ISSN 2432-8375

BULLETIN OF THE

LABORATORY FOR ADVANCED NUCLEAR ENERGY

VOL. 3 2018

LABORATORY FOR ADVANCED NUCLEAR ENERGY
INSTITUTE OF INNOVATIVE RESEARCH
TOKYO INSTITUTE OF TECHNOLOGY

BULLETIN OF THE LABORATORY FOR ADVANCED NUCLEAR ENERGY

(Formerly, BULLETIN OF THE RESEARCH LABORATORY FOR NUCLEAR REACTORS)

Abbreviation of the "**BULLETIN OF THE LABORATORY FOR ADVANCED NUCLEAR ENERGY**" is BULL. LAB. ADV. NUCL. ENERGY

All communications should be addressed to the editor, Laboratory for Advanced Nuclear Energy, Institute of Innovative Research, Tokyo Institute of Technology (Tokyo Kogyo Daigaku),
2-12-1-N1-16, O-okayama, Meguro-ku, Tokyo 152-8550, Japan.

TEL. +81-3-5734-3052, FAX. +81-3-5734-2959, E-mail bulletin@lane.iir.titech.ac.jp

http://www.lane.iir.titech.ac.jp/

BULLETIN OF THE LABORATORY FOR ADVANCED NUCLEAR ENERGY
BULL. LAB. ADV. NUCL. ENERGY, Vol.3, 2018

CONTENTS

Research Staffs ····· 1

I. Research Reports
A. Innovative Nuclear Energy System Division

A.1 Progress in Innovative Nuclear Energy Systems Study and Criticality Safety Study
Toru OBARA ····· 3

A.2 Development of solid oxide electrolysis cell for carbon recycling driven by high temperature gas cooled reactor
Yukitaka KATO and Hiroki TAKASU ····· 5

A.3 Collapse Behavior of Core Structure Materials by Molten Metallic Corium in Boiling Water Reactor Plants during Severe Accidents
Yoshinao KOBAYASHI and Takehiro SUMITA ····· 7

A.4 Integration of Ultrasonic Measurement and Robotic System for Measurement in NPP Decommissioning for Fukushima
Hiroshige KIKURA and Hideharu TAKAHASHI ····· 9

A.5 Study on the development of ultrasonic transducer for three -dimensional velocity profile measurement
Hideharu TAKAHASHI and Hiroshige KIKURA ····· 10

A.6 Numerical Investigation of Thermocline in Thermal Energy Storage System using Stone
Hiroshige KIKURA, Hideharu TAKAHASHI and Yutaka TAMAURA ····· 11

A.7 Development of Enhanced Inspection Methodology for 1F
Hiroshige KIKURA and Hideharu TAKAHASHI ····· 12

A.8 Microscopic Bubble behavior in suppression pool during wetwell venting
Hiroshige KIKURA, Hideharu TAKAHASHI and Hideo NAGASAKA ····· 13

A.9 Numerical Simulation of Cavity Receiver with Parallel Tubes for Cross Linear Concentrated Solar System
Hiroshige KIKURA, Hideharu TAKAHASHI and Yutaka TAMAURA ····· 14

A.10 Material compatibility study on liquid lead alloys and liquid tin alloys for innovative nuclear reactors
Masatoshi KONDO ····· 15

B. Actinide Management Division

B.1 Research activity of metal ion separation in Takeshita Laboratory from solvent extraction, adsorption to contactor work
Masahiko NAKASE, Yusuke INABA, Miki HARIGAI, Kazuo UTSUMI and Kenji TAKESHITA ····· 19

B.2 Study on remediation of contaminated soil generated by Fukushima Nuclear Power Plant Accident with hydrothermal treatment technique
Yusuke INABA, Xiangbiao YIN, Miki HARIGAI, Kazuo UTSUMI, Masahiko NAKASE and Kenji TAKESHITA ····· 23

B.3 Development of methodology for evaluation of nuclear fuel cycle from the viewpoint of waste management and disposal
Tomohiro OKAMURA, Masahiko NAKASE, Kota KAWAI, Eriko MINARI, Hidekazu ASANO and Kenji TAKESHITA ····· 25

B.4 Direct Extraction of Actinides from Acidic Solution using the Hydrophobic Interactions of poly (N-isopropylacrylamide) with Diamide-typed Ligands
Kaname SAGA and Takehiko TSUKAHARA ····· 26

B.5 Microchemical Analysis of Gamma-Emitting Actinides in Radioactive Wastes Generated From Nuclear Accidents
Brandt AILEEN, Kazuki MATSUSHITA and Takehiko TSUKAHARA ····· 27

C. Global Nuclear Security Division

C.1 Accumulation of metal cations by sorbents
Toshihiko OHNUKI, Yuria SEKINE and Qianqian YU ····· 29

C.2 Impacts of 240Pu self-shielding effect and uncertainties of σ(n,γ) at resonance energy on the reactivity controllability in HTGR inert matrix fuel
Takeshi AOKIA, Hiroshi SAGARA and Chi Young HAN ····· 31

C.3 Applicability study of the photofission based nuclear material isotopic composition measurement method on the Thorium-Uranium system
Rei KIMURA, Hiroshi SAGARA, Satoshi CHIBA ····· 32

C.4 User Interface of Atmospheric Dispersion Simulation for Nuclear Emergency Countermeasures, Energy Procedia, Volume 131, December 2017, Pages 279-284
Hamza El-ASAAD, Hiroshi SAGARA, Haruyasu NAGAI ····· 33

C.5 Characterization and Fluorine-Plasma Exposure Behavior of Dense Yttrium Oxyfluoride Ceramics
Katsumi YOSHIDA, Toru TSUNOURA, Anna GUBAREVICH and Toyohiko YANO ····· 34

C.6 Combustion synthesis of MAX phases for accident-tolerant fuels
Anna GUBAREVICH, Toyohiko YANO and Katsumi YOSHIDA ····· 37

C.7 Agendas and Issues of Participatory Dialogues by Junior-High and High School Students from Fukushima Hama-doori and Capital Area -Recognition for thyroid examination of six years after the accident and future issues-
Tetsuo SAWADA ····· 40

D. Advanced Medical Application Division

D.1 Applied Research on Proton-Induced X-ray Emission at LANE, IIR
Yoshiyuki OGURI, Yuchao HU and Wenkai TENG ····· 43

D.2 Molecular Mechanisms for Repair of DNA Double-strand Breaks
Mikio MATSUMOTO ····· 44

D.3 DNA damage response in human induced pluripotent stem cells after ionizing radiation exposure
Mikio SHIMADA ····· 47

D.4 Flow Direction Control of Laser-produced Plasma by a Magnetic Nozzle
Jun HASEGAWA ····· 49

D.5 Numerical Analysis of Particle Dynamics in a Linear Inertial Electrostatic Confinement Fusion Device
Jun HASEGAWA ····· 51

E. Fundamental Research Division

E.1 Study for nuclear fission and its application
Chikako ISHIZUKA and Satoshi CHIBA ····· 53

E.2 Diagnostics of Microwave Discharge Low-Pressure Argon Plasma by Multi-Optical Emission Line Analysis Based on Collisional-Radiative Model

Hiroshi AKATSUKA and Atsushi NEZU ····· 55

E.3 Spectroscopic study on CO b 3Σ+ state in microwave discharge CO2 plasma and the effect of rare-gas admixture
Hiroshi AKATSUKA and Atsushi NEZU ····· 56

E.4 Heat Transfer of Submerged Ar Arc Plasma to Water for the Decommissioning of Degraded Nuclear Power Plant
Hiroshi AKATSUKA and Atsushi NEZU ····· 57

II. Co-operative Researches

II.1 Co-operative Researches within Tokyo Institute of Technology ····· 59

II.2 Co-operative Researches with outside of Tokyo Institute of Technology ····· 59

III. List of Publications ····· 63

Research staffs of
THE LABORATORY FOR ADVANCED NUCLEAR ENERGY,
TOKYO INSTITUTE OF TECHONOGY
AS OF 2018 JAPANESE FISCAL YEAR

Director

Kenji TAKESHITA	Professor

Innovative Nuclear Energy System Division

Toru OBARA	Professor
Yukitaka KATO	Professor
Yoshinao KOBAYASHI	Professor
Tatsuya KATABUCHI	Associate Professor
Hiroshige KIKURA	Associate Professor
Masatoshi KONDO	Associate Professor
Jun NISHIYAMA	Assistant Professor
Hiroki TAKASU	Assistant Professor

Actinide Management Division

Kenji TAKESHITA	Professor
Koichiro TAKAO	Associate Professor
Takehiko TSUKAHARA	Associate Professor
Masahiko NAKASE	Assistant Professor

Global Nuclear Security Division

Toshihiko OHNUKI	Professor
Hiroshi SAGARA	Associate Professor
Katsumi YOSHIDA	Associate Professor
Tetsuo SAWADA	Assistant Professor
Anna GUBAREVICH	Assistant Professor

Advanced Medical Application Division

Yoshiyuki OGURI	Professor
Noriyosu HAYASHIZAKI	Professor
Yoshihisa MATSUMOTO	Associate Professor
Jun HASEGAWA	Associate Professor
Mikio SHIMADA	Assistant Professor

Fundamental Research Division

Shunji IIO	Professor
Satoshi CHIBA	Professor
Hiroshi AKATSUKA	Associate Professor
Hiroaki TSUTSUI	Associate Professor
Chikako ISHIZUKA	Assistant Professor

Advanced Research and Education Program

Akira NISHIMURA	Specially Appointed Professor

Common Staffs

Hiroshi UETSUKA	Specially Appointed Professor
Kazutoshi FURUKAWA	Specially Appointed Professor
Hiroyasu MOCHIZUKI	Specially Appointed Professor
Tadashi NARABAYASHI	Specially Appointed Professor
Satoru TSUSHIMA	Specially Appointed Associate Professor
Hideharu TAKAHASHI	Specially Appointed Assistant Professor
Maletaskic JELENA	Specially Appointed Assistant Professor
Tuya DELGERSAIKHAN	Specially Appointed Assistant Professor
Takatoshi TAKEMOTO	Visiting Associate Professor

Technical Staffs

Masamitsu IMAI	Senior Technical Specialist
Mitsuo MATSUZAKI	Senior Technical Specialist
Hitoshi FUKUDA	Senior Technical Specialist
Ken-ichi TOSAKA	Senior Technical Specialist
Atsushi NEZU	Senior Technical Specialist

I. Research Reports

A. Innovative Nuclear Energy System Division

A.1 Progress in Innovative Nuclear Energy Systems Study and Criticality Safety Study

Toru OBARA

Studies on innovative nuclear systems and criticality safety have been performed. The studies were focused on the Breed and Burn reactors, High Temperature Gas-cooled reactors, and criticality safety analysis.

1. Study on CANDLE burning reactor with melt-refining process

One of the ideas to keep integrity of fuel cladding in CANDLE burning reactor is to introduce melt-refining process. In the study, the effects of cooling during the melt-refining process in the reactor was investigated. The introduction of cooling time during the melt and refining process had an impact on the CANDLE burning. A cooling time of one, two, four and eight years were simulated at each melt and refining cycle. The effects of cooling on excess reactivity varied with the cooling time. A longer cooling time may reduce the excess reactivity of a CANDLE burning reactor in the equilibrium condition to negative. In this case, the core design of the CANDLE might need to be optimized to compensate for the decrease of excess reactivity due to the accumulation of Am-241 during the cooling period [1].

2. Study on CANDLE burning reactor with start-up core using plutonium from LWR spent fuel

A CANDLE burning fast reactor can achieve effective utilization of uranium resources. Once it is started up, it needs only natural or depleted uranium, but the initial core must be constructed with enriched uranium or plutonium fuel. In this study, numerical calculations were performed to find the minimum amount of plutonium needed for a loaded fuel distribution of the initial core to start up many CANDLE burning fast reactors using plutonium from light water reactor spent fuel. Results showed that a minimum amount of 3.58 tons of plutonium in the initial core could keep a reactor critical during its entire operation period [2].

3. Study on High Temperature Gas-cooled reactor with ROX fuel

The Japan Atomic Energy Agency has proposed rock-like oxide (ROX) fuel as a new, once-through type fuel concept. In the study, burnup performance using ROX fuel was simulated in a pebble bed reactor with an accumulative fuel loading scheme. The MVP-BURN code was used to simulate the burnup calculation. Fuel of 5g-HM/pebble with 20% ^{235}U enrichment was selected as the optimum composition. Discharged burnup could reach up to 218 GWd/t, with a core lifetime of about 8.4 years. However, high excess reactivity occurred in the initial condition. Initial fuel enrichment was therefore reduced from 20% to 4.65% to counter the initial excess reactivity. The operation period was reduced by the decrease of initial fuel enrichment, but the maximum discharged burnup was 198 GWd/t. Burnup performance of ROX fuel in this reactor concept was compared with that of UO_2 fuel obtained previously. Discharged burnup for ROX fuel in the PBR with an accumulative fuel loading scheme was as high as UO_2 fuel. Maximum power density could be lowered by introducing ROX fuel compared to UO_2 fuel. However, PBR core lifetime was shorter with ROX fuel than with UO_2 fuel. A negative temperature coefficient was achieved for both UO_2 and ROX fuels throughout the operation period [3].

4. Study on Criticality Accident Analysis in Coupled Fuel Debris

Analysis of a possible criticality accident during decommissioning of the Fukushima Daiichi NPS (1FNPS) by evaluating the potential energy and dose release is important for safety. Yet choosing an appropriate method for such analysis can be challenging because of the unknown state of fuel debris inside the reactors. Past experience with the TMI-2 accident, however, suggests that fuel debris at 1FNPS could be highly heterogeneous in terms of both composition and geometry consisting of physically distinct but neutronically coupled debris regions. Conventionally, a one-point kinetic model (PKM) supplemented with deterministic method was used for transient analysis. However, the PKM fundamentally does not provide space-dependent quantities. Thus, an integral kinetic model (IKM) aided by Monte Carlo transport method is more suitable because it takes space/region-dependency into account. As a preliminary analysis for the long term effort of analyzing criticality accidents involving fuel debris, in this study an effect of surrounding debris during a supercritical transient in simple two-region coupled debris systems of symmetric and asymmetric geometry were investigated using the IKM with simple Doppler feedback mechanism. The obtained results included region-wise fission rate profile and energy release. The results indicated that total energy release decreased about exponentially as the distance between two regions increased [4].

5. Study on Improved Approach to Multi-region Supercritical Transient Analysis

An approach to multi-region supercritical transient analysis based on the integral kinetic model (IKM) and Monte Carlo method is further developed with new features. The IKM describes the region-dependent fission rate during the transient in a system of arbitrary geometry using a secondary fission probability density function, which

takes the explicit neutron transport time between successive fissions across the regions into account. The new features of the improved approach include treatment of the multi-region transient using repeated multi-dimensional linear interpolation between pre-obtained kinetic functions (i.e., secondary probability density function), a new method for calculating the kinetic functions using the continuous-energy Monte Carlo code MVP2.0, and utilization of kinetic functions directly in the IKM without the fitting function that introduces a fitting error. The improved approach is verified by applying it to the supercritical transient in simple Godiva systems of different region combinations without feedback. In addition, we attempt to validate the improved approach by applying it to the supercritical transient in a simplified Godiva system with thermal expansion feedback and compared the obtained and experimental results. The verification results indicate the improved approach works well with different combinations of regions while the validation results show promising agreement with the experimental results. This study is part of an ongoing research activity on the development of **M**ulti-region **I**ntegral **K**inetic code (MIK code) for general space- and time-dependent kinetic analysis [5].

Reference

1. Julia Abdul Karim, Jun Nishiyama, Toru Obara: Effects of cooling interval time in melt and refining process for CANDLE burning; Annals of Nuclear Energy, Vol. 105, pp.144-149 (2017).
2. Hiroki Osato, Jun Nishiyama, Toru Obara,: Study on CANDLE Burning Fast Reactor with Initial Core Using Plutonium from LWR Spent Fuel; Energy Procedia, Vol. 131, pp. 15-20 (2017).
3. Irwan Liapto Simanullang, Toru Obara: Burnup performance of rock-like oxide (ROX) fuel in small pebble bed reactor with accumulative fuel loading scheme; Annals of Nuclear Energy, Vol. 107, pp. 110-118 (2017)
4. Delgersaikhan Tuya, Toru Obara: Supercritical transient analysis in coupled fuel debris systems of symmetric and asymmetric geometry using integral kinetic model**;** Annals of Nuclear Energy, Vol. 109, pp. 113-119 (2017).
5. Delgersaikhan Tuya, Hiroki Takezawa, Toru Obara: Improved approach to multi-region supercritical transient analysis based on the integral kinetic model and Monte Carlo method; Nuclear Science and Engineering, Vol. 188, pp. 33-42 (2017).

A.2 Development of Solid Oxide Electrolysis Cell for Carbon Recycling Driven by High Temperature Gas Cooled Reactor

Yukitaka KATO and Hiroki TAKASU

1. INTRODUCTION

The increase of carbon dioxide (CO_2) emissions due to the consumption of fossil fuels causes global environmental problems. In Japan, almost all primary energies are imported from other countries. Reductions of CO_2 emissions and primary energy imports have been difficult problems to be addressed. However, a new low-carbon energy system has been proposed, which is referred to as an active carbon recycling energy system (ACRES)[1]. With ACRES, carbon energy materials such as carbon monoxide (CO) are regenerated from CO_2 and reused cyclically. CO has a higher exergy ratio (ΔG / ΔH) than hydrogen (H_2) and methane, which makes CO an important candidate as a recycling media for ACRES. In ACRES, CO_2 separated from exhaust gas is reduced to CO, as shown in Eq. (1), and the regenerated CO is used cyclically as an energy medium.

$$CO_2 \rightarrow CO + 1/2\ O_2 \quad (1)$$

CO_2 reduction into CO is a key technology for the establishment of ACRES. It is possible to reduce CO_2 into CO by an electrolysis process, such as with a solid oxide electrolysis cell (SOEC), which employs the opposite operation of a solid oxide fuel cell (SOFC)[2].

ACRES is expected to be applicable with iron-making processes, because CO can be used directly for the reduction of iron ore. After CO_2 generated from a blast furnace is captured, CO is regenerated from CO_2 using the SOEC. The regenerated CO is recirculated in a blast furnace, so that the quantity of coke (reducing agent) required can be reduced. A proposed application of ACRES for an iron-making process referred to as a smart iron-making system based on ACRES (iACRES) is shown in Fig. 1 [3]. As primary energy sources for a high-temperature gas cooled reactor (HTGR) used for ACRES, renewable energies such as solar and wind, and waste heat from high-temperature industrial processes are proposed as candidates. The HTGR, in particular, is a chief candidate for iACRES because it is capable of sufficiently high-temperature heat production up to 950 °C and stable heat output for iACRES.

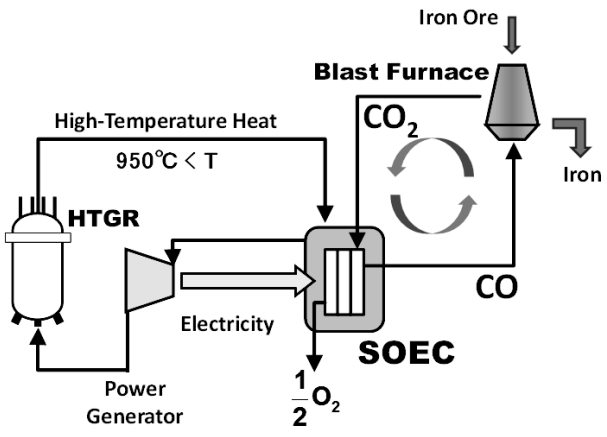

Fig. 1 Schematic of the iACRES concept.

Although previous studies demonstrated CO_2 electrolysis, however, knowledge about availability of SOEC CO_2 electrolysis under operation conditions of gas compositions and temperatures for iACRES was still small. Then, in this study, a disk-type SOEC was prepared and the SOEC electrolysis performance was measured experimentally at the laboratory scale. The availability of a practical iron-making system based on iACRES was evaluated using the experimental results for the SOEC.

2. PRINCIPLE OF SOEC

A SOEC electrolyzes carbon dioxide by the application of an overvoltage in the cell. SOEC has a three-layer structure of cathode|solid electrolyte|anode. CO_2 is supplied to a porous cathode and diffuses through the micropores of the electrode. CO_2 is then decomposed into CO and O^{-2} by electrons supplied to cathode, as shown in Eq. (2):

$$CO_2 + 2e^- \rightarrow CO + O^{2-} \quad (2)$$

The oxygen ions generated are transported to the anode through ionic defects in the solid oxide electrolyte and oxygen is generated:

$$O^{2-} \rightarrow 1/2O_2 + 2e^- \quad (3)$$

The overall reaction from Eqs. (2) and (3) gives Eq. (1). The energy change for Eq. (1) is given by

$$\Delta H = \Delta G + T\Delta S \quad (4)$$

where ΔH [J mol^{-1}], ΔG [J mol^{-1}], and ΔS [J mol^{-1} K^{-1}] are the Gibbs free energy, enthalpy, and entropy changes for the reaction, respectively, and T [K] is the reaction temperature. For establishment of the reaction by the supply of ΔH, the ΔG term is covered by the use of electricity, while the $T\Delta$S term is provided by thermal energy. The decomposition voltage of CO_2 ($E°$ [V]) is dependent on ΔG, which is expressed as

$$E° = -\Delta G / (nF) \quad (5)$$

where n is the number of the valence electrons and F is Faraday's constant (= 96500 C/mol). The catalytic reactions at the electrodes, gas diffusion in the electrode

layer, and ohmic resistance must be considered for performance improvement of SOEC. Yttria-stabilized zirconia (YSZ) is mainly used as solid oxide electrolytes, which become oxygen ion conductors at high temperatures around 700–1000 °C.

3. EXPERIMENTAL AND RESULTS

The experimental apparatus was constructed to measure the performance of the SOEC [4]. CO_2 gas is introduced to the reactor as a reaction gas, and Ar is used as a carrier gas at the cathode side. N_2 is used as a carrier gas for oxygen generated via electrolysis at the anode side. The reacted gases were analyzed using gas chromatography.

The disk-type ceramic-supported (CS) SOECs prepared for this study had an electrolyte disk as shown in Fig. 2 (20 mm diameter and 1.0 mm thick), which supported the cell's integrity and was made of yttria-stabilized zirconia (YSZ) powder (40 nm particle diameter, TOSOH Corp.) formed by using metal mold subjected to uniaxial pressing and cold isostatic pressing at 200 MPa, then sintered at 1500 °C for 2 hours. The YSZ disk prepared had a diameter of 20 mm and a thickness of 1 mm, and the electrode layers (cathode and anode) were formed on the top and bottom surfaces of the disk using squeegee of a screen-printer. The name NiSDC1280 SOEC has that cathode and anode materials were NiO:SDC (50:50 by weight) and LSCF, respectively. SDC and LSCF stand for samarium-doped ceria (20 mol%samarium) and $La_{0.6}Sr_{0.4}Co_{0.2}Fe_{0.8}O_{3-\delta}$ (lanthanum strontium cobalt ferrite), respectively.

The SOEC was held by two outer alumina tubes (20 mm outer diameter) and sealed with glass rings. The electrolyte cell thickness was relatively thicker than conventional cell, then, it was thought that IR loss of the cell was relatively larger than conventional one. It was expected that electrolysis performance would be improved by the reduction of the thickness. Reaction gases were supplied through inner tubes (6 mm outer diameter). The electrical current was collected using platinum mesh (7×7 mm^2) attached to each end of the inner tubes. The glass ring seals were melted at 950 °C prior to operation of the SOEC. In this study,

A current density of 131.4 mA cm^{-2} was measured between the cathode and anode at 2.3 V and 900 °C. The CO and O_2 production rates were close to theoretical as shown by the Faraday efficiency values of the data points.

Based on the experimental results, iACRES as a combination of ACRES with a blast furnace was evaluated when CO_2 of 30% in the blast furnace gas (BFG) was reduced to CO by the SOEC. Heat and electricity generated from the HTGR were used together for the high-temperature CO_2 electrolysis in the SOEC. The required HTGR unit numbers and SOEC surface area for a blast furnace were calculated.

An evaluation employed the experimental results of NiSDC1280 was assumed to be used for iACRES. A blast furnace used conventionally in large ironworks with an annual pig-iron production of 2.5 Mt y^{-1} was employed as a model for the evaluation. An HTGR plant, in which the secondary coolant has 600 MW-thermal (MWt) at 850 °C, was employed for the electrolysis. From measured current density of 0.163 A cm^{-2} at 800°C, CO_2 decomposition rate of 0.783×10^{-6} mol s^{-1} cm^{-2} was calculated, and required surface area of SOEC cell was estimated as 0.047 km^2 for required CO_2 decomposition rate of 371 mol s^{-1}. 28.8 MWt and 246 MWe were required for the SOEC reduction of the CO_2. Then, total thermal output from HTGR of 576 MWt was needed. The thermal output was corresponding to output of 0.96 HTGR unit. It was understood that the improvement of SOEC performance was important way for reduction of volume of CO_2 reduction facility. These evaluated values would be useful information for system scale evaluation in feasibility studies of iACRES.

Fig. 2 Developed Cell for SOEC.

4. CONCLUSION

SOEC experimental apparatus was fabricated for CO_2 reduction to CO. The SOEC experiment was conducted. The iACRES evaluation indicated that 0.96 HTGR units and an electrode surface area of 0.047 km^2 were required for the reduction of 30% of the CO_2 in conventional blast furnace gas. These results indicate the possibility of carbon recycling with iACRES driven by nuclear powers.

References

[1] Y. Kato, *ISIJ Int'l*, 50(1), pp. 181-185 (2010).
[2] A. L. Dipu, J. Ryu, Y. Kato, *ISIJ Int'l.*, 52(8), pp. 1427–1432 (2012).
[3] Y. Kato, *Prog. Nuc. Eng*., 82, pp. 53-57 (2015).
[4] M. C. A. Nepomuceno, Y. Kato, *Energy Procedia*, 131, pp. 101-107 (2017).

A.3 Collapse Behavior of Core Structure Materials by Molten Metallic Corium in Boiling Water Reactor Plants during Severe Accidents

Takehiro SUMITA and Yoshinao KOBAYASHI

1. Introduction

A severe accident (SA) occurred at Fukushima Daiichi Nuclear Power Plant due to a great earthquake and a subsequent tsunami that happened on March 11, 2011, in Japan. During the accident, the temperature of the reactor core rose up to approximately 3000 K through the radioactive decay and Zircaloy oxidation due to the loss of coolant in the units 1, 2, and 3. After a SA, it is necessary to understand the fracture behavior of the core construction materials, such as the core support structure and the vessel walls, during the accident, to decommission the boiling water reactors. Fig. 1 presents the schematic illustration of the core of a Boiling Water Reactor (BWR) and its composition. At high temperature, the melt occurs between the core component materials, such as control rods (B_4C) and their claddings (stainless steel (SS)) at approximately 1447 K, and the fuel rods (UO_2) and the fuel claddings (Zircaloy) below the UO_2 melting point. Liquid phases, called corium, are then formed. The formed corium flows down to the bottom of the pressure vessel, and a portion reaches the bottom of the reactor container while dissolving the core support structure mainly made of SS.

The corium that might have been formed during the SA could be composed of the following materials: SS-B_4C melt from the control rods, oxidic corium (UO_2-ZrO_2) from the fuel rods (both at the initial stage of the SA), molten steel with small quantities of metallic U and Zr, or molten steel enriched with metallic U and Zr (both after the stratification occurred). In particular, the eutectic melt between the control rods (B_4C) and their cladding (SS) has been a concern since the accident in Fukushima as the B_4C used for this BWR could have been at the origin of a reaction that never previously occurred in a PWR. This reaction caused SS-B_4C melt, having a low melting point in the core component materials. It is considered that this SS-B_4C melt can damage the core construction materials in the early stage of a SA before the fuel rods and their cladding melt. Therefore, the fracture behavior of SS by SS-B_4C melt should be investigated in order to predict the damage condition of a reactor after the accident. However, there are few reports on the reaction between SS-B_4C melt and solid SS.

This study aims to investigate the fracture behavior of core structure materials by molten metallic corium. Immersion experiments of SS rod with molten metallic corium (SS- B_4C melt) were carried out.

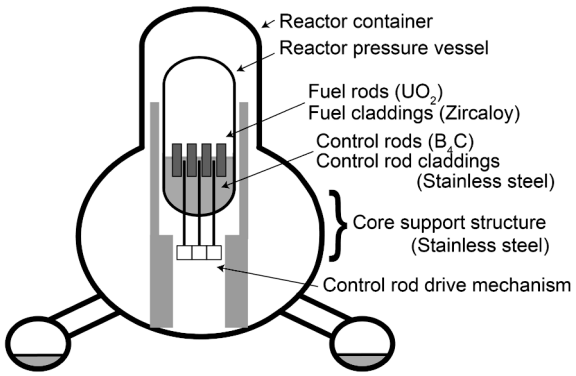

Fig. 1 Schematic illustration of BWR

2. Experimental

2.1. Sample preparation

Samples simulating metallic corium originated from control rods were prepared in a mullite crucible (11 mm in inner diameter x 15 mm in outer diameter x 120 mm in height) by melting a mixture of SUS 304 powder and B_4C powder at 1723 K for 90 min. In Ar-3%H_2, followed by water quenching. This alloy was synthesized to obtain a B concentration of 3.7wt%; this is similar to the Fe-B eutectic alloy composition having a low melting point based on the Fe-B phase diagram, having 5wt% of B concentration.

Samples simulating structural material of SS was prepared by machining the SUS 304 rod to have the shape of immersed part having the length of 50 mm and diameter of 7 mm as shown in Fig.2. This immersed part of the sample was ground with abrasive SiC papers (#100 - #2000).

Table. 1 Chemical composition of mock metallic corium

	Fe	Cr	Ni	B	C
mass%	71	17	7.6	3.7	1.0
at.%	59	15	6.0	16	4.0

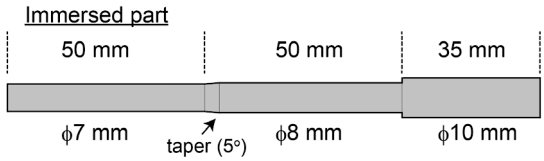

Fig. 2 SS rod sample

2.2. Experimental Procedure

About 14 g of metallic corium was placed in a mullite crucible having the same size as above, and was put in a furnace. The sample was pre-melted at 1573 K in an Ar atmosphere for 45 min. After that, SS rod was charged into the furnace just above the crucible and preheated for 2 min. Thereafter the rod sample was immersed in molten metal for the intended time, followed by water quenching as shown in Fig.3. After the experiment, the sample was cut out from the immersed part and mounted in epoxy followed by grounding with abrasive SiC papers (#100 - #2000) and polishing with diamond paste (2 μm). Scan electron microscopy (SEM), electron dispersion spectrum (EDS), and wavelength dispersion spectrum (WDS) were used to characterize the reaction zone.

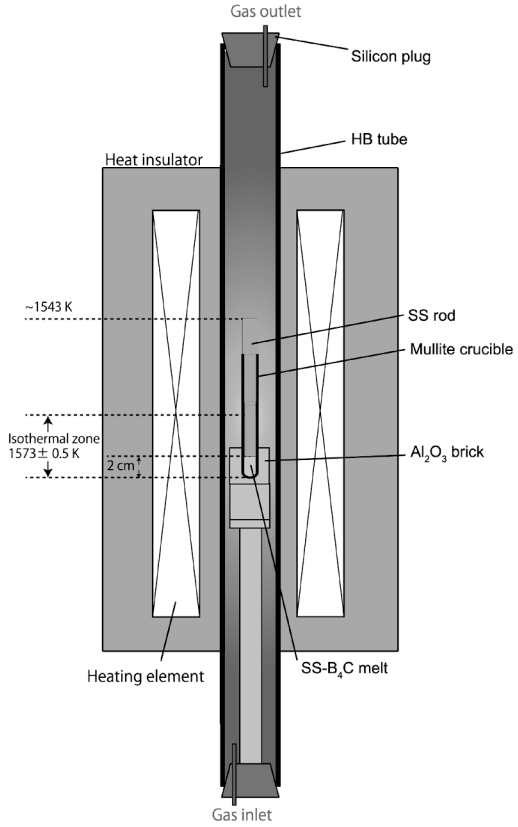

Fig. 3 Immersion experiment

3. Results and Discussion

Fig. 4 shows the Optical Microscopic Images (OMI), and Backscattering Electron Images (BEI) of the sample after 4 min immersion experiment. Since the interface between the SS rod and the SS-B_4C alloy was distinguishable in both the OMI and BEI, the infiltration of SS-B_4C melt into the SS grain boundaries was observed. This infiltration phenomenon was also observed in the case of interaction between molten Cu and solid Fe

This finding suggests that grains may fall off from the rod due to infiltration. In fact, it was found that fallen grains were observed in longer immersion experiment. Thus, it is predicted that, besides chemical dissolution reaction (called eutectic melting) between SS and B_4C, physical dissolution (called erosion) is caused by the grains falling off from rod due to infiltration of molten metal.

Obtained result imply that the dissolution mode of this system has two types: (1) chemical dissolution by eutectic melting at the SS interface and (2) physical dissolution which is caused by the grains falling off from rod due to infiltration of molten metal called corrosion-erosion.

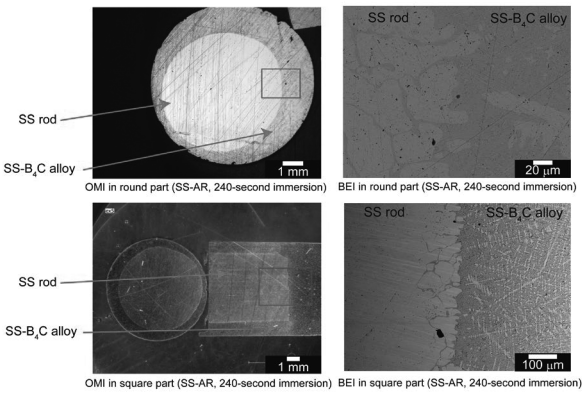

Fig. 4 Optical Microscopic Images (OMI), and Backscattering Electron Images (BEI) of the sample after 4 min immersion experiment

Acknowledgment

This study is financially supported by the project of "Accessibility for removal of fuel debris in BWR plant after severe accident" in The Center of World Intelligence Project for Nuclear S&T and Human Resource Development, Ministry of Education, Culture, Sports, Science and Technology.

Reference

1. Takehiro Sumita, Kentaro Urata, Yuya Morita, Yoshinao Kobayashi: Dissolution behavior of core structure materials by molten corium in boiling water reactor plants during severe accidents; *Journal of Nuclear Science and Technology*, Vol. **55**, pp. 267-275(2018).

A.4 Integration of Ultrasonic Measurement and Robotic System for Measurement in NPP Decommissioning for Fukushima

Hiroshige KIKURA and Hideharu TAKAHASHI

1. Introduction

After the Fukushima Daiichi Nuclear Power Plant Accident, a significant amount of radioactive material was released into the atmosphere, and three of the plant's six reactors suffered core meltdowns (unit 1, 2 and 3). The long-term goal is to decommission the damaged vessels. Nevertheless, before starting the decommissioning process, the highly radioactive fuel debris must be removed from the PCV and RPV. However, at present relatively little is known about the state of the vessels and the location and distribution of the fuel debris. The inspection presents a wide range of engineering challenges due to limited access and the harsh radioactive environment. For example, the fuel debris within 1F is currently being cooled by continuously addition of water and so the PVC/RPV are flooded meaning that the areas of interest are underwater. Meanwhile, by addition of cooling water, there is water leakage from damaged primary containment vessels (PCVs) to the groundwater.

Therefore, for decommissioning purpose, we designed a deployment and manipulation system for the ultrasonic sensor robot considering the condition of the vessels[1]. The focus will be on examining measurement from above the grating in the PCV (see **Fig. 1**) by projecting a telescopic arm down through the grating and into the water.

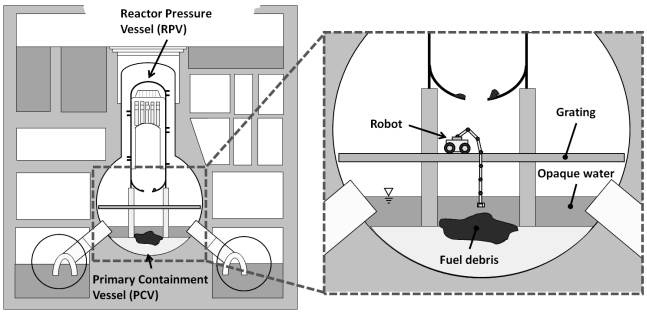

Fig. 1. 1st floor of Primary Containment Vessel (PCV) is covered by gratings. The robotic assess to the flooded vessels is through holes in this grating.

2. Ultrasonic Measurement and Robot System

We propose to use ultrasonic sensor arrays to both measures the water leakage and to map out the location of the fuel debris. We will explore a method known as the Ultrasonic Velocity Profiler (UVP) by multiple measurements using a sensor array which can produce a velocity flow map. This velocity flow map can then be used to indicate the leakage points from the behavior of the surrounding fluid.. We also explore advanced ultrasonic array imaging to inspect the shape and state of the fuel debris. This method is called the Aperture Synthesis method; the ultrasound echoes from the target are combined to produce high-resolution images of the shape of the target. We designed and built lab-based replicas of the immersed regions of PCV and RPV and the access points. This apparatus will be used to test the ultrasonic measurements and their robotic deployment (see **Fig. 2**).

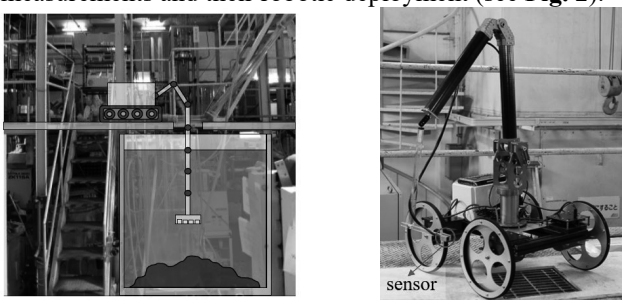

(a) (b)

Fig. 2. (a). A laboratory scale replica of the PCV geometry will be used to test the sensors and robotic deployment systems. (b). Robot and ultrasonic system.

3. Results summary

Figure 3 shows a measurement result from phased array UVP for identifying a water leakage in the water tank[1].

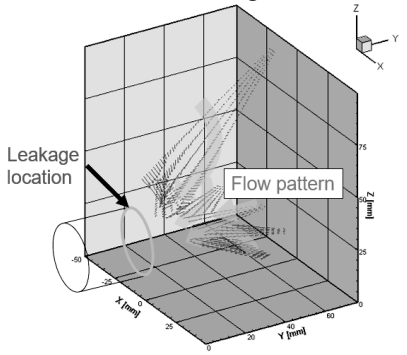

Fig. 3. Identifying a leakage location by phased array UVP and constructed in 3D.

The key feature of this study is that we proposed to combine the ultrasonic imaging of the debris with ultrasonic velocity profiler method for velocity profiles, thus, create a compact sensor system for assessment of the damaged reactor cores. The sensor system will be mounted on a specially designed robotic platform. Thus, the study represents a significant step forward in our ability to decommission the Fukushima Dai-ichi nuclear power plant.

Reference

1. A. Hamdani, *et al.*: Transactions of the American Nuclear Society, ANS 2017, October 29-November 2, 2017, Washington DC, United States, Vol. 117, pp. 917-919 (2017).

A.5 Study on the development of ultrasonic transducer for three-dimensional velocity profile measurement

Hideharu TAKAHASHI and Hiroshige KIKURA

1. Introduction

In fluid engineering, the actual flow often exists as multi-dimensional flow. Previously, we developed the two-elements transducer [1] to obtain two-dimensional velocity profile. In this study, we tried to improve the measurement system by developing the measurement system with five elements transducer to measure three-dimensional velocity profile at the same time to complete the velocity information. We proposed the transducer design and tested the design performance by sound pressure simulation using MATLAB® code.

2. Five-elements ultrasonic transducer

The transducer has elements configuration of 1 center transmitter and four side transmitter/receiver (see Fig.1). With this design, we expected to obtain four Doppler frequencies from 1 measurement volume with a different orientation to each element. Thus, the three-dimensional velocity can be obtained by using two Doppler frequencies in each axial and radial plane (see Fig.2) and can be constructed with the equation below.

$$V_x = \frac{c}{2f_o}\frac{f_{d1} - f_{d2}}{\sin\theta} \quad (1)$$

$$V_y = \frac{c}{2f_o}\frac{f_{d1} + f_{d2}}{1+\cos\theta} \quad (2)$$

$$V_z = \frac{c}{2f_o}\frac{f_{d3} - f_{d4}}{\sin\theta} \quad (3)$$

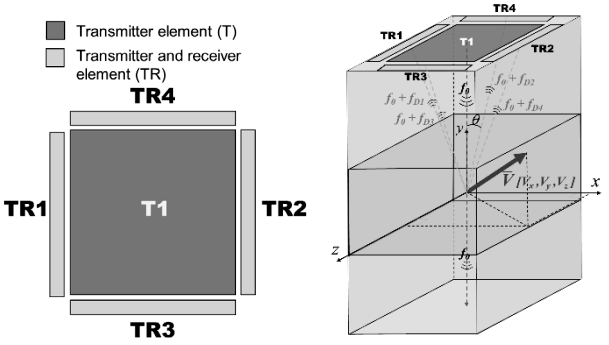

(a) Element configuration. (b) Measurement principle.

Fig.1 Five-elements transducer.

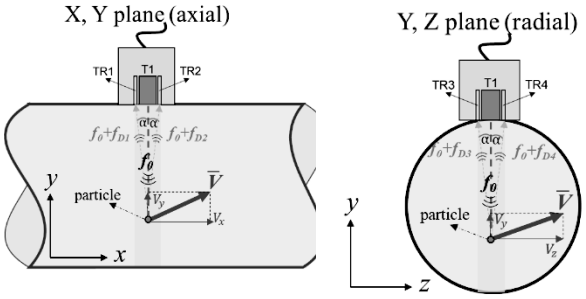

(a) Axial plane (b) Radial plane

Fig.2 Three-dimensional velocity measurement.

3. Sound pressure simulation

Before manufacturing the transducer, the design was evaluated by sound pressure simulation (MATLAB® code) to know the ultrasound propagation characteristic (see Fig.3). From the result, we found that there is one main lobe existing in the center. Therefore, we expect that the three-dimensional velocity measurement possible.

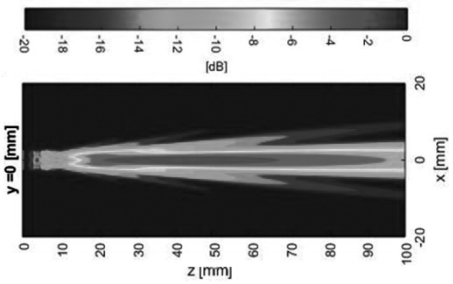

Fig.3 Sound pressure simulation result

4. Conclusion

The five-elements sensor was studied, and the design was tested by simulation. From the simulation result, we found that the ultrasound propagation has one measurement volume. Thus the three-dimensional measurement is possible.

Reference

[1] Jevin Tanius Owen *et al.*, Proceedings of ASTECHNOVA 2017 Int Energy Conference, Yogyakarta, Indonesia (2017-11)

A.6 Numerical Investigation of Thermocline in Thermal Energy Storage System using Stone

Hiroshige KIKURA, Hideharu TAKAHASHI and Yutaka TAMAURA

1. Introduction

Recently, Nuclear- Solar combination system has been proposed and discussed by Kikura et al. (Fig.1) [1]. In this system, solar heat energy will be used to superheat and reheat the steam for operating turbine at maximum possible load. In addition, the supply of solar heat energy will be kept by economical stone heat storage system. Generally, one of problem in solar energy system is the duration of energy production itself, which depends on the time and weather condition. To solve this problem, utilization of Thermal Energy Storage (TES) becomes an essential requirement. By utilizing TES, time and rate mismatch between energy supply and energy demand can be reduced. In this paper, a thermocline in TES using air as the heat transfer fluid was numerically investigated. Stone was selected as storage material because of its economical, chemical inertness, no maintenance and good heat transfer performance. Advantages of air as heat transfer fluid are no cost, non-corrosive, non-toxic and no need to preheat. The effects of several influencing factors on thermal stratification, such as the effects of stone size and the mass flow rate, are taken into consideration.

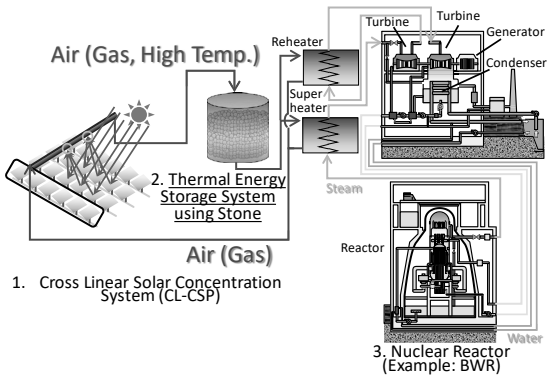

Fig.1 Nuclear – Solar Combination System [1]

2. Numerical Analysis

CFD simulations for 2D axisymmetric geometry (shown in Fig. 2) were performed under laminar flow condition by using a commercial CFD software ANSYS Fluent. Air was used as the heat transfer fluid, with limestone selected as the storage material. A tank of the *H/D* value greater than one was examined. The inside of the tank was filled with a packed bed of crushed limestone at 4 variations of size and the void fraction of 0.45. Local thermal non-equilibrium (LTNE) model for heat transfer in a porous medium was selected, with separate energy equations for the fluid and solid phases. Heat transfer between air and limestone was computed using Wakao and Kaguei correlation (for fluid flow through a packed bed with minimal contact area between the particles).

$$Nu = 2.0 + 1.1\mathrm{Re}^{0.6}\,\mathrm{Pr}^{1/3} \quad (1)$$

3. Results and Discussions

CFD simulations were focused on heat transfer between air and limestone inside the storage tank. Four different stone sizes and three mass flow rate variations were taken into consideration. The simulation result of dimensionless temperature of the packed bed (θ) as a function of dimensionless tank height (x/L) under mass flow rate $\dot{m}_3$ during charging process is presented in Fig. 2.

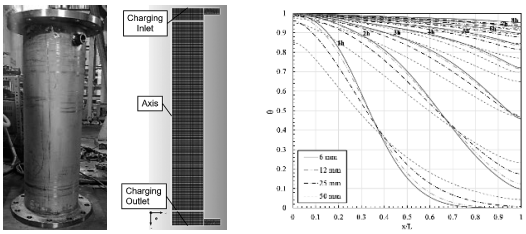

Fig.2. 2D Axisymmetric Geometry of TES and Comparison of Dimensionless Temperature θ inside TES Unit using $\dot{m}_3$, during Charging Process (Inlet air temp. condition: 200°C) [2].

Selection of a higher mass flow rate during charging process resulting in a higher energy stored inside the TES unit. In contrast, selection of a high mass flow rate results to a faster drop in outlet air temperature and to be avoided. The temperature of air became lower when the bigger size of stones were filled into the TES. Rapid decrease of the outlet air temperature during discharging occurred when the bigger size of stones was filled. However, the selection of a small size of limestone inside the TES during both processes results in a higher pressure drop inside the packed bed region and need to be considered for the TES design and operation.

The final step in achieving the optimum parameters of the thermocline TES operating condition is to perform an optimization analysis using Response Surface Methodology (RSM). The optimum operating conditions of the TES unit during charging process were found to be at the inlet air mass flow rate between 0.003-0.004 kg/s and using stone size between 11-25 mm. For the discharging process, optimum conditions were found to be at the inlet air mass flow rate lower than 0.002 kg/s and using stone size between 11-20 mm.

4. Conclusion

Selection of a higher mass flow rate during charging process resulting in a higher energy stored inside the TES unit. In contrast, selection of a high mass flow rate results to a faster drop in outlet air temperature and to be avoided. The optimization result from the RSM analysis shows that the use of different mass flow rate during the charging and discharging cycle might lead to the expected outcome from the TES unit. Moreover, to avoid a high pressure drop inside the TES, the limestone should be bigger than 10 mm.

Reference

1. H. Kikura, et al.; International Conference “Recent Trends on Energy Storage & Hydrogen Energy”, April 28-29, RGPV, Bhopal, India, (2017).
2. R. Pratama, et al.; International Conference “Recent Trends on Energy Storage & Hydrogen Energy”, April 28-29, RGPV, Bhopal, India, (2017).

A.7 Development of Enhanced Inspection Methodology for 1F

Hiroshige KIKURA and Hideharu TAKAHASHI

1. Introduction

Recently, optical inspections have been implemented for the decommissioning of the Fukushima Dai-ichi nuclear power plant (1F). The objective of these inspections is to assess the conditions within the primary containment vessel (PCV) of units 1,2 and 3 at the site, and some achievements has been made so far. However, the inspections have not yet unveiled the locations of leaks or accurate distribution of fuel debris. The two main problems for optical inspection of the plant are: suspended particulates in the coolant water leading to an opaque medium and high-dose radioactivity, to which optical systems are not well suited.

Ultrasonic measurement is considered as a promising non-optical inspection method. Ultrasonic sound can be used in opaque liquids and ultrasonic transducers are generally suited to high radiation levels. In my study, an ultrasonic velocity profiler (UVP) and total focus method (TFM) were focused for identifying leakage points and determining the distribution of fuel debris, respectively. Then, combining of those methods, a measurement system was developed as an enhanced inspection methodology since they don't conflict with each other in signal processing.

This paper describes applicability of the methodology.

2. Methods

2.1 Ultrasonic Velocity profiler

UVP obtains a velocity profile from estimating Doppler frequency in an echo signal. In this method, an ultrasonic pulse is emitted into fluid in which tracer particles are suspending and echo signal are captured afterwards. This procedure is repeated at the pulse repetition frequency and Doppler frequency is calculated with each of the adjacent captured signal using auto-correlation. It is expressed as;

$$f_D(x) = \frac{f_{PRF}}{2\pi} \sum_{x=1}^{N_{rep-1}} Z_x^* \cdot Z_{x+1} \qquad (1)$$

Where subscript index, x is sampled data location of capture signal from sensor, f_{PRF} is pulse repetition frequency, $N_{rep}$is number of repetition, Z is demodulated complex signal with center frequency.

Then, the velocity profile on ultrasonic beam path can be obtained by;

$$V(x) = \frac{f_D(x)}{2f_0} c \qquad (2)$$

Where f_0 is center frequency of sensor, c is sound speed of fluid.

2.2. Total Focusing Method

In this method, an ultrasonic array sensor is used. An ultrasonic pulse from an element is emitted into the media and reflected echo signals are received by all elements in the array sensor. This procedure is repeated for all elements in order to capture signals of all combination of transmitter-receiver pair in the array sensor. A region of interest in front of the array is defined as a number of 'pixels' and echo intensities at each pixel is then calculated using all of the signals. It is expressed by;

$$I_p = \sum W_{ij}^p S_{ij}(\tau_i + \tau_j) \qquad (1)$$

Where subscript index i,j and p are transmitter, receiver and pixel point, respectively, and W is weighting factor S is the captured echo signal and τ is time delay. In this work, element directivity and direction of echo signal are considered as weighting factor.

3. Development

To realize the methodology, a developed system consists of an ultrasonic array sensor (8MHz,128ch.), pulser/receiver, multi-plexer, digital convertor and PC. All signal processing is carried out with LabVIEW program written for the methodology.

4. Experiment & Result

Experiments were conducted evaluate performance of the developed system as showed in Fig.1(a). As a result, shape of the mocked fuel debris and location of leakage point are determined and assumed as white line and intensive downflow(red), respectively in Fig.1(b) and those looks good agreement with the actual shape and location.

Thus, applicability of the methodology was confirmed.

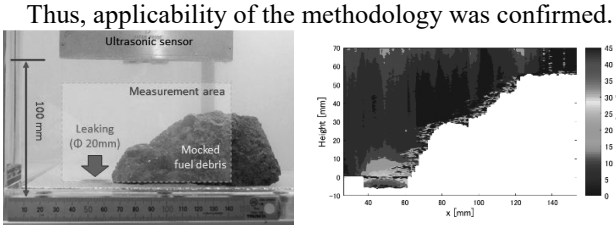

(a) Measurement area. (b) Combined image.

Fig.1 Result of the experiment.

Reference

1. T.Kawach, *et al*: Development of Simultaneous Measurement System for Flow Visualization and Surface Reconstruction using Ultrasonic Array Sensors; CO.122, 9th World Conference on Experiment Heat Transfer, Fluid Mechanics and Thermodynamics (2017).

A.8 Microscopic bubble behaviour in suppression pool during wetwell venting

Hiroshige KIKURA, Hideharu TAKAHASHI and Hideo NAGASAKA

1. Introduction

The retention of fission products in the suppression pool is called pool scrubbing effect. It is a complex process governed by several fission product (FP) removal mechanisms, such as diffusiophoresis, gravitational sedimentation, etc. These mechanisms enhance the efficiency of pool scrubbing effect. The total efficiency, determined by decontamination factor (DF), is introduced in pool scrubbing codes, such as SUPRA, SPARC, and BUSCA. In the codes DF is calculated based not only on FP parameters, but also on bubble parameters. Important bubble parameters are diameter and rise velocity. However, correlations used in the codes were developed under different conditions.

2. Experimental method

2.1. Test facility

A new test facility was constructed to observe and visualize rising bubble in suppression pool under wetwell venting conditions. The facility (Fig. 1) consists of two pressure vessels - drywell (D/W, 1.2 m long, 0.345 m in diameter), and wetwell (W/W, 2.5 m high and 0.355 m in diameter), steam generator, air compressor, and heat exchanger. D/W and W/W are connected with downcomer pipe.

Bubble visualization is performed adopting backlit shadowgraphy technique. The high speed camera Photron Mini AX50 is used to records rising bubbles.

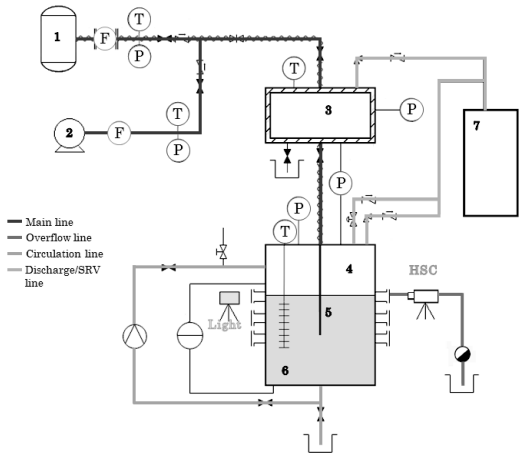

Fig. 1 Test facility. 1 - steam generator, 2 - air compressor, 3 - drywell, 4 - wetwell, 5 - downcomer pipe, 6 - suppression pool, 7 - heat exchanger.

2.2. Initial test conditions

18 experimental tests were conducted. All experiments were done using ID 12.48 mm downcomer pipe. W/W pressure was kept atmospheric. Rising bubbles were observed and visualized at the pool surface. The mixture of steam and air from drywell to wetwell was flowing due to the pressure difference just slightly higher than the pressure head in the downcomer pipe.

The initial conditions vary by submergence of downcomer outlet, S/P temperature, and air content. 6 tests were conducted having lower submergence (0.63-0.67 m), and 12 tests were conducted having higher water level (1.47-1.54 m) in the S/P. S/P temperature was ranged from 30 °C to 90 °C. Half of the tests were done having uniform temperature distribution. Another half was done having thermally stratified S/P. Air content was ranged 4-43%.

3. Results

Experimentally obtained data was analyzed evaluating influence of conditions in the pool (temperature, content of non-condensable gas, downcomer submergence), and comparing with the results from the correlations used in the pool scrubbing codes.

Pool temperature, downcomer submergence and air content in the carrier gas resulted in bubble diameter increase. Air content and pool temperature had the greatest effect on bubble diameter. Bubble were rising faster in the pool with deeper submergence and having higher air content in the flow. Rising pool temperature had negative effect on bubble rise velocity.

The obtained bubble diameter (represented by Sauter Mean Diameter SMD) (Fig. 2) and rise velocity show effect of suppression pool temperature and air content tendency. On the other hand, correlations in the codes result in almost constant values.

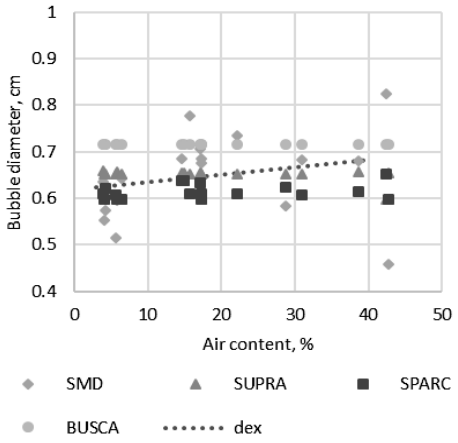

Fig. 2 Bubble diameter over air content in the flow.

4.Conclusions

Experimentally obtain bubble parameters show a different dependency on several parameters comparing with the pool scrubbing codes. Therefore, bubble diameter and velocity under well controlled conditions is necessary.

Reference

1. G. Zablackaite, et al. 14th *14th International Conference on Fluid Control, Measurements and Visualization (FLUCOME2017)* October 8-12, Notre Dame, Indiana, USA

A.9 Numerical Simulation of Cavity Receiver with Parallel Tubes for Cross Linear Concentrated Solar System

Hiroshige KIKURA, Hideharu TAKAHASHI and Yutaka TAMAURA

1. Introduction

Concentrated solar power (CSP) is a very promising technology for renewable energy. Tokyo Institute of Technology takes part in its development by inventing the novel Cross Linear Concentrated Solar Power (CL-CSP) system. A 30kW CL-CSP plant has been commissioned at Rajiv Gandhi Technological University (RGPV) and utilizes a new receiver model which is called Cavity Linear Receiver (CLR), as shown in Fig. 1. Study on the new receiver could be essential for the development of the novel CL-CSP system and applicable to other CSP systems.

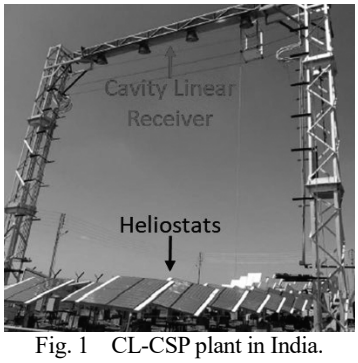

Fig. 1 CL-CSP plant in India.

2. Numerical simulation method

This work focused on the improvement of the CLR performance through a parametric study of the receiver geometry based on numerical simulation. The improvement in the CLR performance can give significant effect on the CL-CSP system efficiency. The numerical simulation is divided into two parts as seen in Fig. 2. The optical simulation used the Monte Carlo Ray Tracing Method (MCRT) and the CFD simulation used Finite Volume Method (FVM) [1]. The simulation considers the non-uniformity of solar heat flux and temperature on receiver tubes.

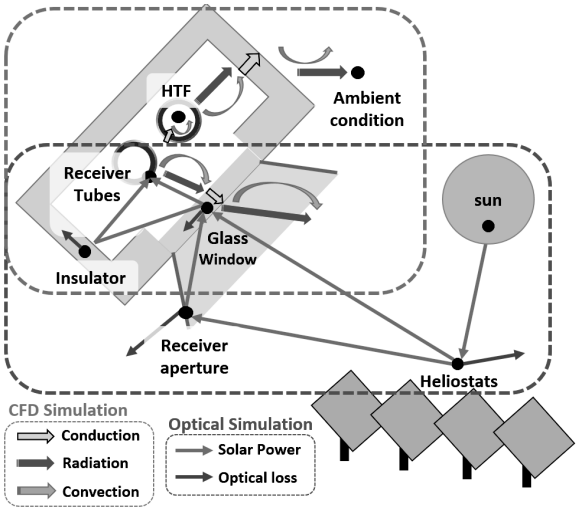

Fig. 2 The optical and CFD simulations.

3. Geometrical parameters

A parametric study for the CLR geometry has been done by varying the distance of the receiver tube center from the cavity top wall (d), cavity height (h), the distance between tubes (p), and cavity width (w) as seen in Fig. 3.

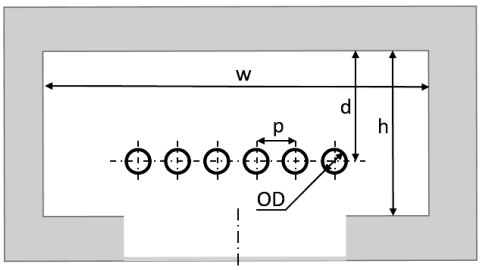

Fig. 3 Geometrical parameters of CLR.

4. Result and discussion

Effect of the geometrical parameters variation on the CLR optical and thermal efficiency has been investigated and can be seen in Fig. 4. The result implies that the variation of geometry has a more significant impact on the optical efficiency than that on the thermal efficiency. In addition, the maximum surface temperature is also an important thing to be considered, due to high non-uniformity of temperature near the cavity window.

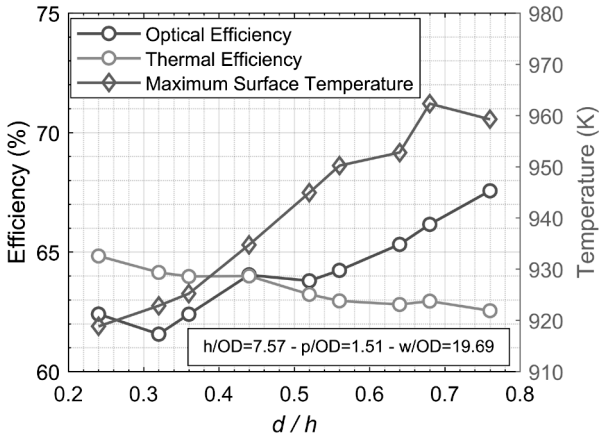

Fig. 4 Geometrical parameter effect on CLR efficiency.

5. Conclusion

The combination of optical and CFD simulation was successfully utilized in this work to perform optimization for geometrical configuration of Cavity Linear Receiver (CLR). The highest optical efficiency is achieved when the tubes are close to the cavity window and the distance between the tubes is small.

Reference

1. Renata, R. S., **et al**.; International Conference Recent Trends on Energy Storage & Hydrogen Energy, April 28-29, 2017, Rajiv Gandhi Proudyogiki Vishwavidyalaya, Bhopal, India (2017).

A.10 Material compatibility study on liquid lead alloys and liquid tin alloys for innovative nuclear reactors

Masatoshi KONDO

1. Introduction [1]

Liquid lead (Pb) and liquid lead–bismuth eutectic alloy (Pb–Bi) are candidate coolants of fast reactors (FRs) owing to their excellent nuclear characteristics and chemical stabilities. Liquid Pb–Bi is also a candidate target material of accelerator-driven systems (ADSs). Liquid lithium–lead alloy (Pb–17Li) is a candidate tritium breeder for fusion reactors owing to its excellent tritium breeding performance. Liquid tin (Sn) and liquid tin lithium alloy (Sn-20Li) are promising coolants of plasma facing component (PFC) of fusion reactors, because of it's very low vapor pressure. However, material compatibility of these liquid metals with structural materials is a critical issue for the development of the innovative nuclear reactors. This paper reviews recent corrosion studies performed by authors. The kinetics of corrosion and corrosion–erosion of various steels in the heavy-liquid- metal coolants are explained. The effectiveness of oxide layers and ceramic coatings as a corrosion barrier in the liquid metals is then discussed. Technology for in-situ monitoring of corrosion barriers is introduced.

2. Test materials

Table 1 shows the materials tested in the corrosion studies. 316 type austenitic steel is one of the candidate structural materials of the innovative reactors. The reduced activation ferritic martensitic (RAFM) steels such as JLF-1 (Fe-9Cr-2W-0.1C) and F82H (Fe-8Cr-2W-0.1C) are candidate structural materials for fusion reactors. Aluminum (Al)-rich steels (Such as Recloy10 and NTK04L) are candidate structural materials of nuclear reactors with heavy liquid metal coolants according to its excellent chemical compatibility. The Al-rich steels form a protective alumina (Al_2O_3) layer and can protect their surface in liquid metals, when the oxygen potential is adequately controlled.

3. Experimental conditions

The material compatibility tests have been performed at various conditions, as presented in Table 1. The material compatibility in flowing Pb-Bi was investigated by means of corrosion tests with a forced-convection loop. The oxygen concentration in flowing Pb–Bi was measured by solid electrolyte sensors [2]. The oxygen concentration was controlled by means of injection of a H_2/H_2O gas mixture or PbO-type mass exchanger.

The corrosion characteristics of RAFM steel JLF-1 in liquid Pb–17Li were investigated by means of corrosion tests with a static pot, a mixing pot and a non-isothermal mixing pot. The static pot was used to investigate the chemical interaction between steel and liquid metals. The mixing pot was used to investigate the influence of flow conditions on corrosion behavior. The non-isothermal mixing pot was equipped with a cold trap cooled by an air cooler. The corrosion characteristics of the RAFM steel under non-isothermal conditions were investigated.

The chemical behaviors of the oxide layers in liquid Pb were studied by means of electrochemical impedance spectroscopy (EIS). Cylindrical specimens were immersed into static Pb as a working electrode. The impedance response of the oxide layers formed on the specimen surface was then obtained by periodically scanning.

Corrosion characteristics of JLF-1 steel and 316 type in liquid Sn were investigated by means of corrosion tests with static pot.

4. Corrosion behaviors of steels in liquid metals

4.1 Corrosion-erosion in flowing Pb alloys [3, 4]

Erosion occurrence on the specimen surface was detected in the corrosion tests under flowing Pb–Bi, when its oxygen potential was controlled at a relatively low condition. Fig. 1 (a) shows the trace of corrosion-erosion occurrence. First, the surface was corroded by dissolution of steel alloying elements and the penetration of Pb–Bi into the steel matrix. The Pb–Bi penetration mainly occurred along the grain boundaries of the steel. The corroded surface was then mechanically eroded by the flowing Pb–Bi. This phenomenon is known as corrosion–erosion. Similar phenomenon was detected in the flowing Pb-17Li as shown in Fig. 1 (b).

4.2 Alloying corrosion in liquid Sn and Sn-20Li alloy

The corrosion of the steels in liquid Sn was caused by the alloying reaction between liquid Sn and Fe of the steel element. The reaction layer of FeSn was formed on the steel surface. In the same time, Fe dissolved into the melt through the layer. The corrosion characteristics of the steels in liquid Sn-20Li were closed to that in liquid Sn. The corrosion was caused by the formation of the alloying layer of FeSn and the dissolution of Fe into the melt.

4.3 Formation of oxide layer in liquid metals [5-7]

Steels formed oxide layers in flowing Pb-Bi on their surface when its oxygen potential was higher than that for formation of Fe-Cr oxide layers. The oxide layers were effective as a corrosion barrier to mitigate dissolution-type corrosion and the penetration of Pb–Bi into the steel matrix. The occurrence of corrosion–erosion was not detected. However, some oxide layers were removed by the flowing Pb–Bi at certain intervals owing to their porous structure. Repetition of their removal and formation induced oxidation corrosion of the steels. Steel with higher Cr content (430 steel) exhibited resistance against oxidation corrosion, attributed to the formation of a Cr-rich compact

oxide layer on its surface. The Al-rich steels (Recloy10 and NTK04L) showed excellent corrosion resistance in flowing Pb–Bi. Al-rich compact oxide layers formed on their surfaces, and the layers exhibited excellent corrosion resistance. The results of recent works indicated that severe alloying corrosion by liquid Sn was also suppressed by the formation of Al-rich protective layers.

4.4 EIS of oxide layers in liquid Pb [8, 9]

In situ monitoring of the oxide layer soundness in a liquid metal is being developed based on electrochemical impedance spectroscopy. In corrosion tests in liquid Pb, impedance of the oxide layer formed on the specimen surface was measured by in-situ electrochemical impedance spectroscopy. Large impedance was detected by the EIS when the oxide layers of Y_2O_3 or ZrO_2 formed on the specimens of Y and Zr. The impedance response was evaluated based on equivalent circuit models and the formation of horizontal cracks in the oxide layer was then detected.

Conclusions

1. Corrosion–erosion was caused by the destruction of the corroded surface of steels in flowing Pb alloys.
2. Dissolution-type corrosion of steels could be suppressed by the formation of oxide layers on their surfaces in flowing Pb–Bi; however, oxidation corrosion was caused by the exfoliation of porous oxide layers.
3. Al-rich steels formed a compact oxide layer, which significantly improved their corrosion resistance in liquid metals.
4. In situ monitoring of the oxide layer soundness in a liquid metal is being developed based on electrochemical impedance spectroscopy.

REFERNCE

[1] A. Alemberti, K. Tucek, T. Obara, M. Kondo, A. Moiseev, C. Simith, Y. Wu, I. S. Hwang, THE GENERATION-IV LEAD FAST REACTOR ACTIVITIES, Innovative designs and technologies of nuclear power of nuclear power, V International Scientific and Technical Conference, Collection of papers, JSC NIKIET, pp. 1935–1946, (2018).

[2] P. M. Adhi, M. Kondo, M. Takahashi, Performance of solid electrolyte oxygen sensor with solid and liquid reference electrode for liquid metal, Sens. Actuators B Chem., 241, pp.1261–69 (2017).

[3] M. Kondo, M. Takahashi, T. Suzuki, K. Ishikawa, K. Hata, S. Qiu, H. Sekimoto, Metallurgical study on erosion and corrosion behaviors of steels exposed to liquid lead-bismuth flow, J. Nucl. Mater., 343, pp. 349–359 (2005).

[4] M. Kondo, Y. Hishinuma, T. Norimatsuc, T. Muroga, Corrosion‐erosion and mass transfer dynamic behaviors of reduced activation ferritic/martensitic steel in a nonisothermal Pb-17Li system, Fus. Eng. Design, 136, B, pp. 1581-1587 (2018).

[5] M. Kondo, M. Takahashi, N. Sawada K. Hata, Corrosion of Steels in Lead–Bismuth Flow. *J. Nucl. Sci. Technol*., 43, 107–16 (2005).

[6] M. Kondo, M. Takahashi, Corrosion resistance of Al- and Si-rich steels in lead bismuth flow. *J. Nucl. Mater*., 356, pp.203-12 (2006).

[7] M. Kondo, M. Tada, Y. Ohtsuka, Y. Hishinuma, T. Muroga, Corrosion resistance of alumina forming steel and ceramic materials in liquid tin, 30th symposium on fusion technology, Book of abstracts, p. 507, (2018).

[8] M. Kondo, N. Suzuki, Y. Nakajima, T. Tanaka, T. Muroga, "Electrochemical impedance spectroscopy on in-situ analysis of oxide layer formation in liquid metal", Fus. Eng. Des., 89, 1201-1208 (2014).

[9] M. Kondo, Experimental study on material compatibility for heavy liquid metal coolants, Innovative designs and technologies of nuclear power of nuclear power, V International Scientific and Technical Conference, Collection of papers, JSC NIKIET, pp. 1935-1946, (2018).

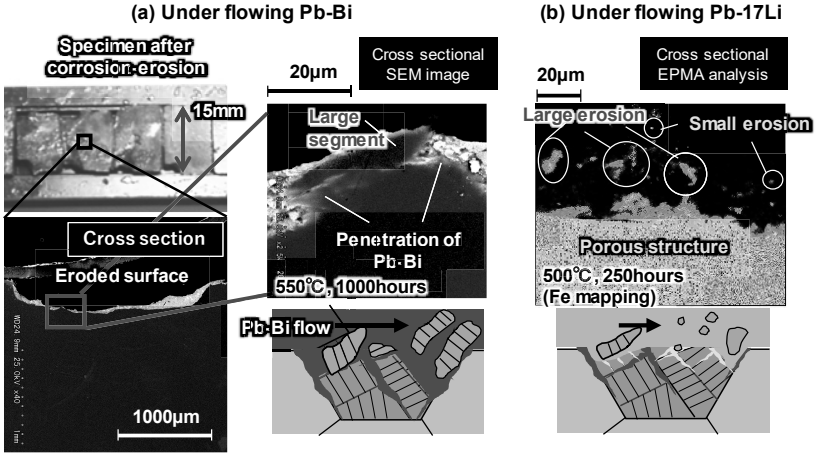

Fig .1 Corrosion–erosion in flowing Pb alloys;
(a) F82H steel in flowing Pb–Bi [3] and (b) JLF-1 steel in flowing Pb–17Li [4]

Table 1 Chemical compositions of test materials (mass %)

	Cr	Mo	W	Si	others	Fe	Application and Remarks
SCM420	1.2	0.2	-	0.2	-	Balanced	Low alloy steel
NF616	9	0.5	1.8	0.3	-	Balanced	
STBA26	9	1	-	0.2	-	Balanced	High temperature boiler
STBA28	8.6	1		0.4	-	Balanced	
HCM12	12.1	1.1	1.0	0.3	-	Balanced	
HCM12A	12	0.3	1.9	0.3	0.9Cu	Balanced	
JLF-1	9	-	2	-	0.1C	Balanced	Reduced activation ferritic martensitic (RAFM) steel for Fusion reactors
F82H	7.7	-	1.94	0.11	0.01Ti-0.01Cu	Balanced	
ODS	11.7	-	1.9	-	0.29Ti-0.23Y_2O_3 - 0.18Y	Balanced	Fast reactors
SUH3	11	-	-	**2**	0.4C	Balanced	
316	18	2-3	-	0.1	10-14Ni	Balanced	
SS405	12	-	-	1	0.1Al	Balanced	
SS430	**18**	-	-	0.75	-	Balanced	
Recloy10	17.7	-	-	1	**0.9Al**	Balanced	Al-rich steels
NTK04L	17.7	0.14	-	0.4	**3.3Al**	Balanced	

Table 2 Experimental conditions

	Test apparatus	Test materials	Temperature [K] /Oxygen content [wt%]	Flow Velocity [m/s]	Time [hr]
Pb–Bi	Forced convection loop	Mainly HCM12A, 316, NTK04L, Recloy10	823 / $2x10^{-9}$	2	1000
			823 /$1.7x10^{-8}$	1	1000
			823 /$1.7x10^{-6}$	1	500
					2000
Pb–17Li	Static pot	JLF-1	773 / -	Static	500
	Mixing pot	JLF-1	773 / -	8.63×10^{-2}	250
				8.63×10^{-2} or 16.3×10^{-2}	500
	Non-isothermal Mixing pot	JLF-1	749 / -	8.63×10^{-2}	500
					1000
Pb	Electrochemical impedance spectroscopy	Fe, Cr, Y, JLF-1	648 - 973 (Mainly 773) /$3x10^{-5}$	Static	1841
		Zr	698–898 /$1.2x10^{-5}$		458
Sn	Static pot	JLF-1, NTK04L Al_2O_3, Cr_2O_3	873	Static	250
			773		500
Sn-20Li	Static pot	JLF-1 and 316	873	Static	250
					750

B. Actinide Management Division

B.1 Research activity of metal ion separation in Takeshita Laboratory from solvent extraction, adsorption to contactor work

Masahiko NAKASE, Yusuke INABA, Miki HARIGAI, Kazuo UTSUMI and Kenji TAKESHITA

1. Introduction

Separation of minor actinide (MA) from lanthanide (Ln) and other fission products (FPs) after the Pu, U recovery can make the burden for vitrification process minimized and space needed for final disposal becomes much smaller than direct disposal. In Takeshita Laboratory, we are studying separation science and technology mainly related to advanced nuclear fuel cycle; separation of MA from Ln, mutual separation of Ln, separation of platinum group elements (PGMs) from simulated high lever liquid waste (sHLLW), separation of Cs and Sr which are heat emitting FPs from nitric acid solution. In this report, some of the general results about separation works obtained in the fiscal year of 2017 are reported.

Selective recognition and separation of trivalent actinides over lanthanides is difficult owing to the chemical similarity of these species. The ionic radii of trivalent f-elements in solution are similar. Particularly in nuclear reprocessing, separating trivalent actinides such as Americium (Am) from lanthanides (Ln) is important to minimize the burden of final disposal. Solvent extraction is a conventional and one of the most reliable methods for metal separation (Figure 1(a)), and is used for continuous large-scale separation. However, solvent extraction also has some demerits; under some conditions, a third phase that is immiscible with the aqueous and organic phases is produced that disrupts stable operation. Furthermore, during highly radioactive processes, such as nuclear fuel reprocessing, organic solvent tends to form secondary radioactive waste and is a source of unwanted radical species. To overcome such demerits, we are also developing gel adsorbent for differentiation of f-elements. The schematics of gel/liquid extraction is illustrated in Figure 1(b). By introducing ligands to thermosensitive gel, the extraction behavior can be controlled by changing the gel conformation through temperature or pH without using an organic phase. Not only extraction/adsorption studies, but also we are recently engaging in structural study to understand the mechanism in detail. Each activity will be briefly explained.

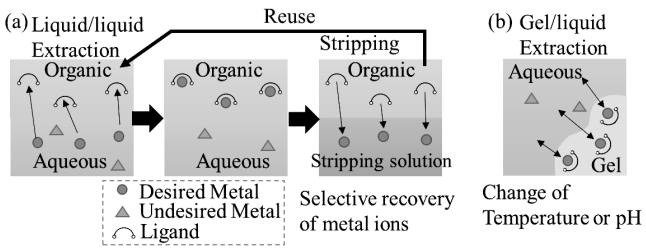

Figure 1 Schematic of (a) liquid/liquid (solvent) extraction and (b) gel/liquid adsorption

2. General experimental results and achievements

2.1. Solvent Extraction

Some of the *N*,*O*-hybrid donor ligands such as 1,10 -phenanthroline-2,9-dicarboxyamide (PTDA) derivatives with different alkyl chains were synthesized and extraction experiments with a series of Ln and MA were implemented. One master course student joined summer internship at Japan Atomic Energy Agency (JAEA) and some roadwork was carried out as a collaborative work. In Takeshita laboratory, PGM separation from nitric acid solutions has been attracting attention in the field of nuclear waste management. HLLW from the PUREX process contain significant amounts of PGMs dissolved in nitric acid of high concentrations. Removal of PGM from HLLW before vitrification process can lead to more stable operation and higher quality of the glass. For this purpose, extractants which can efficiently separate PGM from high nitric acid solutions are studied. The extraction performance and mechanism of PGM extraction by thyodiglycolamide derivatives was carried out as a collaborative work with The National Institute of Advanced Industrial Science and Technology (AIST).

2.2. Contactor work

In the fiscal year of 2017, we performed a unique separation based on extraction kinetics using a liquid-liquid countercurrent centrifugal contactor that induces Taylor-Couette (TC) flow as shown in Figure 2.

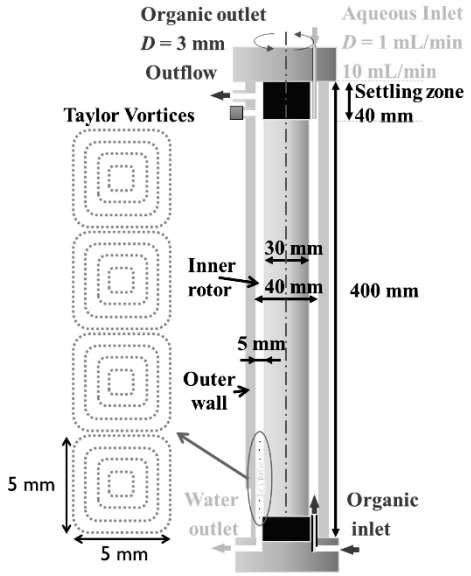

Figure 2 Schematic of liquid-liquid countercurrent centrifugal contactor with Taylor vortices

Conventional extraction systems typically involve a mixer-settler extractor, which relies on an equilibrium being established. In the case of the countercurrent TC flow, extraction with multiple theoretical stages is possible. We have been studying a lot about the relation between oil-water dispersion flow and number of theoretical multiple stages [1–7].

Recently, we found out the extraction kinetics plays quite important rules for separation performance [8]. The specie with faster extraction kinetics can be extracted more significantly then those with slower extraction kinetics in TC contactor which enables unique separation operation. As an example, we demonstrated unique separation based on the difference in extraction kinetics with Fe(III)/Y(III) separation by using di(2-ethylhexyl) phosphoric acid (D2EHPA), for which the extraction kinetics are fast for Fe(III) but slow for Y(III). In Figure 3, distribution ratio and separation factor in equilibrium case (batch extraction) and non-equilibrium case (continuous extraction by TC contactor). The distribution ration, D and separation factor SF are defined as equation (1) and (2), respectively.

$$D = (C_{ini} - C_{after}) / C_{after} \quad (1)$$

$$SF_{A/B} = D_A / D_B \quad (2)$$

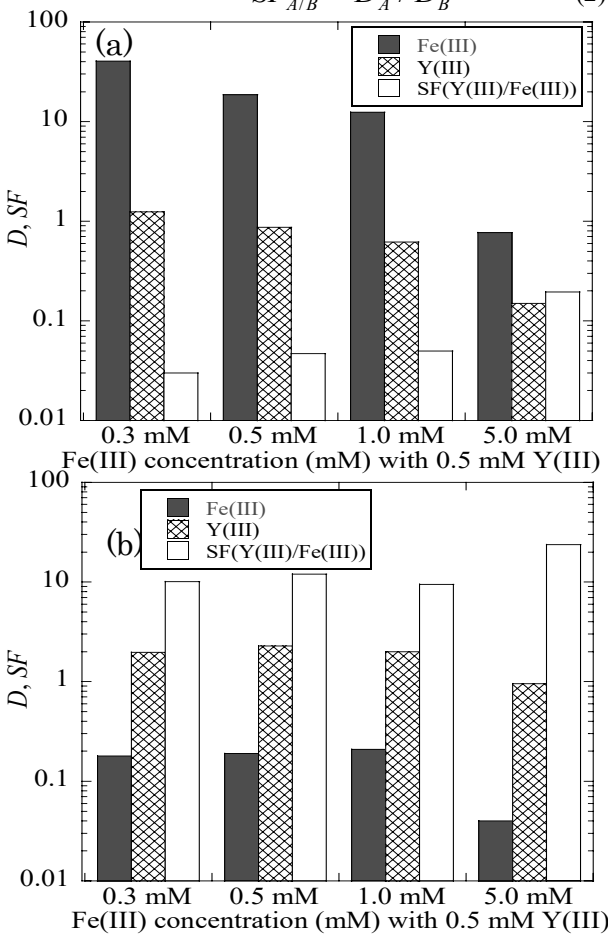

Figure 3 Comparison of *D* and *SF* for Fe(III) and Y(III); (a) batch extraction (equilibrium) and (b) continuous extraction with TC flow (non-equilibrium).

Under equilibrium conditions, Fe(III) is more readily extracted than Y(III), but during countercurrent operation with TC flow, the order of extractability is reversed, with Y(III) being more readily extracted than Fe(III). For the condition where the metal ion concentrations are higher than the ligand concentration, which is a more competitive extraction condition for metal ions, the *D* values for both Y(III) and Fe(III) were decreased, but the selectivity for Y ($SF_{Y/Fe}$) increased. It was clarified that the TC contactor enables unique separation based on the difference in extraction kinetics. We also clarify the effect of flow geometry on extraction performance by both numerically and experimentally [9]. Also, we are developing some complexants and planning to develop special complexants suitable for TC contactor [10]. Next year, we will apply to more extraction cases as well as solid/liuid extraction to TC contactor system.

2.3. Gel/liquid extraction and adsorption

In the fiscal year of 2017, some of the *N*,*O*-hybrid donor ligands such as PDA and PTDA with polymerizable functional groups were synthesized and polymerized with *N*-isopropylacrylamide (NIPA) in aid of N,N'-methylenbisacrylamide (BIS), which produced thermosensitive gels. In Takeshita Laboratory, we have been studying TPEN-NIPA gel for MA/Ln separation (TPEN;*N*,*N*,*N'*,*N'*-Tetrakis(2-pyridylmethyl)ethylene diamine). This year, a new manuscript related to TPEN/NIPA gel was reported [11]. Also, some of the preliminary data about extraction and adsorption behaviors by *N*,*O*-hybrid donor, PTA and PTDA gels were acquired. The difference in complex structure of PDA-Nd and PDA-Eu were also surveyed by EXAFS experiments at SPring-8 [12]. The schematics of ligand and immobilized gel are shown in Figure 4. The radial structural functions obtained by EXAFS experiments for solution case and gel case were compared with Nd(III) and Eu(III). The NIPA-BIS-PDA gel in both cases of Nd(III) and Eu(III) showed shifts in the first peak with increasing temperature, but not for Nd(III) solution, Eu(III) solution and Eu(III)-NIPA in nitric acid. Also, it was suggested that the coordination is different in organic solvent and in gel by comparison of Eu(III)-NIPA -BIS-PDA gel and Eu(III)-PDA in methanol. The results indicated a slight change in complex structure. Understanding the difference in complexation in solution and gel further should allow the selective recognition and separation of specific f-block elements in the future.

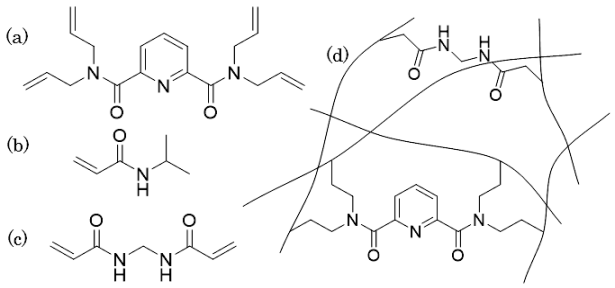

Figure 4. Structures of (a) tetraallyl-PDA, (b) NIPA, (c) BIS, and (d) NIPA-BIS-PDA gel.

Also, U.Th separation experiment was done at Tohoku University for the first time. Contact time, acid concentration and temperature dependencies on adsorption of U and Th were surveyed and the results and insight will be reported in next year. Since we are interested in Th utilization, we will continue and expand this work.

Adsorption separation of PGM elements from HLLW was also studied. In Takeshita Laboratory, we found that an aluminum hexacyanoferrate (AlHCF) adsorbent has high adsorption capability of PGMs and Mo from HLLW. The AlHCF is composed of Al^{3+} and $Fe(CN)_6^{4-}$ and depending on the synthetic condition, slight difference can be observed depending on the amount of defect and composition. Then, the general adsorption behaviors of Pd, Ru, Rh, and Mo was continuously studied. The general performance in radiation condition was reported [13]. The further structural study to elucidate the adsorption mechanism will be implemented by both theoretical and experiments approaches with external collaborators.

2.4. Ionic liquid extraction

Recently, we are also studying about metal ions extraction by ionic liquid. In Takeshita laboratory, we studied about TPEN derivatives, which has high affinity with MA. New TPEN-type *N*,*O*-hybrid donor ionic liquid was synthesized and the extractability and coordination mechanism of cadmium(II), zinc(II) and lanthanide(III) were studied [14, 15]. The appropriate combination and composition of ionic liquid will be surveyed as well as the better lionic-liquid TPEN extractant. A structural study of will also be implemented in next year.

3. Conclusion

Research activity about separation science and technology in Takeshita Lab during the fiscal year of 2017 was reported. We did a lot of extraction and adsorption work and from next year, we are planning to implement more structural studies by single crystal X-ray diffraction and EXAFS experiments to understand the ion recognition and separation mechanism. We will understand the relation between extraction/adsorption and complex structure for development of better extractant and adsorbent.

Acknowledgment

Our activity about separation work in the fiscal year of 2017 was supported by some of the research funds.

1. Study on ion recognition mechanism and separation of f-block element by multidentate *N,O*-hybrid donor ligand immobilized gel, Grant-in-Aid for Young Research, Japan Society for the Promotion of Science (JSPS)
2. Study of effective ion recognition and selective separation of f-series elements based on higher oxidation states of Americium, Grant-in-Aid for JSPS Overseas Research Fellowship, JSPS, 434
3. Absorption study on specific trivalent lanthanide and valence-different uranium ions by ligand-immobilized soft materials, Inter -University Cooperative Research Program of the Institute for Materials Research, Tohoku University), 17K0086
4. Separation of trivalent minoractinide by new ionic liquid containing TPEN structure, Grant-in-Aid for JSPS Research Fellow, JSPS
5. Development of cyano-crosslinked coordination polymer material with high sorption ability of platinum group elements for high quality and volume reduction of vitrified glass for high level radioactive wastes, H29_commissioned research from Nagoya University, Japan Science and Technology Agency (JST)

Reference

1.M.Nakase et al., Scale-up Effect of Oil-water Countercurrent Centrifugal Extractor on Extraction Performance, *Transactions of the American Nuclear Society*, 107, 277-278(2012).
2.M.Nakase et al., Relation between oil-water flow and extraction performance in liquid-liquid counter -current centrifugal extractors with Taylor vortices*J Nucl Sci Technol*, 50, 287–295(2013).
3.M.Nakase et al., Multi-staging for extraction of cesium from nitric acid by a single liquid -liquid countercurrent centrifugal extractor with Taylor vortices *J Nucl Sci Technol*, 50, 1089–1098(2013).
4.M.Nakase et al, Numerical and Experimental Study on Oil-water Dispersion in New Countercurrent Centrifugal Extractor *Procedia Chemistry*, 7, 288–294(2013).
5.M.Nakase et al., High-performance extraction operation using emulsion flow protected by surfactants in a liquid–liquid countercurrent centrifugal extractor *J Nucl Sci Technol*, 50, 723-730(2013).
6.M.Nakase et al., Synergistic extraction of lanthanides in a liquid-liquid countercurrent centrifugal extractor *Separ Sci Technol*, 49, 2478–248(2014).
7.M.Nakase et al., Continuous mutual separation of lanthanides by a liquid-liquid countercurrent centrifugal extractor with Taylor Vortices, *Energy Procedia*, 71, 106–111(2015).
8.M.Nakase et al., Unique separation based on extraction kinetics using a liquid-liquid countercurrent centrifugal contactor with Taylor vortices; *ISEC2017*, pp.187-193(2017).
9.M.Nakase et al., Modified flow geometry for higher extraction performance with a liquid–liquid centrifugal contactor with Taylor vortices; *J Nucl Sci Technol*, 55(8), 829–837(2018).
10.T.S. Grimes et al, Thermodynamic, Spectroscopic

and Computational Studies of f-Element complexation by *N*-hydroxyethyl-diethylene etriamine-*N*,*N*′,*N*″,*N*‴-tetraacetic Acid; *Inorg Chem*, 56(3), 1722–1733(2017).
11. T.Kawamura and K.Takeshita, Extraction and recovery of soft metal ion by porous silica coated by hydrophilic polymer gel with hexavalent nitrogen-donor ligand; *Separ Sci Technol*, 53(9), 1319–1326(2018).
12. M.Nakase et al., Extended X-ray absorption fine structure study on gel/liquid extraction of f-block elements; *Nucl Sci Technol* (accepted)(2018).
13. T.Onishi et al., Adsorption of platinum-group metals and molybdenum onto aluminum ferrocyanide in spent fuel solution; *Energy Procedia*, 131, 151–156(2017).
14. H.Wu, et al., Selective separation of cadmium(II) from zinc(II) by a novel hydrophobic ionic liquid including an *N*,*N*,*N*′,*N*′-tetrakis(2-methyl pyridyl) -1,2-phenylenediamine-4-amido structure: a hard –soft donor combined method; *Dalton Trans*, 47(30), 10063–10070(2018).
15. H.Wu et al., Extraction Behavior of Lanthanides by a Novel Ionic Liquid Including *N*,*N*,*N*′,*N*′ -Tetrakis(2 -pyridylmethyl)-1,3-diamino propane-2 -amido Structure: A Soft–Hard Donor Combined Strategy; *Chem Lett*, 47(6), 732–735(2018).

B.2 Study on remediation of contaminated soil generated by Fukushima Nuclear Power Plant Accident with hydrothermal treatment technique

Yusuke INABA, Xiangbiao YIN, Miki HARIGAI, Kazuo UTSUMI, Masahiko NAKASE and Kenji TAKESHITA

1. Introduction

After the Fukushima Nuclear Power Plant Accident occurred in 2011, we started studying about the remediation technique for recovering the contaminated soil and water. In Takeshita laboratory, separation of Cs from soil by hydrothermal treatment (HTT) has been studied extensively. Last year, the effect of cations into hydrothermal treatment in batch system was reported by publications and a series of talks in domestic and international conferences [1-14]. Implementation of HTT several times to vermiculitized biotite (VB) made almost 100 % desorption of Cs without destroying the structure of soil. To expect rapid ion exchange, effect of the additional cations, such as K^{+}, NH^{4+}, Mg^{2+}, Ca^{2+} and La^{3+} on Cs removal by HTT was tested this year. As a result, addition of cation enhanced the ion exchange rate drastically which resulted in more efficient desorption operation. In HTT situation, property of water changes; solubility product constant becomes enhanced and relative permittivity is changed which result in higher solubility. Also, the ion exchange equilibrium constant and rate constant may also be increased. Previously in Takeshita Laboratory, HTT was carried out with batch system. In batch system, the temperature was increased firstly and kept constant to sustain subcritical condition at 250ºC. After 30 minute, temperature was decreased and when the water temperature became lower than 60ºC, the water was collected and proceeded to the concentration measurement by Atomic Absorption Spectrometry (AAS) or Inductively Coupled Plasma-Atomic Emission Spectrometry (ICP-AES). However, this process requires heat-up and cool-down which are quite significant energy loss. By applying column system, continuous operation without changing temperature. Also, the re-adsorption during the cooling process before retrieving was strongly suggested in batch operations. If the re-adsorption can be minimized, it is expected to make HTT system more efficient and over spec design of the removal process will be neglected. Therefore, HTT in continuous Cs removal system by column apparatus was developed and some preliminary results were obtained. The latest results are now preparing for publication, hence, a brief explanation about HTT with continuous column experiments is reported.

2. Experimental

The experimental setup of column system is illustrated in Figure 1. Cationic aqueous solution is introduced in the column and pass through the packed soil in subcritical condition with rapid ion exchange. Then the subcritical water containing Cs is pushed out while it is hot which can minimize the unwanted re-adsorption. Then concentration of Cs in the retrieved aqueous samples were proceeded to measurement.

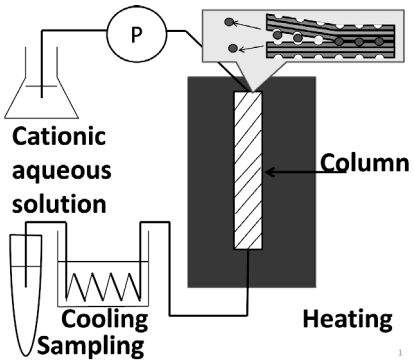

Fig. 1 Column system for continuous removal of Cs from soil by HTT

3. Result

The continuous Cs removal by HTT in column apparatus was successful accomplished. 100% removal of Cs from VB was achieved and the addition of cations were also confirmed. The results in detail will be come up in next year since the results are waiting for publication. From the viewpoint of commercial use, the column systems seem to have more merits than batch system from the viewpoints of desorption ratio and energy consumption. The performance of column operation is highly depending on the flow rate, residence time, solid/liquid ration and some other parameters. To seek the suitable design and operational condition of the column apparatus, more fundamental knowledge about desorption, re-adsorption and kinetics is needed as well as the operational results with different condition.

4. Conclusion and Future Work

The continuous Cs removal apparatus by HTT was developed and the preliminary tests were done. To upgrade this continuous system, we will have to understand in detail about adsorption/desorption mechanism in detail. To do so, we will not only use column system, but also use batch system to derive adsorption equilibrium constants at higher temperature and kinetic data. Reaction analysis is also implemented. We will also expand HTT technique to many other situations such as the decontamination of Cs from burned residue such as ash and mud in the ponds in Fukushima area.

Reference

1. X.Yin et al.; Effect of Temperature on K+ and Mg2+ Extracted Desorption of Cs from Vermiculitized Biotite, Chem Lett, Vol.46, No.9, pp.1350-1352(2017).
2. X.Yin et al.; Effects of NH^{4+}, K^{+}, and Mg^{2+} and Ca^{2+} on the Cesium Adsorption/Desorption in Binding Sites of Vermiculitized Biotite ; Environmental Science & Technology, Vol.51, pp.13886-13894(2017) .
3. R.Sannomiya et al.; Recovery of Cesium from Contaminated Soil by Hydrothermal Treatment with Metal Ions, RCWM2017, Fukushima, Japan, June 20, (2017).
4. L.Zhang et al.; Removal of Cs from Clay Minerals by Hydrothermal Treatment Using Organic Acids; Fukushima, Japan, June 20, (2017).
5. X.Yin et al.; Effective and Efficient Removal of Cs from Clay Minerals for Volume Reduction of Radioactive Soli in Fukushima, ASNFC 2017, Lanzhou, China, July 17-21, (2017).
6. K.Takeshita et al.; Rapid ion exchange of Cs from classified solid by metal ion containg subcritical water and volume reduction of vitrified glasses (1) oveall research plan and overview; 6th Annual Conference on SRRCE, Fukushima, Japan, July 19-20, S8-1 (2017).
7. K.Takeshita et al.; Rapid ion exchange of Cs from classified solid by metal ion containing subcritical water and volume reduction of vitrified glasses (2)Cs removal experiments by metal containing subcritical water; 6th Annual Conference on SRRCE, Fukushima, Japan, July 19-20, S8-2. (2017).
8. Y.Inaba et al.; Rapid ion exchange of Cs from classified solid by metal ion containing subcritical water and volume reduction of vitrified glasses (3) Cs vitrification into glass by from subctirical water; 6th Annual Conference on SRRCE, Fukushima, Japan, July 19-20, S8-3 (2017).
9. H.Takahashi et al.; Rapid ion exchange of Cs from classified solid by metal ion containg subcritical water and volume reduction of vitrified glasses (4) Cs vitrification into borosillicate glass containing solid acid; 6th Annual Conference on SRRCE, Fukushima Japan, July 19-20, S8-4 (2017).
10. N.Horiuchi et al.; Rapid ion exchange of Cs from classified solid by metal ion containg subcritical water and volume reduction of vitrified glasses (5) system assessment and future perspective; 6th Annual Conference on SRRCE, Fukushima, Japan, July 19-20, S8-5, (2017).
11. K.Takeshita et al.; Recovery of Cs from Contaminated Soil by Subcritical Water Containing Metal Ions and Its Solidification using Inorganic Materials for Volume Reductionn(1) oveall research plan and overview; The Japan Atomic Energy Society Fall 2017, Sapporo, Japan, September 13-15, 3I01, (2017).
12. N.Horiuchi et al.; Recovery of Cs from Contaminated Soil by Subcritical Water Containing Metal Ions and Its Solidification using Inorganic Materials for Volume Reduction(2) Cs removal from contaminated soil by rapid ion exchange in subcritical water condition; The Japan Atomic Energy Society Fall 2017, Sapporo, Japan, September 13-15, 3I02 (2017).
13. X.Yin et al.; Recovery of Cs from Contaminated Soil by Subcritical Water Containing Metal Ions and Its Solidification using Inorganic Materials for Volume Reduction (3)Mechanism of Enhanced Cs Desorption from Clay Minerals under Hydrothermal Condition; The Japan Atomic Energy Society Fall 2017, Sapporo, Japan, September 13-15, 3I03 (2017).
14. H.Takahashi et al.; Recovery of Cs from Contaminated Soil by Subcritical Water Containing Metal Ions and Its Solidification using Inorganic Materials for Volume Reduction (4) Cs selective recovery by subcritical water and Cs vitrification into glass; *The Japan Atomic Energy Society Fall 2017*, Sapporo, Japan, September 13-15, 3I04 (2017).

B.3 Development of methodology for evaluation of nuclear fuel cycle from the viewpoint of waste management and disposal

Tomohiro OKAMURA, Masahiko NAKASE, Kota KAWAI, Eriko MINARI, Hidekazu ASANO and Kenji TAKESHITA

1. Introduction

Due to the Fukushima nuclear power plant accident, our energy policy, especially the future perspective of nuclear fuel cycle (NFC), became unclear. Therefore, NFC have to be rethought from various aspects such as technology, safety, cost, waste management and so on. The authors started research project since 2014 and studied to evaluate the entire NFC to reduce the impact of high-level radioactive waste management including disposal and promotion of the use of plutonium. We recently focus on reducing the geological disposal area as well as reducing environmental impact.

To reduce the geological disposal area, characteristics of vitrified waste, especially a number of vitrified waste produced from the upper process and its thermal property are important. Also, these two factors are greatly affected by the composition of radionuclide contained in the vitrified waste. On the other hand, the nuclide composition depends on NFC conditions; ① Nuclear fuel composition, ② Fuel burn-up, ③ Cooling period of spent fuels (SFs), ④ Partitioning technologies in reprocessing process, and ⑤ Waste loading of vitrified waste. Therefore, it is necessary to comprehensively and quantitatively evaluate how these conditions affect the thermal characteristics and the number of vitrified waste. In this report, current situation of methodology development is briefly introduced. Our final goal is to find out more sophisticated NFCs from the viewpoint of waste management and disposal.

2.3. CAERA index

To evaluate the NFC jointly from front-end to back-end processes from the aspect of geological disposal area reduction, CAERA (Comprehensive Analysis of Effects on Reduction of disposal Area) index was introduced as shown in (1) [1].

$$\mathrm{kg/m^2} = \frac{\text{Waste loading [wt\%/glass unit]} - \mathrm{Na_2O}\ \text{[wt\%/glass unit]}}{\text{Occupied area [m}^2\text{/glass unit]}} \times \text{Weight of vitrified waste form [kg]} \times \frac{1}{100} \quad (1)$$

By using this index, quantitative analysis of the relationship between effectiveness of occupied area reduction and conditions of NFC is proven to be possible. The CAERA indicates the weight of disposable HLW per unit occupied area. Therefore, higher CAERA indicates more amount of waste can be disposed in unit area, in other words, the geological disposal area can be reduced. In the reference case, the value of CAERA was calculated as 0.973 kg/m^2 under the 44.4 m^2 of occupied area per waste package and 20.8 wt% of waste loading per glass unit. The CAREA index is highly depending on the conditions of SNF such as ①～⑤. Therefore, by verifying individual conditions and evaluating disposal area with CAERA index, we can clarify the influence of each condition of NFC on the disposal area.

3. Result and Discussion

Scenario study by CAERA index successfully revealed that the separation condition greatly affected on the disposal area reduction. Since manuscripts related to this research are under preparation and under review process, only the brief results are compiled as following;

1. CAERA was developed and scenario study with various NFC situation was carried out. By comparing CAERA index, NFC conditions which can contribute to reduce the disposal area was sought.

In the case of UO_2 fuel cycle;

2. Approximately 40% of waste occupied area can be reduced by the separation of Cs, Sr, Mo and PGM from HLLW without removal of MA. This is because the separation of Cs, Sr can reduce the heat generation and Mo, PGM separation can increase waste loading in vitrified waste.
3. Approximately 40% of waste occupied area can be reduced by MA separation in consideration of prolonged cooling period of SFs. In such case, waste loading of vitrified waste can also be increased due to the reduced heat emission from MA.

4. Future Work

The insights obtained in this year are now compiling into publication. We have also done series presentation at AESJ conferences, we had 6 presentations in 2018 spring and will make 5 more presentations in 2019 spring. In addition, we will implement some experimental approach such as fabrication of simulated glass. We will survey the stability and validity of the glasses when the chemical component and waste loading are varied depending on our scenario. Also, we will evaluate the merit of simplified separation process and consequent reduction effect of waste occupied area. The methodology and index will also be updated in a framework of collaboration with external research institutes, JAEA, RWMC and IAEA.

Reference

[1] K. Kawai. Establishment of back-end systems for load reduction of geological repository. 2018, Ph.D. thesis.

Acknowledgment

This research was supported by Radioactive Waste Management Funding and Research Center

B.4 Direct Extraction of Actinides from Acidic Solution using the Hydrophobic Interactions of poly (*N*-isopropylacrylamide) with Diamide-typed Ligands

Kaname SAGA and Takehiko TSUKAHARA

In order to establish partitioning methods for high level liquid wastes, various separation techniques of minor actinide (MA) and lanthanide (Ln) ions, which are based on liquid-liquid solvent extraction process and chromatographic process using resins impregnated with specific extractants, have been investigated. However, their processes require repeated time-consuming chemical operations, and produce large amount of secondary wastes. herefore, rapid and efficient separation method is expected to be established for overcoming such disadvantages. On the other hands, a thermoresponsive poly(N-isopropylacrylamide) [poly(NIPAAm)] has been recognized as unique materials which exhibit hydrophilicity-hydrophobicity phase transition at the lower critical solution temperature (LCST = 32 °C). We have recently found that the poly(NIPAAm) can be suddenly converted to the gel in acidic solutions at the temperatures above LCST due to the hydrophobic interactions of isopropyl groups in poly(NIPAAm). When an acidic solution containing poly(NIPAAm), chelating agents with hydrophobic groups, and target metal ions is just heated from below to above the LCST, the metal complexes with chelating agents can be captured onto poly(NIPAAm) and recovered as poly(NIPAAm) gel because of their hydrophobic aggregation (see Figure 1). Therefore, in this study, we aimed to realize direct separation of MA and Ln species in HNO_3 solutions by using the phase transition-based gelification method without any organic solvents and eluents. For MA ions separation, we used 2-ethylhexyl diamide amine(ADAAM(EH)) having five 2-ethylhexyl hydrophobic alkyl chain (see Figure 2).

We synthesized poly(NIPAAm) by means of free radical polymerization, and the structure and the number-average molecular weight were measured by NMR and GPC, respectively. ADAAM(EH) was obtained from Chemicrea, Inc.(Tokyo, Japan). Radioactive isotopes (Am(III), Cm(III), and Eu(III)) were purchased from Japan Radioisotope Association (Tokyo, Japan). The separation test for Am(III), Cm(III), and Eu(III) was performed as the following steps. The initial HNO_3 solution was prepared by dissolving Am(III), Cm(III), and Eu(III) with the concentrations of sub-ppb level. Moreover, the specified quantity of NH_4NO_3 was added into the solution. Poly(NIPAAm) and ADAAM(EH) were injected in the HNO_3 solution and mixed by a stirrer at 10 °C (below the LCST). After mixing, the solution was heated until at 40 °C (above the LCST). When the solution mixing at 40 °C was maintained for about 1 hour, the gelification of poly(NIPAAm) capturing metal-ADAAM(EH) complexes was generated. The remaining solution was picked up using a membrane filter, and measured the concentrations of each radioactive isotope by an α-silicon semiconductor detector (GCD-20180X SEIKO EG&G) and a γ-spectrometer (BSIGCD-20180X). The γ-ray measurement results showed that the separation efficiencies of Am(III) and Eu(III) in 0.1 M HNO_3 and 3M NH_4NO_3 solution could be determined as 63.0% and 10.0%, respectively. From the α-ray measurements, we found that Am(III) and Eu(III) were separated 64.1% and 29.2% in the same solution conditions, respectively. The extraction percentages were found to be consistent with bulk solvent extraction using organic solvents.

These results suggest that the phase transition-based gelification method makes it possible to separate target metal ions in aqueous solutions by controlling just temperatures.

References

1. K.C. Park, N. Idota, and T. Tsukahara, *Reactive & Functional Polymers*, **2014**, 79, 36-46.
2. H. Tateno, K.C. Park, and T. Tsukahara, *Chem. Lett*. **2018**, 47, 318–321.

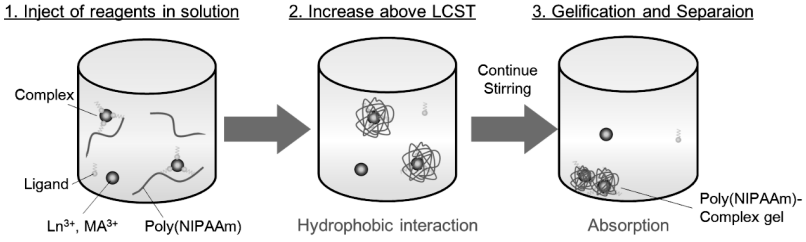

Figure 1. Conceptual illustration of the phase transition-based gelification method.

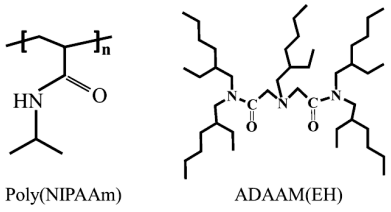

Figure 2. Molecular structure of (left) poly(NIPAAm) and (right) ADAAM (EH).

B.5 Microchemical Analysis of Gamma-Emitting Actinides in Radioactive Wastes Generated From Nuclear Accidents

Brandt AILEEN, Kazuki MATSUSHITA, and Takehiko TSUKAHARA

By the TEPCO Fukushima Dai-ichi Nuclear Power Plants accident, large amounts of radioactive wastes including contaminated water, soil, structural materials, and nuclear fuel debris have been generated. To realize safe treatment and disposal of these wastes, analysis of radioactive metal species in the wastes should be essential. However, conventional bulk-scale chemical analysis requires time-consuming operations, and produces large amounts of secondary wastes and radiation toxicities. On the other hand, microfluidic devices are expected to resolve the problems associated with bulk-scale analysis. We have previously performed efficient redox reactions and extraction of uranium using microchannels [1,2]. There was no need to consider the impact of radiation doses to microfluidic devices, because uranium (U-238) is typically alpha-emitting nuclide. However, the applicability of the microdevices to gamma-emitting nuclides should be investigated, because of its high-dose radiation. Therefore, in this study, we carry out micro solvent extraction of important gamma-emitting actinides (Ac) and lanthanides (Ln), which are generated as fission products, and evaluate the extraction performances.

A quartz microchip with a Y-shaped microchannel was fabricated by means of photolithography and HF wet-etching techniques. After a toluene solution containing 1.0 wt% octadecyltrimethoxysilane (ODS) was introduced into the microchannel and dried the solution, a portion of the ODS-modified microchannel VUV (vacuum UV) light was irradiated by under N_2 atmosphere. The ODS on the irradiated area was decomposed and converted to the hydrophilic surface. In the Y-shaped hydrophobic-hydrophilic patterning microchannel, a 1.0 M nitric acid solution containing Am-241, Cm-243, and Eu-152 and an dodecane solution containing N,N,N',N'-tetraoctyl-3-oxapentane-1,5-diamide (TODGA; 0.1, 0.5, 1.0 M) were introduced simultaneously, and aqueous/organic plug flows were formed (Figure 1). The aqueous/organic phases were recovered at the channel outlets, and measured using Ge semiconductor detector.

The gamma-ray spectra of solutions before and after extraction could be obtained (Figure 2). Each main peak of Am-241, Cm-243, and Eu-152 was assigned at the energy of 59.5kev, 278.5kev, and 345kev, respectively. The concentrations were determined from the peak areas, and each distribution coefficient (*D*) was calculated. The obtained *D* values for Am-241, Cm-243, and Eu-152 were shown in Figure 4. We found that the *D* values for actinides (Am-241 and Cm-243) increased with increasing TODGA concentrations, and arrived at about 100 at 1.0 M TODGA. The *D* values for Cm-243 were higher than those for Am-241 in the whole concentration range, while lanthanide (Eu-152) at 0.1 M TODGA had the highest D value (about 20). Namely, the TODGA concentration dependence of *D* values showed the opposite tendency between Ac and Ln. The extraction time (about 3 sec) for this micro-scale extraction was quite faster than that of a few hours for bulk-scale one.

The results suggest that Ac(III) having the high affinity to nitrogen donor of TODGA could be effectively extracted compared with Ln(III) even in the microchannel.

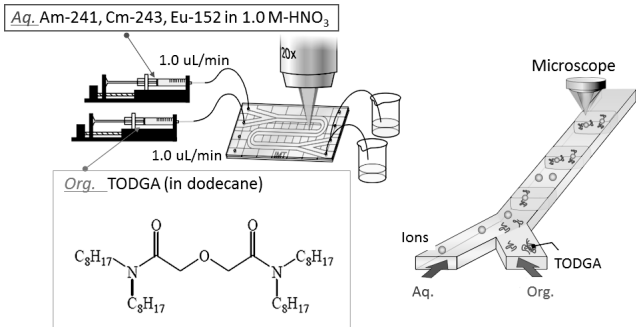

Figure 1. Schematic illustration of a micro plug flow-based extraction system using an aqueous phase containing Am-241, Cm-243, and Eu-152 and an organic phase containing TODGA.

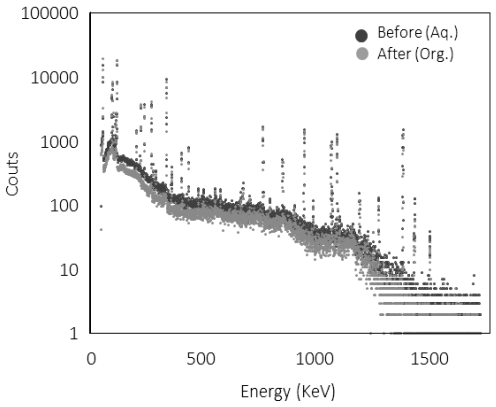

Figure 3. Typical gamma-ray spectra of Am-241, Cm-243, and Eu-152 in solutions before and after micro extraction. The main peaks appeared at 59.5kev, 278.5kev, and 345kev, respectively. Other peaks which appeared at the high energy regions corresponded to the decay energy produced from Eu-152.

References

1. T. Tsukahara, H. Hotokezaka, M. Harada, Y. Kikutani, M.Tokeshi, and Y. Ikeda, Microfluid Nanofluid., **2013**, 14, 989.
2. T. Tsukahara, and Y. Ikeda, *Prog. Nucl. Energy*, **2011**, 53, 935.

C. Global Nuclear Security Division

C.1 Accumulation of metal cations by sorbents

Toshihiko OHNUKI, Yuria SEKINE, Qianqian YU

Since the accident at the Fukushima-Daiichi nuclear power plant (FNPP) in 2011, there has been an immense need for novel ways to remove radioisotopes from contaminated water. A substantial number of radioisotopes such as strontium-90 (^{90}Sr), cesium-134 (^{134}Cs), and cesium-137 (^{137}Cs) were released from FNPP into the environment, thereby contaminating the seawater, groundwater, and land surface. The radioactivity of the Sr and Cs released from FNPP onto the land surface was estimated to be around 8.56 PBq for ^{90}Sr and 288 PBq for ^{134}Cs and ^{137}Cs, whereas that of the strontium and cesium directly released into the ocean was estimated to be 52 GBq for ^{90}Sr and 3.5 PBq for ^{134}Cs and ^{137}Cs. Thus, studying the migration of ^{90}Sr, ^{134}Cs and ^{137}Cs in solution and determining suitable decontamination procedures are important issues to be researched. Thus, we have conducted the sorption of Sr and Cs by Ca-deficient hydroxyapatite[1] and Manganese dioxides of birnessite and todorokite[2].

The physical–chemical characterization of Ca-deficient hydroxyapatite (DEF-HAP, Ca/P = 1.38) is as follows: average length of ~43 nm, and average width of 17 nm, zeta potential of -20.1 mV at pH 7. Transmission electron microscopy (TEM) images of the materials show that DEF-HAP forms rod-like crystals. For comparison, we used stoichiometric hydroxyapatite (ST-HAP, Ca/P = 1.68).

The effect of competing cations on the Sr^{2+} sorption capacity of DEF-HAP and ST-HAP was evaluated using an aqueous solution containing HAPs (35 mg), Sr^{2+} (0.05 mmol/L), and either Mg^{2+} or Ca^{2+} (0–50 mmol/L) in MilliQ water (7 mL). The solution was stirred for 5 h at pH 7. The supernatant was obtained by centrifugation and filtration, and the concentration of Sr^{2+} was determined using inductively coupled plasma-mass spectrometry (ICP-MS). Notably, the equilibrium time for the sorption was confirmed to be 1 h; hence, five hours were sufficient to evaluate the sorption properties of the HAP materials. Based on the concentration of Sr^{2+} in the supernatant, the sorption efficiency (A_{eff}) of DEF-HAP and ST-HAP was calculated as follows:

$$A_{eff}(\%) = 100 \times (1-C/C_0)$$

where C_0 and C are the initial and final (after 5 h) concentrations (mg/L) of Sr^{2+}, respectively.

The Ca-deficient hydroxyapatite maintained a high Sr^{2+} sorption ratio of above 80% in the presence of Mg^{2+} and Ca^{2+} at the concentrations between 0.1 and 1.0 mmol/L, whereas the stoichiometric hydroxyapatite showed a lower ratio even in the presence of small amounts of Mg^{2+} and Ca^{2+} (72% for Mg2+ and 51% for Ca2+ at 0.1 mmol/L). For solutions with various Sr^{2+} concentrations between 0.01 and 10 mmol/L, Ca-deficient hydroxyapatite exhibited a higher Sr^{2+} sorption ratio than stoichiometric hydroxyapatite. The bonding states of Sr^{2+} on the Ca-deficient hydroxyapatite were evaluated by extended X-ray absorption fine structure measurements. The results indicated that there are specific sorption sites in Ca-deficient hydroxyapatite where Sr^{2+} is stably and preferentially immobilized.

Birnessite and todorokite were prepared according to Feng et al.[3]. The cationic exchange capacity (CEC) is 2.50 $\times 10^{-3}$ mol/g for todorokite and 4.57 $\times 10^{-3}$ mol/g for birnessite. The XRD patterns for the birnessite precursor, the intermediate products, and the final products are shown in Fig. 1a. The XRD pattern of the birnessite precursor showed characteristic reflection peaks at 7.16 Å, 3.58 Å, and 2.49 Å. The peaks at 7.16 Å (001) and 3.58 Å (002) reflect the basal diffraction between the MnO_6 layers. After a complete exchange with the $MgCl_2$ solution had occurred, the interlayer spacing expanded from ca. 7.16 Å to ca. 9.71 Å to form Mg-buserite as indicated by the appearance of the diffraction peaks at 9.71 Å, 4.87 Å, and 3.24 Å. The basal diffraction peaks were more intense for the Mg-buserite than for the birnessite precursor, implying that the ion exchange process enhances the crystallinity and long-range ordering of the layers, which is in agreement with previous reports[4].

The XRD patterns for the Cs-exchanged birnessite and Cs-exchanged todorokite are shown in Fig. 1b. As the interlayer cations were exchanged by Cs, the basal diffraction peaks were left-shifted from 7.16 Å, 3.58 Å to 7.47 Å, 3.71 Å, respectively. Moreover, the ratio of the 001:002 peak intensities decreased from 4.1 to 1.1 (Fig. 1a, b). This result was attributed to the exchange of heavy X-ray scatters into the birnessite interlayer, which is consistent with previous reports[5]. The XRD pattern for todorokite changed slightly after being exchanged with Cs. A peak shift was not observed and the ratio of the 001:002 peak intensities slightly increased from 1.2 to 1.9.

The adsorption isotherms for birnessite and todorokite

exhibit a non-linear feature (Fig. 2a). This non-linear feature seems to be consistent with the existence of two different adsorption sites. A linear region with a slope of 1 was observed at low concentration and the slope decreased when the Cs adsorbed amount was> 1×10^{-4} mol/g for birnessite and > 5×10^{-6} mol/g for todorokite. The changes in the slope indicate a saturation of the adsorption sites (T_1 site). Therefore, the density of the T_1 sites could be estimated directly from the point where the slope started to decrease (marked by an arrow in Fig. 2a). After the saturation of the T1 sites, another region of linear adsorption appeared until the Cs adsorbed amount approached the CEC value (4.57×10^{-3} for birnessite, and 2.50×10^{-3} mol/g for todorokite), although the second linear segment is not as clear for birnessite as for todorokite. Therefore, the remainder of the CEC was assigned to the T2 site.

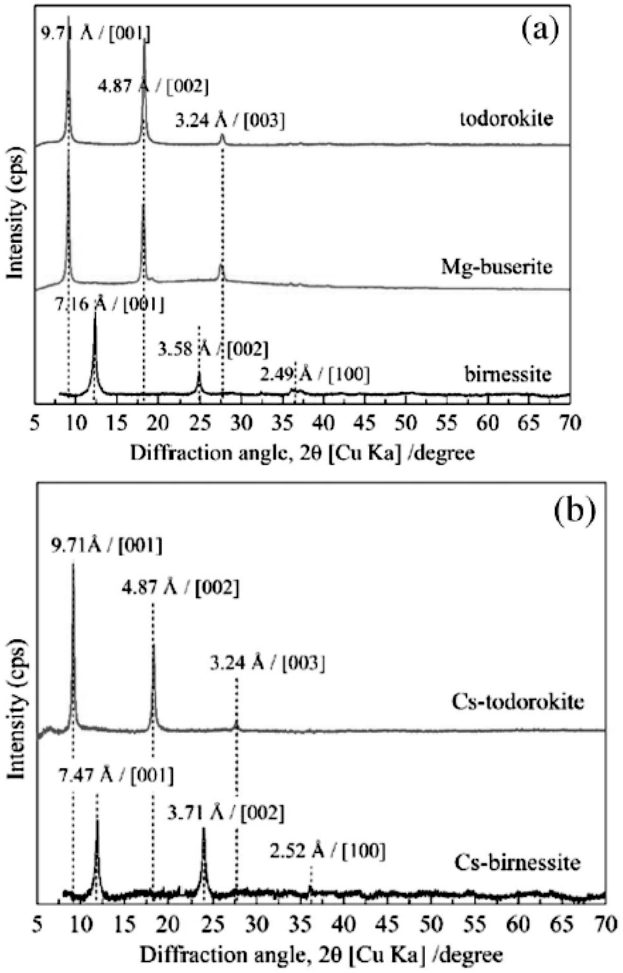

Fig. 1. X-ray diffraction patterns for birnessite and todorokite (a) before and (b) after exchange with Cs.

Although birnessite showed a higher Cs adsorption capacity than todorokite, most of the Cs adsorbed onto birnessite was desorbed by ion exchange. Two types of adsorption sites were observed for todorokite. Despite low density, the selectivity coefficient was much higher for the T1 site ($Log_{Na}\ ^{Cs}K_{sel}$ = 4.2) than for the T_2 site ($Log_{Na}\ ^{Cs}K_{sel}$=−0.6). Sequential extraction was carried out at Cs concentrations of 1×10^{-9} mol/L and 1×10^{-3} mol/L. At lower concentrations, approximately 34% of the adsorbed Cs was residual in the todorokite after the sequential extraction; this value was much higher than the results for the Cs-adsorbed birnessite as well as the Cs-adsorbed todorokite at higher concentrations. The present results indicate that the structural factors of Mn oxides significantly affect the retention capacity of radioactive Cs. Aside from phyllosilicate minerals, todorokite also contributes to the fixation of radioactive Cs in soils.

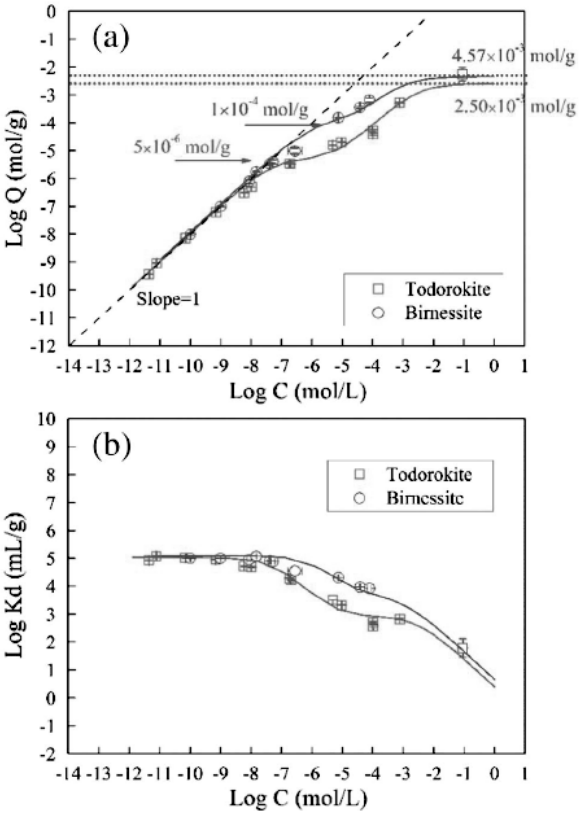

Fig. 3. Cs sorption isotherms for birnessite and todorokite at pH 7.0 ± 0.2 with an ionic strength of I= 1 mmol/L. (a) Data are expressed as Log C vs. Log Q and (b) data are expressed as Log C vs. Log K_d. The lines represent the fitting result with the parameters shown in Table 1. The CEC value for the two samples is marked with a dotted line.

Reference

1. Y. Sekine, et al., *Scientific Reports*, 7, 2064S(2017).
2. Q. Yu, et al., *Chemical Geology*, 470, 141(2017).
3. T. Ohnuki, et al., Scientific Reports, 6:29866 (2016).
4. Atkins, A.L., et al., 2014. *Geochim. Cosmochim. Acta* 144, 109(2014).
5. Lopano, C.L., et al., *Am. Mineral*. 94, 816(200).

C.2 Impacts of ^{240}Pu self-shielding effect and uncertainties of σ(n,γ) at resonance energy on the reactivity controllability in HTGR inert matrix fuel

Takeshi AOKIA, Hiroshi SAGARA and Chi Young HAN

1. Introduction

In the study on deep-burning, utilization of inert matrix fuel (IMF) which is TRU oxide diluted with neutronically inert matrix has been proposed for low initial excess reactivity and higher fuel burnup by reducing self-shielding effect of ^{240}Pu. Especially, a significant resonance capture cross section (σ(n,γ)) at 1.056 eV of ^{240}Pu contributes to the self-shielding effect was discussed.

2. Methodology

The core model used is the Clean Burn reactor, a prismatic block type HTGR developed by JAEA based on GTHTR300. **Fig.1(a)** shows the calculation model based on a two-dimensional infinite body, which is created from the fuel block to simulate equivalent incineration features. Each fuel compact is composed of a graphite matrix and many tristructural isotropic (TRISO) fuel particles randomly dispersed in the graphite matrix.

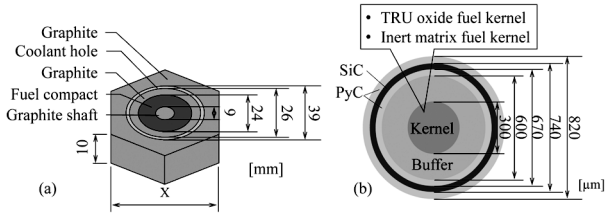

Fig. 1. Geometry of calculation models: (a) two dimensional infinite body and (b) cross section of the TRISO fuel particle

3. Summary of Results

The effect of the dilution of the fuel kernel on incineration features was studied, maintaining the fuel compact pitch of 6.1 cm. **Figure 2** shows the variations of k_∞ with burnup for five different compositions of IMF: TRUOx:YSZ = 100:0; 90:10; 77:23; 60:40; and 49:51 wt.%. Higher dilution rates resulted in lower initial excess reactivity, smaller burnup reactivity swing, and higher burnup indicating that this mitigation of the self-shielding effect of ^{240}Pu increased the neutron capture reaction rate of ^{240}Pu and the ^{241}Pu production. The excess reactivity will be managed by negative reactivity insertion with control rod. Less initial excess reactivity and burnup reactivity swing can be easily and efficiently controlled with the control rods. This study showed that the IMF design with TRUOx:YSZ = 49:51 wt.% could achieve better reactivity controllability and higher burnup.

Figure 3 shows the variation in the relative neutron capture reaction rates of ^{240}Pu for different depths to the peak at surface of kernel in (a) the TRUOx kernel and (b) the optimized IMF kernel and fuel block, in which TRUOx:YSZ = 49:51 wt.% and the pitch is 5.1 cm. The sharp decrease in the macroscopic capture reaction rate at resonance regions in the inner layer of the IMF kernel caused by the spatial self-shielding effect; remarkably, this decrease was recovered, especially in the vicinity of the resonance. Therefore, the mitigation of the self-shielding

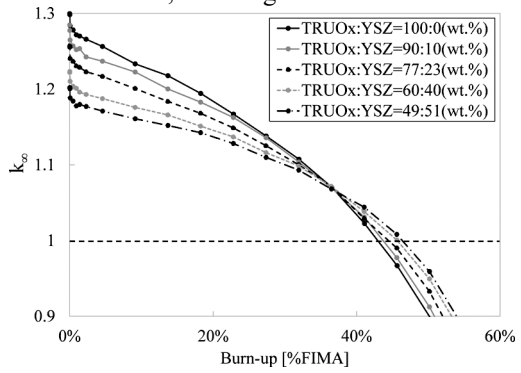

Fig. 2. Variation in k_∞ relative to burnup for IMF kernels with different compositions

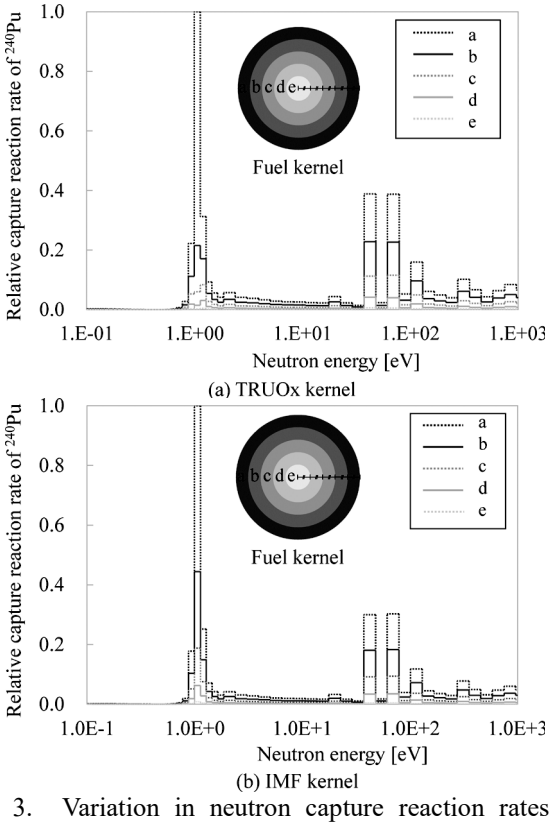

Fig. 3. Variation in neutron capture reaction rates for different depths in (a) TRUOx and (b) IMF kernels

Reference

1. Takeshi Aoki, Hiroshi Sagara and Chi Young Han; Progress in Nuclear Science and Technology, Vol. 5 (2017).

C.3 Applicability study of the photofission based nuclear material isotopic composition measurement method on the Thorium-Uranium system

Rei KIMURA, Hiroshi SAGARA, Satoshi CHIBA

1. Introduction

A principle of new nondestructive assay (NDA) technique based on the photofission reaction ratio (PFRR) has been developed, which is aimed at measuring the isotopic composition of nuclear fuel materials without relying on their self-generated neutron information. The feasibility of the PFRR method was validated in the ^{235}U-^{238}U system previously. However, applicability of the PFRR method in the other material is not yet validated. In this study, applicability of PFRR method to the ^{232}Th-^{233}U system was confirmed, PFRR method showed good reproducibility of predicted value of ^{232}Th and ^{233}U isotopic composition.

2. Summary of Results

The Fig. 1 shows the cross-section of photo fission reaction described as (γ, n), and photo-2n reaction described as (γ, n). From the figure, it can be predicted that fission reaction count rate ratio of 11MeV/6MeV case is larger than 10MeV/8MeV case due to large photofission cross section difference as shown in Fig. 1.

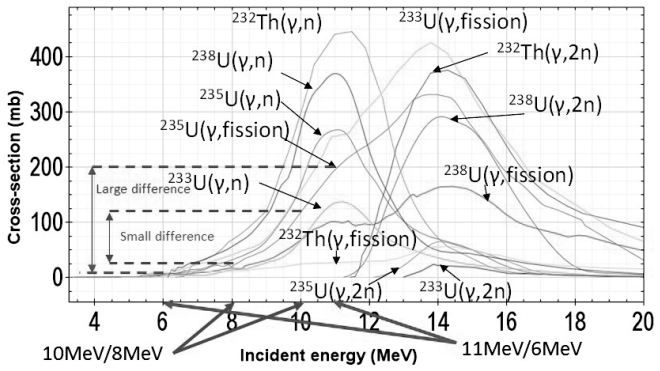

Fig. 1 Photonuclear cross section of each actinide nuclide

The Fig. 2 shows the fission reaction count rate ratio in (a) and predicted value of the ^{233}U enrichment in ^{232}Th-^{233}U system in (b), by 11MeV/6MeV photon beams with Gaussian-shaped energy distribution incident to 1mm thickness target. This figure shows good reproducibility of predicted value of the ^{233}U enrichment as well as ^{235}U-^{238}U system. For this reason, the PFRR method was shown that it has applicability to ^{232}Th-^{233}U system.

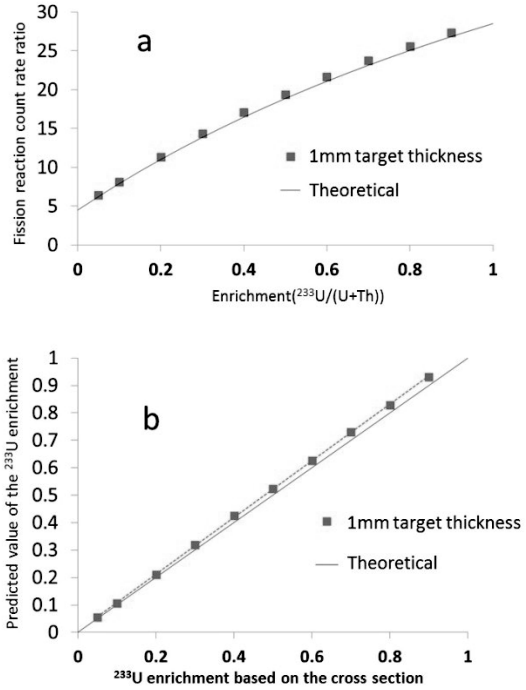

Fig. 2 (a) Fission reaction count rate ratio; (b) Predicted value of the ^{233}U enrichment, in case of the 11MeV/6MeV incident photons that has Gaussian-shaped energy distribution

Acknowledgement

We would like to express great gratitude to Dr. K. Kosako for providing the ACE format photonuclear cross section library of the ^{232}Th and ^{233}U.

Reference

1.Rei Kimura, Hiroshi Sagara, Satoshi Chiba, “Applicability study of the photofission based nuclear material isotopic composition measurement method on the Thorium-Uranium system,” Energy Procedia, Volume 131, December 2017, Pages 264-273.

C.4 User Interface of Atmospheric Dispersion Simulation for Nuclear Emergency Countermeasures, Energy Procedia, Volume 131, December 2017, Pages 279-284

Hamza El-ASAAD, Hiroshi SAGARA, Haruyasu NAGAI

1. Introduction

In the event of a nuclear emergency, evacuation experts will have very limited time to make life saving decisions. Therefore, it is very important to provide these experts with knowledge of plume characteristics which are generated by an intuitive user interface; backed by simulations of radionuclide dispersions to better assist experts in evacuation planning. This study aims to verify the effectiveness of the user interface that can provide a one year meteorological and dispersion data based on WSPEEDI-II library. Such a user interface might be beneficial to risk and crisis management planning in case of a radioactive dispersion.

2. Methodology development

The user interface will use the data from the library to provide short summaries of various scenarios, and finally the user will then decide which of the data provided will be of interest to them. The platform of the user interface can run on any computer running a Linux operating system with the programming language of Fortran 90; hence making the interface friendly and simple to setup and use.

Radioactivity of air concentration $q_{a,i}(x, y, t)$ [Bq/m^3] of nuclide i at each grid point (x, y) and time (t) is obtained by:

$$q_{a,i}(x,y,t)=\sum_j \frac{Q_{j,i}}{Q_1}\times q_{a,1,j}(x,y,t)\exp\left[-\lambda_i\times(t-t_0)\right] \quad (1),$$

Where the release rate for each radionuclide (i), $Q_{j,i}$ [Bq/h] at the j-th release segment in the selected release period, and its radioactive decay (decay constant: λ_i) are applied to air concentration, $q_{a,1,j}(x, y, t)$ [Bq/m^3], of reference radionuclide with unit release (Q_1 =1 Bq/h) in the library. In which the release rate $Q_{j,i}$ is set as decay-corrected value to a specific time, t_0 (for example, shutdown time), for every time segment.

Radioactivity of deposited radionuclide i at each grid point and time, $q_{d,i}(x, y, t)$ [Bq/m^2] is calculated as:

$$q_{d,i}(x,y,t)=\sum_j \frac{Q_{j,i}}{Q_1}\times q_{d,1,j}(x,y,t)\exp\left[-\lambda_i\times(t-t_0)\right] \quad (2),$$

where $q_{d,1,j}(x, y, t)$ [Bq/m^2] is deposition of reference radionuclide with unit release and release period at each grid point (x, y) and time (t). After obtaining the air concentration and deposition of nuclide i, it is possible now to calculate air dose rates from all radionuclides in the plume and deposition, $D_{a,total}(x, y, t)$ and $D_{d,total}(x, y, t)$ [Gy/h], respectively, as:

$$D_{a,total}(x,y,t)=\sum_i C_{a,i}\times q_{a,i}(x,y,t) \quad (3),$$

$$D_{d,total}(x,y,t)=\sum_i C_{d,i}\times q_{d,i}(x,y,t) \quad (4),$$

where $C_{a,i}$ and $C_{d,i}$ are conversion coefficients from air concentration and deposition of the summation of every selected i radionuclide to air dose rate, respectively.

2. Summary of Results

Figure 1. (a) - (b) show how the plume is dispersed immediately after the release until four hours after the event. In Figure 1. (a) the plume is developing in and around the Fukushima Daiichi Nuclear Power Plant (FDNPP1), so it is still highly concentrated in that area, hence a high total air dose rate. However, in Figure 1. (b) the plume is moving upwards (Northeast) into the Pacific Ocean consequently, resulting in a lower total air dose, in fact even stabilizing. These plume conditions can be easily pictured from the short summary in Table 1 and Figure 1. Therefore, the user can easily identify the scenario of interest to them from the huge data set, and they can refer to the WSPEEDI-II library for the full details of that scenario for further analysis.

Along with the short summary it is also very important that experts access this information in a timely manner, so an example comparison is made between manually calculating on WSPEEDI-II the first 24 hours of dispersion after the FDNPP1 and using the interface to make the same calculation, 30 times shorter.

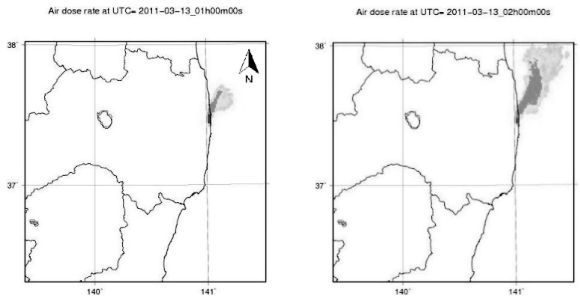

Figure 1. Horizontal distribution patterns of total air dose rate at (a) one hour, (b) two hour after the release start time

Reference

1. H. El-Asaad, H. Sagara, H. Nagai, Energy Procedia, Volume 131, December 2017, Pages 279-284

C.5 Characterization and Fluorine-Plasma Exposure Behavior of Dense Yttrium Oxyfluoride Ceramics

Katsumi YOSHIDA, Toru TSUNOURA, Anna GUBAREVICH, Toyohiko YANO

1. Introduction

Progress toward a society intensively supported by information technology has been made with highly integrated semiconductor-based devices. The semiconductor-based devices have been fabricated with the leading edge of technology by using semiconductor production equipment. The circuit patterns are drawn on silicon wafers by a photoresist in the equipment, and then the wafer is exposed in plasma to form the electric circuit. In plasma irradiation processes, the inside of semiconductor production equipment is also exposed to corrosive plasma, and then particulates are generated and dispersed. As a result, the particulates generated during plasma processes act as a contaminator and they decrease the yield of integrated circuit (IC) production. This problem is crucial when the width of a circuit becomes continuously smaller. It is very important to prevent the IC from particulate contamination in consideration of the yield of IC production.

Particulate contaminators are generated from the surface of the plasma chamber in the semiconductor production equipment. The inside of the plasma chamber must be coated with plasma-resistant materials such as silicon, silica, alumina (Al_2O_3), or yttria (Y_2O_3) in order to protect the IC from contamination. Reactions of silicon and silica with fluorine-based plasma are given as

$$Si + 4F \rightarrow SiF_4 \quad (1)$$

$$SiO_2 + 4F \rightarrow SiF_4 + O_2 \quad (2)$$

Generally, particulate contaminators are not produced from silicon and silica coatings owing to the evaporation of SiF_4. However, their lifetime is very short because of the high vapor pressure of fluoride. Therefore, Al_2O_3 and Y_2O_3 have been used as plasma-resistant coating materials for plasma equipment applying more powerful plasmas. Recently, the Y_2O_3 coating deposited by the aerosol deposition (AD) method as a plasma-resistant material has been adopted instead of the Y_2O_3 coating deposited by the conventional thermal spray method. It is reported that the particulate contaminator from the Y_2O_3 layer formed by the AD method was less in amount than those formed by other methods because these layers are highly dense and consist of very small grains. [17, 18] Al_2O_3 and Y_2O_3 ceramics also react with fluorine plasma, and the reactions are expressed as

$$Al_2O_3 + (3/2)CF_4 \rightarrow 2AlF_3 + (3/2)CO_2 \quad (3)$$

$$Y_2O_3 + (3/2)CF_4 \rightarrow 2YF_3 + (3/2)CO_2 \quad (4)$$

However, the surface of the Y_2O_3 coating was modified by plasma exposure and an altered layer composed of Y-O-F elements was formed after the fluorine-plasma irradiation. The prevention of the generation of the altered layer is believed to reduce particulate generation and thus contamination of ICs. The present authors have paid attention to yttrium oxyfluoride (YOF). YOF is expected to be a more stable material against plasma exposure and to show an excellent plasma resistance property because YOF is a component formed at the surface of the Y_2O_3 coating. It is expected that the YOF coating on the inner surface of the plasma chamber would prevent the particulate contamination of ICs during plasma processes.

There has been no report on the fabrication of YOF ceramics, to the best of our knowledge, and their mechanical and thermal properties are still unknown. In this study, therefore, dense YOF ceramics were fabricated by hot pressing and their mechanical and thermal properties were evaluated to clarify their basic properties. In addition, the fluorine-plasma exposure behavior of the YOF ceramics was also evaluated with reference to that of Y_2O_3 ceramics.

2. Experimental

2.1. Fabrication of YOF ceramics

YOF powder (Nippon Yttrium Co. Ltd., Japan, mean particle size: 0.8 μm) was used as the starting material for the preparation of the dense ceramics. The thermal stability of the YOF powder was evaluated by thermogravimetry and differential thermal analysis(TG-DTA). TG-DTA was conducted with the heating and cooling rates of 10°C/min. The specimen was kept at the maximum temperature of 1050°C for 1 h under Ar flow (100 ml/min).

YOF green bodies were prepared under a uniaxial pressure of 18.4 MPa. Then, YOF compacts were sintered by hot pressing with a unidirectional applied pressure of 36.7 MPa at 1600°C for 1 h under Ar flow (2 L/min). The YOF ceramics were mirror-polished using diamond pastes. The bulk density and open porosity were measured by Archimedes' method using water as media at room temperature.

2.2. Characterization of YOF ceramics

The elastic modulus and Poisson's ratio were measured by the ultrasonic pulse method. Vickers' hardness and the three-point bending strength were measured at room temperature. Vickers' hardness was measured with an applied load of 9.807 N for 15 s (average of 5 indents). The fracture toughness was measured by the indentation fracture method based on the results of Vickers' hardness test. The three-point bending strength was measured using bar-shaped specimens, and applying a lower span of 30 mm and a crosshead speed of 0.5 mm/min, following JIS 1601. The size of the specimens for the bending test was 35^l x 4^w x 3^t mm^3. Thermal conductivity was determined by the laser flash method at room temperature, and linear thermal expansion was measured from room temperature to 1000°C with the heating rate of 10°C/min under helium flow. The

specimen size for thermal expansion measurement was 20^l x 4^w x 3^t mm^3.

2.3 Plasma exposure

The plasma irradiation behavior of the prepared YOF and commercial Y_2O_3 ceramics (Nippon Yttrium Co. Ltd., Japan) was evaluated. Plasma exposure was conducted in a plasma barrel reactor with an RF power of 100 W under 100 Pa CF_4-based gas at room temperature for 30 min. No bias voltage was applied to the specimen. The gas was composed of 80 vol% CF_4 and 20 vol% O_2. After exposure, both YOF and Y_2O_3 ceramics were coated with a Pt layer of about 100 nm thickness to prevent the surface from contamination during polishing with a cross section polisher (CP). After the polishing, cross sections of the fluorine-plasma-exposed ceramics were observed and analyzed with a scanning electron microscope (SEM) equipped with an energy-dispersive X-ray spectrometer (EDS). In addition, cross-sectional thin films were prepared with a focused-ion-beam processor (FIB). Then, the microstructure of the cross sections of the ceramics after plasma exposure was observed with a transmission electron microscope (TEM) and an energy-dispersive X-ray spectroscope (EDS).

3. Results and Discussion

3.1 Characterization of YOF ceramics

In TG-DTA curves of the YOF powder, the weight of the YOF powder was not changed during heating, and DTA peaks were detected at 550°C during heating and at 580°C during cooling. These endothermic and exothermic peaks were considered to be related to the phase transformation of YOF between the rhombohedral phase and the tetragonal phase. It is reported that the rhombohedral phase is stable at temperatures lower than 570°C.

The bulk density and open porosity of the YOF ceramics were 5.21 g/cm^3 and 0.1%, respectively. These results indicated that dense YOF ceramics were successfully fabricated by hot pressing under the present synthesis conditions. From the results of X-ray diffraction (XRD) of the raw YOF powder and pulverized powder of the sintered body, the starting powder was composed of the rhombohedral and tetragonal phases, and sintered YOF ceramics consisted of only the rhombohedral phase of YOF. XRD results support that the phase transformation of YOF occurs at high temperatures and that the rhombohedral phase is a stable phase of YOF at room temperature. Figure 1 shows an SEM image of the polished surface of the YOF ceramics after polishing using CP. Most of the small pores distributed inside the grains of the YOF ceramics, not along the grain boundaries. The grain size of the YOF ceramics measured by the linear-intercept method was around 20 μm.

Vickers' hardness and the fracture toughness of the YOF ceramics were 0.68 GPa and 1.3 $MPa \cdot m^{1/2}$, respectively. The YOF ceramics showed more brittle behavior and lower hardness than other typical oxide ceramics such as Al_2O_3, MgO, Y_2O_3, or mullite. The elastic modulus, Poisson's ratio, and bending strength (an average of three measurements) of the YOF ceramics were 183±6 GPa, 0.29±0.02, and 90±4 MPa, respectively. The mechanical properties of the YOF ceramics were weaker than those of Al_2O_3 and Y_2O_3, but these properties resembled those of fluoride ceramics such as magnesium fluoride (MgF_2) and calcium fluoride (CaF_2), which are also candidate plasma-resistant materials. For example, the fracture strengths of MgF_2 and CaF_2 are 179 and 157 MPa, respectively.

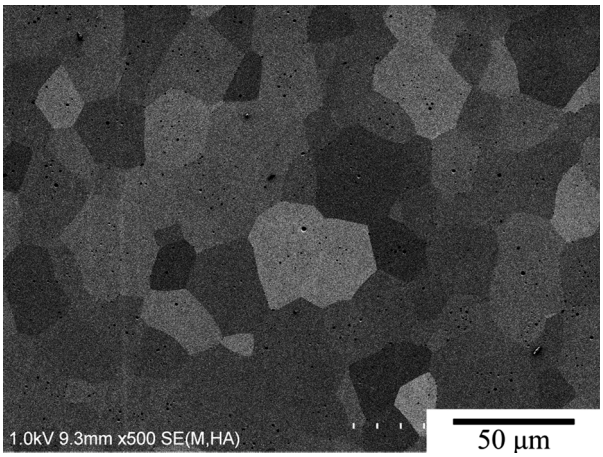

Fig. 1 SEM image of the polished surface of the YOF ceramics

The thermal conductivity κ of the YOF ceramics was calculated as

$$\kappa = \alpha \cdot \rho \cdot c \quad (5)$$

where α is the thermal diffusivity, ρ the bulk density, and c the heat capacity. The thermal diffusivity, heat capacity, and thermal conductivity of the YOF ceramics at room temperature were 3.3 x 10^{-6} ±0.1 x 10^{-6} m^2/s, 0.38±0.01 J/(g·K), and 16.9±0.3 W/(m·K), respectively. From this result of the dilatometry of the YOF ceramics from room temperature to 1000°C, the mean coefficients of thermal expansion (CTE) of the YOF ceramics were 14.1 x 10^{-6}/K at 200-400°C and 18.2 x 10^{-6}/K at 700-900°C. The CTE of the YOF ceramics was expressed by

$$\text{CTE(at 200-400°C)} = 13.5\text{x}10^{-6} + 4.39\text{x}10^{-9}\text{ x } T\,(/\text{K}) \quad (6)$$

$$\text{CTE(at 700-900°C)} = 9.12\text{x}10^{-6} + 8.25\text{x}10^{-9}\text{x } T\,(/\text{K}) \quad (7)$$

where T is the temperature in Kelvin. The length of the YOF ceramics was changed discontinuously at around 570°C because of the phase transformation from the rhombohedral phase to the tetragonal phase during heating. Table 1 lists the mechanical and thermal properties of the YOF, Al_2O_3, and Y_2O_3 ceramics. Compared with conventional plasma-resistant materials such as Al_2O_3 and Y_2O_3, YOF ceramics have lower mechanical properties and larger CTE. Hence, the thermal shock resistance of YOF ceramics should be lower than those of Al_2O_3 and Y_2O_3 ceramics. In consideration of the mechanical and thermal properties of MgF_2 and CaF_2, the thermal shock resistance of YOF would be almost the same as those of MgF_2 and CaF_2. However, YOF ceramics are expected to be applied to semiconductor production equipment as a plasma-resistant coating, and their thermal shock resistance has no problem in practical use. From these results, the mechanical and thermal properties of YOF ceramics seemed to be sufficient for use in semiconductor production equipment.

Table 1 Mechanical and thermal properties of YOF, Al_2O_3, and Y_2O_3 ceramics. Values at room temperature otherwise mentioned.

	YOF	Al_2O_3 (A-601D)	Y_2O_3 (Y0100A)
Vickers' hardness (GPa)	0.68±0.04	17.5	6.0
Fracture toughness (MPa·$m^{1/2}$)	1.3±0.1	5~6	1.1
Three-point bending strength (MPa)	90±4	400	130
Elastic modulus (GPa)	183±6	380	160
Poisson's ratio	0.29±0.02	0.23	-
Thermal conductivity [W/(m·K)]	17.1±0.1	34	14
Linear thermal expansion at 200-400°C (10^{-6}/K)	14.1±0.5	7.2	7.2

3.2 Plasma exposure resistance of YOF ceramics

In cross-sectional SEM images of the Y_2O_3 and YOF ceramics after fluorine-plasma irradiation, an altered layer with slightly darker contrast was observed on the surface of the Y_2O_3 ceramics. On the other hand, the surface of the YOF ceramics was not altered after fluorine-plasma exposure. In the SEM/EDS elemental mapping of the Y_2O_3 and YOF ceramics after plasma exposure, a fluorine-concentrated layer was detected along with the altered layer on the Y_2O_3 ceramics. The concentration of fluorine appeared higher near the surface. The thickness of the altered layer was around 50 nm or less. In contrast, the fluorine-concentrated layer was not formed on the surface of the YOF ceramics. In SEM/EDS spectra of the cross section of the Y_2O_3 ceramics after plasma exposure, the peak derived from fluorine and a slightly weak oxygen peak appeared in the spectra from the red rectangular area, which contained the altered layer. Only a thin area from the surface of Y_2O_3 was corroded and reacted with fluorine plasma because fluorine was not observed in the blue area (inside Y_2O_3). On the other hand, it is obvious that the YOF ceramics has higher fluorine-plasma resistance because both the spectra from the red and blue rectangular portions were almost the same.

From the cross-sectional TEM image of the Y_2O_3 ceramics after fluorine-plasma exposure, this image showed that the distortion of the crystalline lattice and fine grains, observed as a Moiré pattern near the surface, may be due to the damage caused by plasma irradiation. This damaged area may correspond to the altered layer observed by SEM. In TEM/EDS spectra obtained near the surface and inside of a Y_2O_3 grain, fluorine was detected clearly near the surface. This is similar to that observed from the SEM/EDS spectra. It is evaluated that the altered layer consisted of Y-O-F elements. Other elements such as copper and silicon were detected as artifacts from the column and sampling mesh materials of TEM and glass put on ceramics during plasma irradiation. It is supposed that the reaction of fluorine plasma with Y_2O_3 generates new compounds containing fluorine on the surface, and the mismatch of crystals induces the distortion of the lattice and the crystallization of fine grains with a slightly different orientation from the original Y_2O_3 grain. Such damage is believed to be one of the causes contributing to the particulate generation and thus semiconductor contamination.

From a cross-sectional TEM image of the plasma-exposed YOF ceramics, continuous lattice fringes were observed from the surface to the inner part of a grain. TEM/EDS spectra obtained near the surface and inside of a YOF grain showed that the F/Y ratio of the YOF ceramics after plasma exposure was the same as that before plasma exposure. The O/Y ratio in the vicinity of the surface of YOF ceramics appeared to be higher than that of the inside of YOF ceramics. Furthermore, the O/Y ratio in the vicinity of the surface of Y_2O_3 ceramics was higher than those of the inside of Y_2O_3 ceramics. It is considered that the intensity of O should be higher owing to the TEM/EDS measurement method, and it is considered that the higher intensity of O at the outermost surface of Y_2O_3 and YOF ceramics could be ignored. Therefore, the EDS spectra of YOF ceramics indicate that the surface of the YOF ceramics was not corroded under the present fluorine-plasma exposure condition. Therefore, it is concluded that the resistance for fluorine-plasma exposure of the YOF ceramics is superior to that of the Y_2O_3 ceramics.

4. Conclusion

Dense YOF ceramics were successfully fabricated by hot pressing, and their open porosity was less than 1%. The mechanical and thermal properties were sufficient for their use as plasma-resistant materials in semiconductor production equipment. Furthermore, from the results of the fluorine-plasma exposure test, the YOF ceramics showed superior resistance for fluorine-plasma exposure to the Y_2O_3 ceramics. It is concluded that the materials consisting of YOF are excellent for coating or bulk ceramics used in the recent plasma-applying semiconductor production equipment.

C.6 Combustion synthesis of MAX phases for accident-tolerant fuels

Anna GUBAREVICH, Toyohiko YANO, Katsumi YOSHIDA

1. Introduction

The present research is motivated by the existing demand to develop novel materials for accident tolerant fuels (ATF). The ATF are fuels that can tolerate loss of active cooling in the reactor core longer than currently used UO_2-zirconium alloy system while meeting all other operational requirements. In our work we study possibilities to substitute (or protect by coating) currently used in claddings zirconium alloys with materials having improved high-temperature steam oxidation resistance. Among possible candidates for the ATF claddings, we have focused on novel ternary compounds with a general formula $M_{n+1}AX_n$, known as MAX phases, where M is an early transition metal, A is an element of an A group (mostly group 13 and 14 of the Periodic Table elements), X is carbon or nitrogen, and n is typically 1, 2, or 3. MAX phases have an unusual combination of properties, which include good machinability and electrical conductivity, as well as high melting temperature, damage tolerance and high thermal shock resistance. High oxidation resistance was reported for various MAX phases as well.

MAX phases have been attracting a lot of attention as candidate materials for nuclear applications. Ti_3SiC_2 and Ti_3AlC_2 are the most studied MAX phases up to now. Despite of the promising results obtained for the titanium-based MAX phases, from the point of view of neutron economics, titanium has disadvantages related to its high neutron cross-section. Compared to titanium, zirconium has a very low neutron cross-section, and it makes development of zirconium-based MAX phases highly desirable. However, synthesis of zirconium-based MAX phases is very difficult, and no report about pure MAX phases in Zr-Al-C system has been published up to now, and no MAX phases in Zr-Si-C system have been reported yet.

As a way to approach Zr-rich MAX phases we have selected formation of solid solutions of Ti and Zr MAX phases. The MAX phases have a hexagonal crystal structure (space group $P6_3/mmc$), where layers of carbide (such as Ti_3C_2) are interleaved with Si-Si (or Al-Al) layers. The crystal structure of Ti_3AlC_2, visualized in VESTA, is shown in Fig. 1 (a). When Ti-Zr MAX phase solid solution forms, Zr atoms substitute part of Ti atoms (Fig. 1(b)).

As a method of synthesis, we have applied combustion synthesis method, which has merits of simplicity, high time and energy efficiency, as well as suitability for powders fabrication. In the present report, combustion synthesis of titanium-based MAX phases, Ti_3SiC_2 and Ti_3AlC_2, Zr-Ti MAX phase solid solution $Zr_{1.5}Ti_{1.5}AlC_2$, and zirconium-based MAX phase Zr_3AlC_2 is introduced.

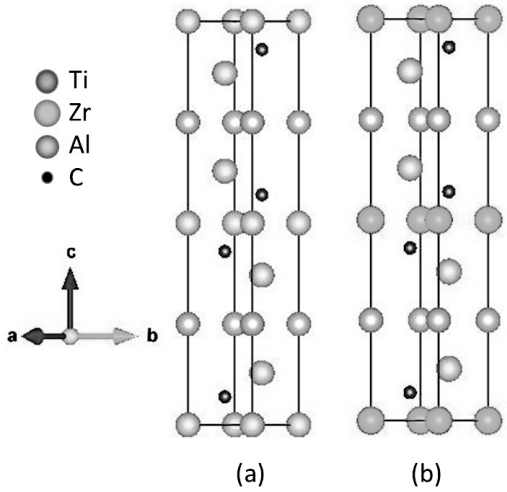

Fig. 1 Crystal structure of Ti_3AlC_2 (a) and $ZrTi_2AlC_2$ (b) MAX phases. (The cell size difference between Ti_3AlC_2 and $ZrTi_2AlC_2$ is not reflected in the Figure.)

2. Experimental

2.1. Set up for combustion synthesis

The experimental apparatus for combustion synthesis has been developed (Fig. 2). A stainless steel chamber (1) is equipped with gas inlet and outlet, which are connected to Ar gas vessel and rotary pomp, and a heater (2). Green pellet of starting materials (3) is placed on a ceramic plate inside the heater (2). Combustion reaction is initiated using an ignition system, based on resistive heating of tungsten filament (4) using voltage transformer. The chamber is equipped with a window (5), through which observation of reaction ignition and propagation is carried out.

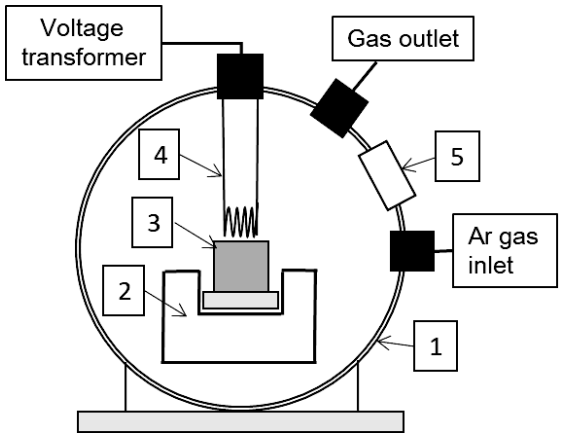

Fig. 2 Simplified scheme of the combustion synthesis set up, where 1) is a stainless steel chamber, 2) is a heater, 3) is a green pellet, 4) is a tungsten filament, and 5) is a window.

2.2. Experimental procedure

Powders of titanium (40 μm, Kojundo Kagaku), silicon (5μm, Kojundo Kagaku), aluminum (30 μm, Kojundo Kagaku), zirconium (less than 30 μm, Wako Chem.), and carbon black (Asahi Carbon) have been used as starting materials. The stoichiometry of mixing was established based on the next chemical reactions.

$3Ti + Si + 2C = Ti_3SiC_2$ (1)

$3Ti + Si + 2C + nAl = Ti_3Si(Al)C_2$ (2),

where n is 0.1 and 0.2.

$xZr + (3-x)Ti + Al + 2C = Zr_xTi_{3-x}AlC_2$ (3),

where x is 0, 1.5, and 3.

In case of synthesis of Ti-based MAX phases (reactions 1 and 2), the elemental powders were mixed in stoichiometric proportions in a ball mill for 24 hours with alumina balls and ethanol as media. After mixing, ethanol was evaporated using rotary evaporator, and powders were dried in a drying furnace for several hours.

In case of synthesis of Zr-containing MAX phases (reaction 3), as a first step, Zr powder, which was kept under water, was dried in a vacuum drying furnace at 60^0C. Then all starting powders were hand-mixed together using an agate mortar and pestle in i-propanol. The mixture was then dried in vacuum drying furnace.

Thus obtained starting mixtures were cold-pressed into green pellets with diameter of 15 mm and height of 10-15 mm. The pellets were set into the chamber (Fig. 2), then chamber was evacuated using rotary pump and filled with Ar gas. The combustion reactions were initiated at room temperature by electroresistive heating of the tungsten filament (Fig. 3 (a)). The applied voltage was 30 or 40 V depending on sample. The ignition and propagation of the reactions were confirmed through the window in the chamber wall (Fig. 3 (b)). After the reaction was finished, the samples were cooled down naturally in the chamber.

For the scanning electron microscopy (SEM) and x-ray diffraction (XRD) measurements, the synthesized products (an example is shown in Fig. 3 (c)) were cut into pieces and crushed into powders. The SEM observation of fractured surfaces was carried out using S-4800 microscope (Hitachi). The XRD measurements of Ti_3SiC_2 powders were done using PW-1700 diffractometer (Phillips) and $Zr_xTi_{3-x}AlC_2$ powders were measured using AERIS diffractometer (Panalytical).

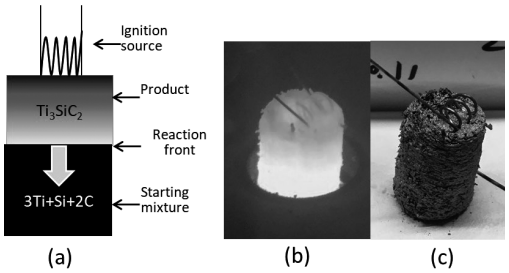

Fig. 3 (a) Self-propagation of combustion reaction, (b) sample during combustion reaction, (c) synthesized product.

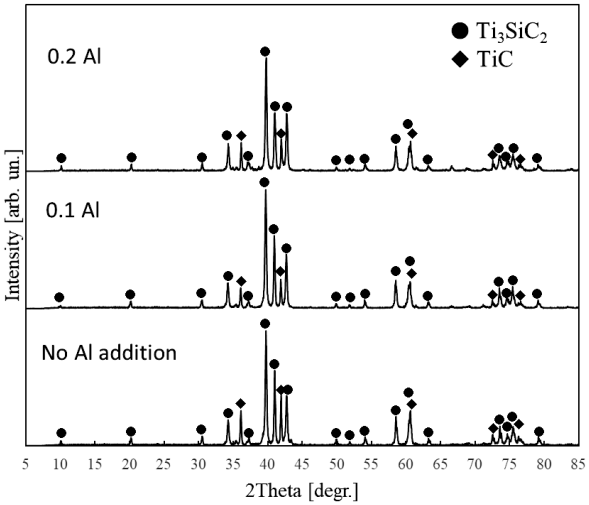

Fig. 4 XRD patterns of the synthesized products with no Al, and 0.1 Al, and 0.2 Al addition.

3. Results and discussion

3.1. Synthesis of Ti_3SiC_3 MAX phase: effect of aluminum addition

XRD patterns of the synthesized products in Ti-Si-C system with and without Al addition are shown in Fig. 4. It can be seen that all specimens consist mainly of two crystalline phases, namely Ti_3SiC_2 (major phase) and TiC (secondary phase). Crystal lattice parameters for the Ti_3SiC_2 phase synthesized without Al addition were calculated as a=3.070 Å and c=17.683 Å.

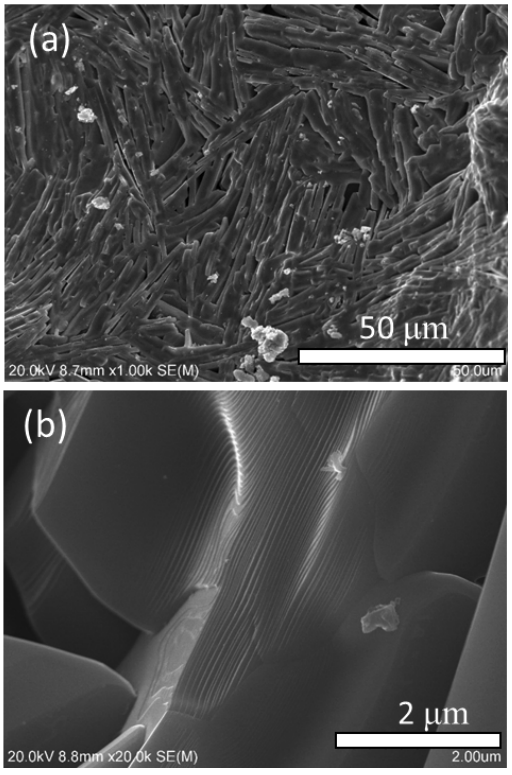

Fig. 5 SEM images of the synthesized Ti_3SiC_2 at low (a) and high (b) magnification.

Phase composition of the specimen synthesized without Al addition was estimated to be 82 vol% of Ti_3SiC_2 and 18 vol% of TiC. With addition of 0.1 mol of Al (reaction 2)), the amount of TiC decreased by 1.6 times to 11 vol%, and the yield of Ti_3SiC_2 phase increased to 89 vol%. Positive effect of Al addition on the yield of the MAX phase is consistent with the results obtained by other synthetic methods. When amount of Al addition was increased to 0.2 mol, the amount of TiC increased to 14 vol%, however it was still lower than in the products synthesized without Al addition.

SEM images of the fracture surface of the specimen synthesized from 3Ti+Si+2C mixture without Al addition are shown in Fig. 5. Lower magnification image (Fig. 5 (a)) shows that the product consists of elongated grains, some of which are as long as 50 μm. The thickness of the grains is several micrometres. Grains form groups with similar orientation. Higher magnification image (Fig. 5 (b)) shows that grains have a nanolaminated structure. Layers with thickness less than 100 nm are stacked together to form a single grain.

3.2. Synthesis of Ti_3AlC_2, Zr_3AlC_2 and $Zr_xTi_{3-x}AlC_2$

Fig. 6 shows XRD patterns of the products synthesized from the 3Ti+Al+2C (x=0), 1.5 Zr+1.5Ti+Al+2C (x=1.5), and 3Zr+Al+2C (x=3) mixtures (reaction 3). Formation of Ti_3AlC_2 and solid solution $Zr_{1.5}Ti_{1.5}AlC_2$ belonging to $P6_3/mmc$ space group was confirmed. Although in a small amount, Zr_3AlC_2 MAX phase was confirmed to be synthesized by combustion synthesis method. As can be seen from the Fig. 6, the diffraction peaks belonging to $Zr_{1.5}Ti_{1.5}AlC_2$ MAX phase (x=1.5) are located between the positions of Ti_3AlC_2 and Zr_3AlC_2 diffraction peaks. All MAX phases have the same crystal structure belonging to $P6_3/mmc$ space group. However, zirconium has a larger atomic radius than titanium, and when Zr substitutes Ti at the same crystal sites, the crystal unit expands and compared to Ti_3AlC_2 peaks of $Zr_{1.5}Ti_{1.5}AlC_2$ MAX phase shift to lower diffraction angles.

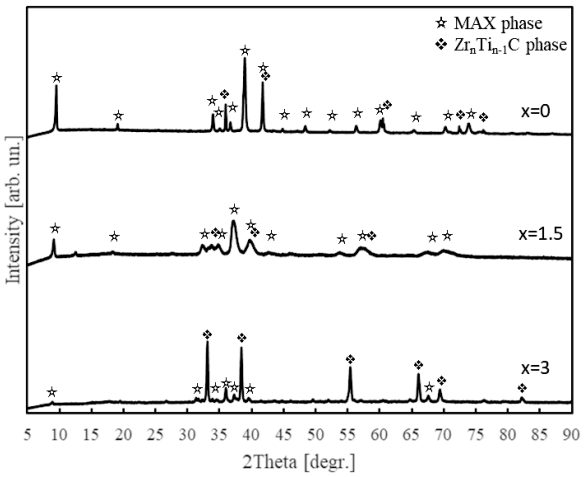

Fig. 6 XRD patterns of the synthesized Ti_3AlC_2 (x=0), $Zr_{1.5}Ti_{1.5}AlC_2$ (x=1.5) and Zr_3AlC_2 (x=3) MAX phases.

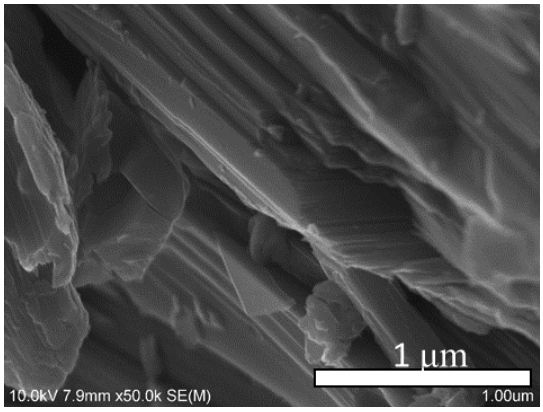

Fig. 7 SEM images of the $Zr_{1.5}Ti_{1.5}AlC_2$ MAX phase solid solution.

From the XRD patterns shown in Fig. 6 it is seen that besides MAX phases secondary phases of titanium carbide TiC (x=0, n=0), zirconium titanium carbide $Zr_nTi_{n-1}C$ (x=1.5, n~0.5), and zirconium carbide (x=3, n=1) were formed. With increasing Zr content in the starting mixtures from 0 to 3, the peak intensity ratio of MAX phases and binary carbides decreased. Future improvement of the yield of MAX phases with higher content of Zr is required.

Fig. 7 shows microstructure of $Zr_{1.5}Ti_{1.5}AlC_2$ MAX phase solid solution. Formation of fine nanolaminated structure, typical for MAX phases, was observed.

4. Conclusion

Combustion synthesis apparatus has been developed for the synthesis of MAX phases. Ti_3SiC_2, Ti_3AlC_2, Zr_3AlC_2 MAX phases and $Zr_{1.5}Ti_{1.5}AlC_2$ MAX phase solid solution have been synthesized by combustion synthesis method in the self-propagating mode. Positive effect of the Al addition on the yield of Ti_3SiC_2 MAX phase has been shown. Further development will include optimization of the synthetic conditions to improve the yield of Zr-Ti MAX phase solid solutions with higher Zr content and investigation of mechanical and thermal properties of the synthesized MAX phase materials.

Acknowledgment

The present research was supported by "Hoga" grant from LANE, TIT, and Research grant from Okura Kazuchika Memorial Foundation. Author acknowledges M. Imai and N. Tsuruoka (LANE, TIT) for the assistance in the experimental set up, and J. Maletaskic (LANE, TIT) for the help in the refinement of XRD data.

Reference

1. A. Gubarevich, K. Yoshida, T. Yano: 6th International Symposium on Advanced Ceramics (ISAC6), March 12-14, Sendai, Japan, (2018).

C.7 Agendas and Issues of Participatory Dialogues by Junior-High and High School Students from Fukushima Hama-doori and Capital Area -Recognition for thyroid examination of six years after the accident and future issues-

Tetsuo SAWADA

1. Introduction

The United Nations Scientific Committee on the Effects of Atomic Radiation (UNSCEAR) stated in the 2013 report on the health effects on the public regarding the thyroid examination conducted for children in all areas of Fukushima Prefecture as follows. That is, it is unlikely that "Thyroid cancer, leukemia and breast cancer incidence will increase in the future at a level that can be distinguished from the natural occurrence rate." Then, for children under the age of 18 in Fukushima prefecture (about 370,000 people), the second round of thyroid examination was carried out between 2014 and 2015. Based on the results, UNSCEAR published the White Paper on 2017. Among them, "This committee continues to be effective in knowledge of the health effects of radiation exposure due to the Fukushima Daiichi Nuclear Power Plant accident in the 2013 report, and received little influence from new information published after that We have reached the conclusion that there is nothing."

2. Where the problem is related to thyroid examination and how to deal with it

2-1. Where the problem is

There are two main problems. (1) The above conclusion issued by UNSCEAR has not arrived in a manner that is easy to understand for the parties, i.e., children under the age of 18 and their close relatives. (2) There is a strong argument in the conclusion of UNSCEAR. For example, Japanese doctors alerting the occurrence of abnormal thyroid cancer on the stage of the International Physicians for the Prevention of Nuclear War (IPPNW) are objections. Also, thyroid abnormality multiple theory is likely to spread through mass media and SNS complicates the situation.

2-2. How to deal with it

To understand the significance and result and interpretation of thyroid examination, the dialogue method utilizing introspective thinking and active learning mainly on the parties is effective in order to resolve the anxiety and doubts of youth who is a party in Fukushima prefecture. It has been confirmed so far [1, 2, 3]. Aware of the four indicators of Socio-Scientific Issue (SSI), that is, training of citizens awaiting scientific knowledge, introspective

development of social responsibility, unremitting thinking and logical discussion, demonstration of critical thinking, through conducting inter-regional dialogue, we confirmed the possibility that the issues with public nature can be seen from collaboration and lead to advocacy (promotion of public policy formation) [4]. Leading to the advocacy, for example, dialogue by middle and high school students of Fukushima Hama-dori and Metropolitan areas conducted 12 questions to be thrown to the medical experts as shown in Fig. 1. In addition, this method also opens the way to resolve post-traumatic stress disorder held by subjects.

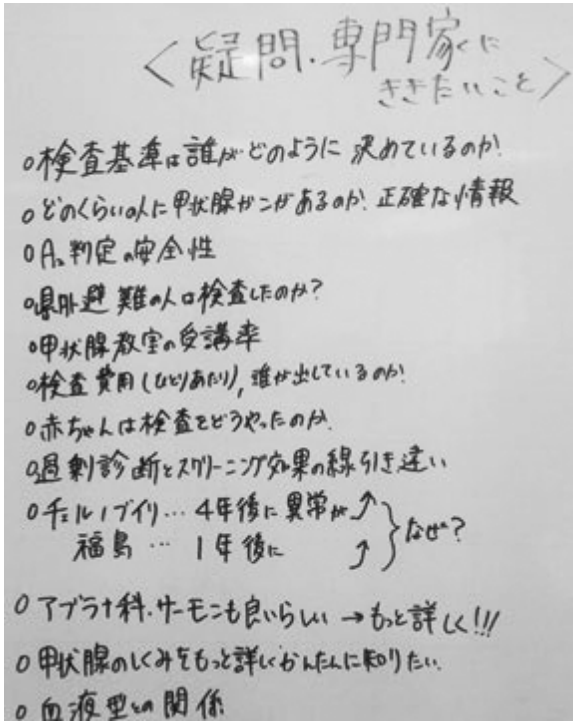

Fig. 1 12 Questions on thyroid examination presented to the concerned experts by middle- and high-school students.

3. Conclusion

Dialogue revealed that middle and high school students can cope with the thyroid problem in a bottom-up manner. In the future, it will be an issue to mobilize expert knowledge and deepen the efforts of the thyroid problem through regional regional collaboration.

Reference

1.～3. T. Sawada, et. al., 2017 Annual Mtg. of AESJ, 2017, 2C13～2C15

4. T. Sawada, et. al., 2017 Fall Mtg. of AESJ, 2017, 1O04

D. Advanced Medical Application Division

D.1 Applied Research on Proton-Induced X-ray Emission at LANE, IIR

Yoshiyuki OGURI, Yuchao Hu, Wenkai TENG

1. Geant4 calculation of X-ray dose distribution of syringe-needle-type proton-induced X-ray source

X-ray dose distribution of the syringe-needle type proton-induced X-ray source[1] is affected by the structure of the needle and conditions of the incident proton beam. To evaluate this effect, we performed a Geant4 calculation[2] of the energy spectrum and distribution of X-ray emission. For this simulation, experimentally measured proton beam emittance was used as input data. The result is shown in Fig. 1. We found that the effect of beam misalignment was significant. It is expected that, after improving this method, we can optimize the source structure for a special dose distribution required for treatment of tumors of arbitrary shape.

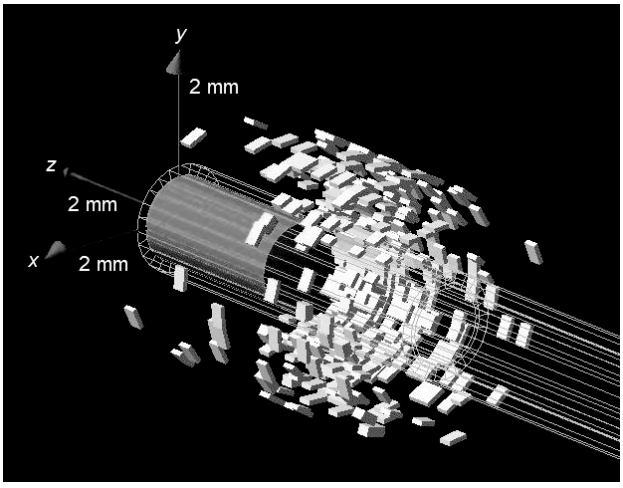

Fig. 1 X-ray distribution calculated by Geant4. White cuboids show cells in which energy was deposited. Straight lines in the *z*-direction show the track of 2.5-MeV incident protons

2. PIXE target preparation by "drop and dry" method using surfactants

X-ray yield in PIXE analysis decreases when the thickness of the sample target becomes comparable to the X-ray attenuation length and/or the proton range. Sample targets prepared by "drop and dry" method can be partially very thick due to inhomogeneous deposition of the evaporation residue. In order to overcome this problem, we applied Triton X-100™ as the surfactant to reduce the surface tension of the sample solution during drying[3].

We used Sr as the element to be analyzed. Sr was introduced in aqueous solutions as $Sr(NO_3)_2$. We prepared two solutions: one with and the other without the surfactant. The Sr concentration was 20 meq/L for both the samples. The concentration of X-100 was 2.5×10^{-4} mol/L. We dropped these sample solutions on 6-μm-thick polypropylene backing films separately, and dried them at room temperature. These samples were PIXE analyzed using a 3-MeV proton beam. The ordinate of the measured X-ray spectra was normalized by the incident proton dose (= beam current × measurement time).

Figure 2 shows PIXE spectra measured for both the samples. We see intensities of Sr X-rays increased when the surfactant was added to the sample solution. Also, when the surfactant was used, the L_α/K_α ratio dramatically increased. These results can be explained by self-absorption of the X-rays and the energy loss of protons in the partially thick target, which was prepared without the surfactant.

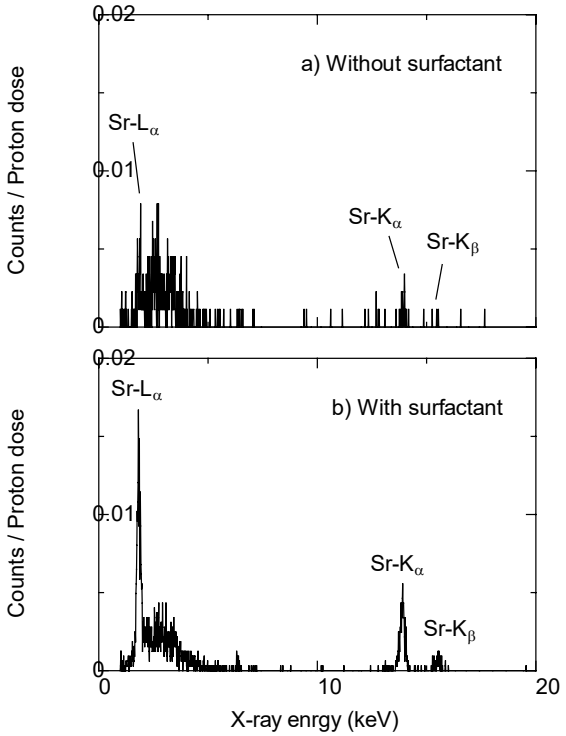

Fig. 2 PIXE spectra measured for samples with and without addition of Triton X-100 surfactant.

Reference

1. Y. Oguri, Y. Hu, K. Kondo, J. Hasegawa: 11th European Conference on Accelerators in Applied Research and Technology, #P99, September 8-13, Namur, Belgium (2013).
2. Y. Hu, H. Fukuda, Y. Oguri: X-Ray Spectrometry, Vol.46, No.5, pp. 356-360 (2017).
3. W. Teng, Y. Oguri, S. Kaseda, H. Fukuda: 33rd PIXE Symposium #3-1, October 19-21, Uji Campus, Kyoto University, Kyoto, Japan (2017).

D.2 Molecular Mechanisms for Repair of DNA Double-strand Breaks

Yoshihisa MATSUMOTO, Mikio SHIMADA, Ali Reza Amiri MOGHANI, Aoi OKAWA, Tomoko MIYAKE, Hisayo TSUCHIYA, Anie Day Asa De CASTRO, Kaima TSUKADA, Naoya KASE, Akane YAMASAKI, Nozomi KAGAWA, Nur Amirah Muhammad NOOR, Mukesh Kumar SHARMA

1. Background

Radiation causes various biological effects, *e.g.*, lethality, infertility, embryonic malformation, carcinogenesis and cancer cell killing, through the generation of damage on the DNA molecule. Among various types of DNA damages, DNA double-strand break (DSB) is considered the most critical type of damage. DSBs are generated exogenously by ionizing radiation or chemicals, including a subset of anti-cancer agents, and endogenously by replication errors or oxidative stress. DSBs also result from recombination, including meiotic recombination in reproductive organs and V(D)J recombination in immune cells. In eukaryotic cells, including human cells, DSBs are repaired through homologous recombination (HR) and non- homologous end joining (NHEJ) (Fig. 1). NHEJ can be further categorized into canonical (or classical) NHEJ (C-NHEJ) and alternative (or atypical) NHEJ (A-NHEJ, also termed TMEJ for theta-mediated end joining).

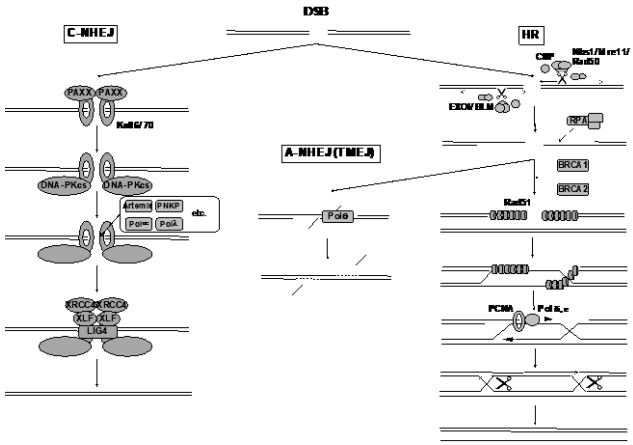

Fig. 1 Mechanisms for the repair of DNA double-strand breaks in human cells.

In DSB repair through HR, undamaged DNA, with identical or homological sequence, serves as a template to reconstitute the original sequence across the break. On the other hand, in DSB repair through C-NHEJ, two broken DNA ends are joined without much regard for the homology at these ends. Therefore, C-NHEJ may sometimes incur nucleotide deletions or insertions at the junction or joining with incorrect partner, leading to chromosomal aberrations like deletions, inversions or translocations. Hence it is considered that C-NHEJ is less accurate than HR. However, vertebrate can utilize only sister chromosome, but not homologous chromosome, as the template for HR and, therefore, the repair of DSB through HR is limited to late S and G2 phases. The majority of the cells reside in G0 or G1 phases in vertebrate body, where only C-NHEJ can operate. Hence C-NHEJ is considered important especially in vertebrates. C-NHEJ operates also in V(D)J recombination.

In some situations, single-stranded DNA generated in HR process undergoes A-NHEJ, an aberrant joining mediated by short stretch of homology. The molecular mechanisms for A-NHEJ has been poorly understood and considered the obstacle for efficient generation of gene knockout cells via gene targeting [1]. Now several groups demonstrated that DNA Polymerase θ (Polθ) plays an essential role in A-NHEJ and deletion of Polθ greatly improves the efficacy of gene targeting.

2. XRCC4 as the Regulatory Hub for C-NHEJ

2.1. Regulation of NHEJ via XRCC4 phosphorylation by DNA-PK

Core C-NHEJ machinery comprises Ku70, Ku86 (also known as Ku80), DNA-dependent protein kinase catalytic subunit (DNA-PKcs), XRCC4, DNA ligase IV (LIG4), XLF (also known as Cernunnos) and PAXX. Ku70, Ku86 and DNA-PKcs forms a protein kinase complex, DNA-PK, which is activated upon DSB. The protein kinase catalytic activity of DNA-PKcs is shown essential for NHEJ but the critical target and the role of phosphorylation remain to be clarified. XRCC4 is constitutively and tightly associated with LIG4 and required for its activity and stability. We have explored the mechanisms of regulating NHEJ via XRCC4.

XRCC4 is shown to be phosphorylated by DNA-PK in vitro and in cultured cells after exposure to ionizing radiation or treatment with DNA damaging chemicals. Mass spectrometry analyses of XRCC4 phosphorylated by DNA-PK in vitro lead to the identification of Ser260 and Ser320 of XRCC4 as the major phosphorylation sites by mass spectrometry. However, it is yet unclear whether these sites are phosphorylated by DNA-PK in vivo. Moreover, XRCC4 mutants lacking these phosphorylation sites appeared functionally normal and, thus, XRCC4 phosphorylation by DNA-PK at these sites was considered unnecessary for DSB repair.

In 2016, we demonstrated that Ser320 of XRCC4 undergoes phosphorylation by DNA-PK in response to DNA damage in cell. This year, we demonstrated XRCC4 Ser260 by DNA-PK in cell [2]. We generated phosphorylation-specific antibodies for XRCC4 Ser260, as well as that for Ser320, which had been generated in the earlier study. By Western blotting analysis using these antibodies, we demonstrated that Ser260 as well as Ser320

undergoes phosphorylation by DNA-PK after irradiation (Fig. 2). XRCC4 S260A mutant exhibit slightly but significantly increased radiosensitivity and delayed DSB repair kinetics (disappearance of γ-H2AX foci) when introduced into a XRCC4-deficient cell. These results indicated that the importance of XRCC4 Ser260 in NHEJ. Moreover, we have identified several additional phosphorylation sites in XRCC4 by DNA-PK and characterized their response to radiation and influence on NHEJ function.

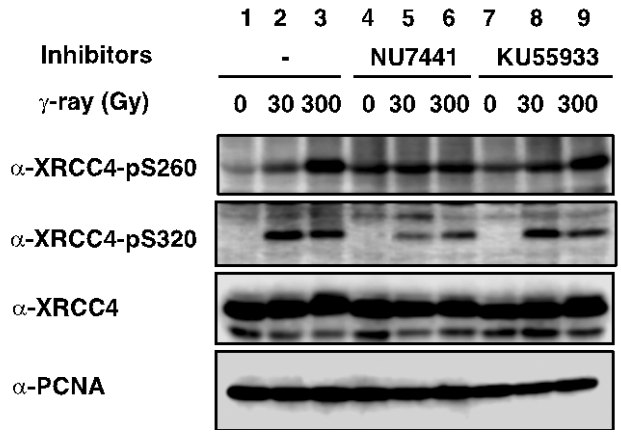

Fig. 2 XRCC4 phosphorylation by DNA-PK induced by γ-irradiation. NU7441 and KU55933 are specific inhibitors for DNA-PK and its related enzyme ATM, respectively [2].

2.2. A Novel Role of XRCC4 in the Regulation of Apoptosis

Apoptosis is an autonomous, programmed cell death to eliminate unnecessary or (potentially) harmful cells in the development or homeostasis of multicellular organisms. Apoptosis is seen, for example, in the process to eliminate cells between fingers in the development of hands and feet. Another example is seen during the generation of immune system, eliminating autoimmune cells. Additionally, DNA damaging agents, including ionizing radiation, induce apoptosis. This is considered one of the mechanisms to eliminate potentially cancerous cells. Dysregulation of apoptosis is frequently seen in cancer cells.

This year, in a collaboration with Yumi Sunatani, Kuniyoshi Iwabuchi and their colleagues at Kanazawa Medical University, we reported the finding of a novel function of XRCC4, regulating apoptosis [3] (Fig. 3). In an earlier study, we found that XRCC4 undergoes cleavage by caspases in apoptosis induced by ionizing radiation or hyperthermia. Caspases are a series of evolutionally conserved proteases, regulating apoptosis. We identified the cleavage site at the carboxy-terminal side of aspartate 265 (D265) and generated caspase-resistant mutant of XRCC4, replacing S265 by alanine (D265A). Introduction of normal XRCC4 to a XRCC4-deficient cell M10 increased apoptosis induced by staurosporine treatment. On the other hand, D265A mutant did not affect staurosporine-induced apoptosis.

One of the most outstanding hallmarks of apoptosis is the formation of "DNA ladder", which is an extensive fragmentation of DNA between nucleosomes. Caspase activated deoxyribonuclease (CAD) is considered the main enzyme for this process. It was found that normal XRCC4 enhances translocation of CAD to nucleus from cytoplasm. The underlying mechanism was clarified further in detail. First, XRCC4 stimulates the phosphorylation of Serine/Arginine-rich Splicing Factor 1 (SRSF1) by SR protein kinase 1 (SRPK1), facilitating the nuclear import of SRSF1. Second, SRSF1 decrease mRNA for the shorter splicing variant of ICAD (ICAD-S, ICAD stands for Inhibitor of CAD). Third, as the result, there is an increase of the complex of CAD and the longer splicing variant of ICAD (ICAD-L), which promotes the nuclear translocation and activation of CAD.

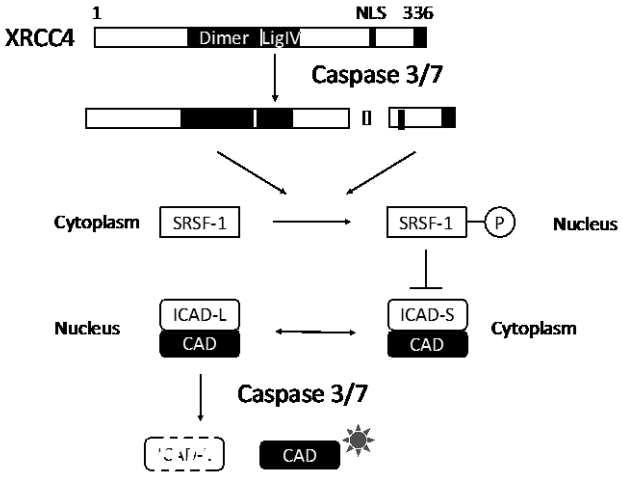

Fig. 3 A model for the regulation of apoptosis by XRCC4.

3. Implication of C-NHEJ in clinical outcome of radiotherapy and congenital diseases

In a collaboration with Koh-ichi Sakata, Masanori Someya and their colleagues at Sapporo Medical University, we have reported correlation between the expression of XRCC4 protein and responses of several types of cancer to radiotherapy. This year, we reported that the expression of Ku70 protein in the tumor tissue and the catalytic activity of DNA-PK in the peripheral lymphocyte predicts the outcome of radiotherapy [4,5].

In 2014 and 2015, several groups in parallel identified XRCC4 mutations in patients of microcephaly and growth defect (Fig. 4). It was surprising that these patients exhibit normal immunological function, whereas the patients with mutation in other NHEJ genes, *i.e.*, DNA-PKcs, XLF and LIG4, exhibit immunodeficiency. Some are the substitution of one amino acid to another one, whereas some others are truncating or frameshift mutations lacking the carboxy-terminal part. Our earlier studies showed that the lysine 271 is essential for the nuclear localization of XRCC4 itself and its binding partner DNA ligase IV. We also showed that the extremely carboxy terminal (XECT) region is highly conserved among vertebrate species and asparagine 326

therein is essential for XRCC4 function conferring cells resistance to radiation. We generated XRCC4 mimicking disease mutations and are currently analyzing the functionality in C-NHEJ.

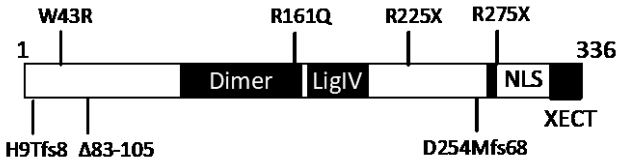

Fig. 4 A diagram of XRCC4 mutations identified in patients showing microcephaly and growth defect. H: histidine, T: threonine, W: tryptophan, R: arginine, Q: glutamine, X: stop codon, D: aspartate, M: methionine, Δ: deletion, fs: frameshift, followed by the number of amino acids up to newly emerged stop codon. Other number indicate the position of amino acid.

Acknowledgment

We thank Kuniyoshi Iwabuchi, Yumi Sunatani, Koh-ichi Sakata, Masanori Someya, their colleagues for fruitful collaborations introduced here, which were conducted in part as RLNR Research Collaboration FY2014 and FY2015, ex-lab members Radhika Pankaj Kamdar, Ravindra Mahadeo Samarth, Rujira Wanotayan, Sicheng Liu, Shoji Imamichi and Mikoto Fukuchi for continuous support and cooperation.

Reference

1. Matsumoto Y. FEBS Journal, Vol. 284, pp. 2745-2747 (2017).
2.Amiri Moghani AR, Sharma MK, Matsumoto Y. Journal of Radiation Research, Vol.59, No.6, pp.700-708, (2018).
3.Sunatani Y, Kamdar RP, Sharma MK, Matsui T, Sakasai R, Hashimoto M, Ishigaki Y, Matsumoto Y, Iwabuchi K. Experimental Cell Research, Vol.362, pp.450-460 (2018).
4. Someya M, Hasegawa T, Hori M, Matsumoto Y, Nakata K, Masumori N, Sakata K. Journal of Radiation Research, Vol.58, No.2, pp.225-231 (2017).
5. Hasegawa T, Someya M, Hori M, Matsumoto Y, Nakata K, Nojima M, Kitagawa M, Tsuchiya T, Masumori N, Hasegawa T, Sakata K. Strahlentherapie und Onkologie, Vol.193, pp.29-37 (2017).

D.3 DNA damage response in human induced pluripotent stem cells after ionizing radiation exposure

Mikio SHIMADA

1. Introduction

Ionizing radiation (IR) induces severe genome instability caused by DNA damage, chromosome aberrations and mutations. In mammalian cells, there are several mechanisms to repair and maintain genome DNA, such as DNA damage response and cell cycle checkpoint. Disruption of these mechanism leads to severe disease such as immunodeficiency, developmental failure and cancer.

Meanwhile, pluripotent stem cells (PSCs) have specific metabolism and gene expression system. It is important to investigate DNA repair mechanism in PSCs to consider IR effect during mammalian development. For this purpose, we established induced pluripotent stem cells (iPSCs) from human neonatal skin fibroblasts NB1RGB. In this study, we analyzed DNA damage response after IR exposure using iPSCs. iPSCs showed altered gene expression and DNA repair activity compared with fibroblasts. These results will contribute understanding of IR effect to the human body and development.

2. Results

2.1. Generation and identification of iPSCs

As reported previously, we generated iPSCs from human neonatal skin fibroblast NB1RGB using mRNA transfection method. iPSCs were identified by immunostaining using PSCs markers, Nanog, SSEA4, OCT4 and KLF4 (Fig 1A) and differentiation to the three germline layers: ectoderm, mesoderm, endoderm (Fig 1B).

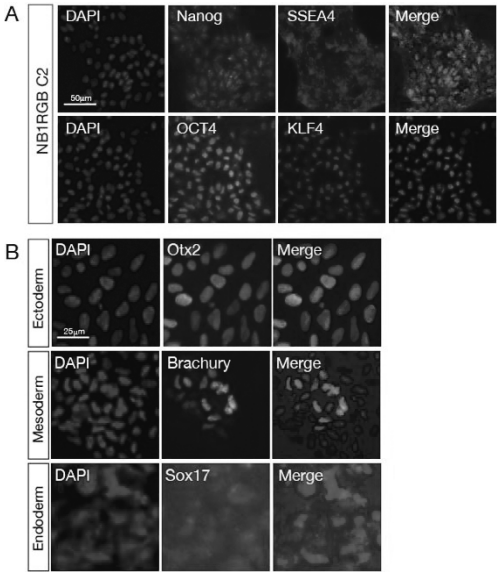

We obtained 10 clones after first transfection and all clones were positive for PSCs markers, Nanog, SSEA4, OCT4 and KLF4. Because of NB1RGB C2, one of 10 clones showed high growth, we used this for next experiments.

Fig. 1 Identification of iPSCs by immunostaining with PSCs markers and differentiation to the three germline layers. (A) iPSCs cells were stained with PSCs markers, Nanog (green), SSEA4 (red), OCT4 (green) and KLF4 (red) and represent positive to the all markers. (B) iPSCs were differentiated to the three germ line layers and stained with each marker: ectoderm (Otx2), mesoderm (Brachury), endoderm (Sox17).

2.2. DNA damage response in iPSCs

To investigate DNA damage response in iPSCs, iPSCs were exposed to gamma-ray irradiation at 2Gy and fixed as indicated time. Cells were stained with DNA damage marker, γ-H2AX and 53BP1 antibodies (Fig 2A and 2B). Although fibroblasts showed γ-H2AX and 53BP1 foci formation after IR exposure at 0.5h and disappearance of foci at 4h and 8h, iPSCs showed delay of disappearance of γ-H2AX and 53BP1 foci compared with fibroblasts. Furthermore, iPSCs showed apoptotic γ-H2AX foci at 4h and 8h after IR exposure.

3. Conclusion

In this study, we showed hypersensitivity of iPSCs to the ionizing radiation exposure. This result was not consistent with previous reports that PSCs show high DNA repair activity. However, we also detected gene expression alteration RNA sequence result using next generation sequencer that high gene expression of DNA damage response factors such as *ATM, ATR, NBS1* and *MRE11* in iPSCs. Furthermore, we found that apoptosis related genes such as *TP53, BAX* and *BID* also upregulated in iPSCs. These results suggested that iPSCs have high DNA repair and apoptosis activity and after DNA damage, first, it is repaired and leads to cell death even DNA repaired cells. To prove this hypothesis, we need further experiments. Our experiments expected to contribute to understand of radiation effect in mammalian development.

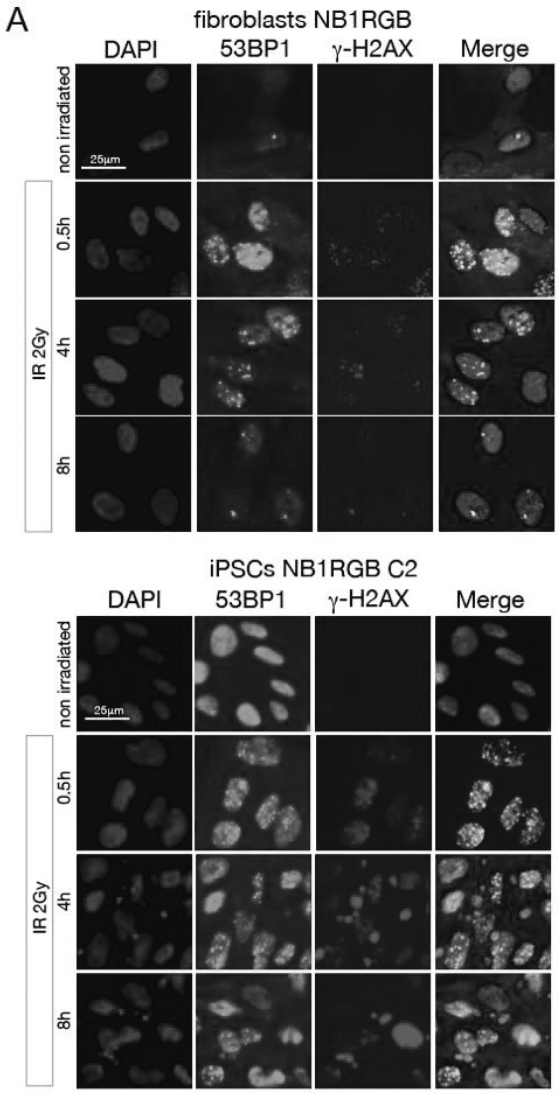

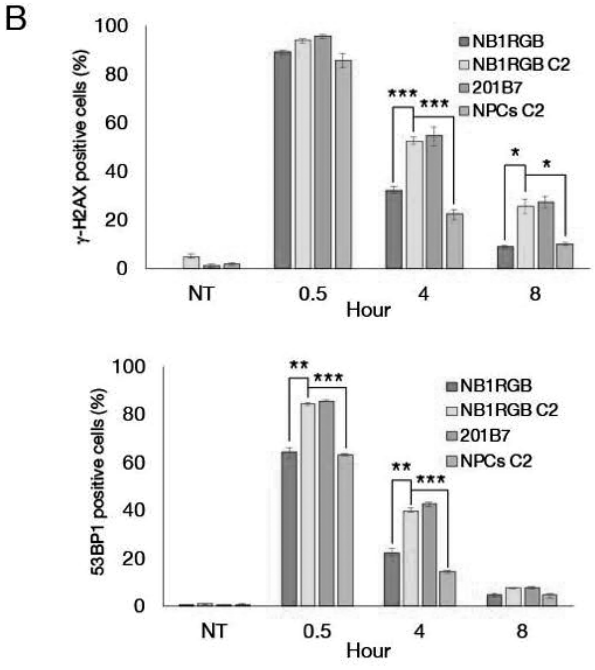

Fig. 2 DNA damage response in iPSCs
After gamma-ray exposure at 2Gy, human fibroblasts and iPSCs were fixed and stained with DNA damage markers γ-H2AX and 53BP1 antibodies(A). 200 Cells with γ-H2AX and 53BP1 foci were counted at least 3 times and graphed (B).

Acknowledgment

Author thanks to Dr. Matsumoto laboratory member for critical discussion and Mr. Isao Yoda for technical assistance.

Reference

1. Mikio Shimada, Naoya Kase, Kaima Tsukada, Yoshihisa Matsumoto: DNA damage response and cell cycle checkpoint in iPSCs; *60th annual meeting of Japanese radiation research society*, Oct. 2017.

D.4 Flow Direction Control of Laser-produced Plasma by a Magnetic Nozzle

Jun HASEGAWA

1. Introduction

The source plasma of the laser-ablation ion source (LAIS) is usually produced by a short-pulsed laser (~10 ns) and then expanded in a long drift space to obtain a pulse length (typically ≥ ~1 μs) suitable for injection into accelerators. Since the laser-ablation plasma becomes collisionless shortly after its generation, plasma ions travel ballistically from a small laser spot in the drift space, enabling us to obtain ion flux having small momentum dispersion in transverse directions at the end of the drift space. This feature of the laser ablation plasma is greatly advantageous in extracting low emittance ion beams. On the other hand, one of the critical issues on the LAIS is a decrease in the plasma ion flux after expansion in the drift space. To suppress the flux decrease, the radial confinement of laser ablation plasmas using a long solenoid magnetic field is often employed. This magnetic confinement of the source plasma is very effective, but it probably degrades the plasma ion directivity because of gyration motions of the ions in the field. One possible way to satisfy both requirements on ion directivity and plasma ion flux is to enhance the plasma ion flux by a divergent magnetic field locally induced near the laser target. When the laser-produced plasma plume interacts with a magnetic field immediately after the laser irradiation, the Lorentz force $\boldsymbol{J}\times\boldsymbol{B}$ acts on the plasma, where $\boldsymbol{J}$ is the diamagnetic current flowing in the surface layer of the plasma plume. When the Lorentz force exceeds the plasma pressure, it can compress the plasma radially and enhance the ion flux density. The purpose of this study is to clarify the magnetic nozzle effects on a laser-produced dense plasma flow and evaluate its potential as a method to enhance plasma ion flux without degradation of ion directivity.

2. Experimental and Numerical Methods

A schematic of our LAIS test bench is given in Fig. 1. The plasma production chamber is evacuated down to about 10^5 Pa by a turbo molecular pump. A KrF excimer laser (λ=248 nm, 200-300 mJ, 30 ns FWHM) is focused onto a plane copper target with an incident angle of 45º and a laser spot size of ~0.5 × 0.5 mm^2. The laser power density on the target is typically 10^8–10^9 W/cm^2. The target is mounted on a remote-controlled two-axis stage to change the laser irradiation position on the target without breaking vacuum. A solenoid coil is located 0.5 mm downstream from the laser target coaxially with the plasma drifting axis. The laser-produced plasma expands and drifts into vacuum through the solenoid. A pulse current up to 2 kA (peak) from a LCR circuit induces a magnetic field of around 300 mT at the center of the solenoid. Because of the skin effect, the induced magnetic field cannot penetrate the copper target in the early stage of field excitation, leading to a nozzle-like field structure. Figure 2 shows the magnetic field at the current maximum calculated by COMSOL Multiphysics®. As shown in the figure, the magnetic flux density strongly depends on the position, so we use the absolute value of the field $|\boldsymbol{B}|$ at the solenoid center to refer the field strength in this study. The timing of laser irradiation with respect to the triggering of the LCR circuit is precisely controlled by a delay and pulse generator. In the present study, the laser was triggered when the induced magnetic field reached the maximum. To monitor the plasma ion flux modulated by the magnetic field, two ion collectors (IC1 and IC2) were used. IC1 was mounted on a rotational motion feedthrough to examine the angular distribution of the ion flux. The angular position of IC1 was varied in a range from 0º to 50º with respect to the center axis (0º corresponds to the direction normal to the target surface). The distance of IC1 from the laser spot was 20 mm or 30 mm depending on the support rod between the cup and the feedthrough. On the other hand, IC2 was mounted on a linear motion feedthrough to measure the plasma ion flux at various positions along the center axis. The axial position of IC2 was changed in a range from 427 mm to 627 mm from the target. Each ion collector was contained in a shielding cage and biased to –50V with respect to the plasma potential to measure ion flux from the

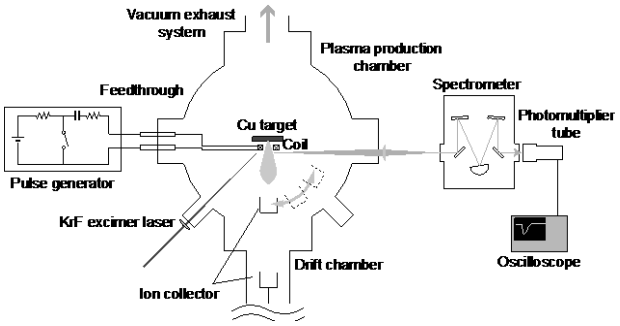

Fig. 1. Schematic of the experimental setup.

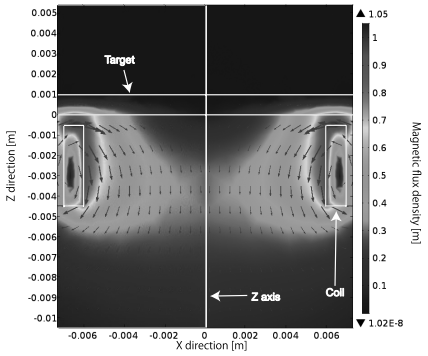

Fig. 2. Magnetic field induced by a coil near the laser target.

source plasma. The sizes of the entrance apertures of IC1 and IC2 are, respectively, 1 mm and 5 mm in diameter. The behavior of a laser-ablation plasma in a divergent magnetic field was investigated also numerically with a 2D hybrid particle-in-cell (Hybrid PIC) code, in which ions are treated as particles and electrons are treated as a continuous fluid. Since we are interested only in the plasma phenomena having a time scale more than microseconds, the motion of each plasma electron is ignored in this numerical model, so the quasi-neutrality condition, i.e., $n_i \approx n_e$, where n_i is ion density and n_e is electron density, is assumed to be always established. The initial velocity distribution of plasma ions were determined so that the calculated ion flux waveform could reproduce the waveform measured in the experiment without the magnetic field.

3. Results and Discussion

Figure 3(a) shows typical waveforms of plasma ion flux observed by IC2 located 427mm downstream from the target. The ion flux increases with increasing magnetic field and a remarkably large enhancement in the ion flux occurs when the magnetic field reaches 0.3 T. The amount of total ion charge deposited on IC1 was evaluated from each ion flux waveform by changing the angular position of the collector from 0º to 50º with an interval of 5º and their angular dependencies are polar plotted in Fig. 3(b)-(d). One can see that the total charge delivered to the direction normal to the target (0º) enhances by a factor of 2 when 0.3 T was applied. This is due probably to plasma compression in the radial direction caused by the $\boldsymbol{J}\times\boldsymbol{B}$ force. Interestingly, the enhancement of the delivered charge is more predominant in the directions from 5º to 25º as shown in Fig. 3(c), where the enhancement reaches 3 with θ=15º. When the distance from the target to IC1 is increased from 20 mm to 30 mm, the angle with which the enhancement reaches the maximum shifts to 5º as shown in Fig. 2(d). This tendency indicates that some ions in the peripheral part of the plasma plume move inward when they travels from z = 20 mm to 30 mm. These results support that the magnetic nozzle improves the

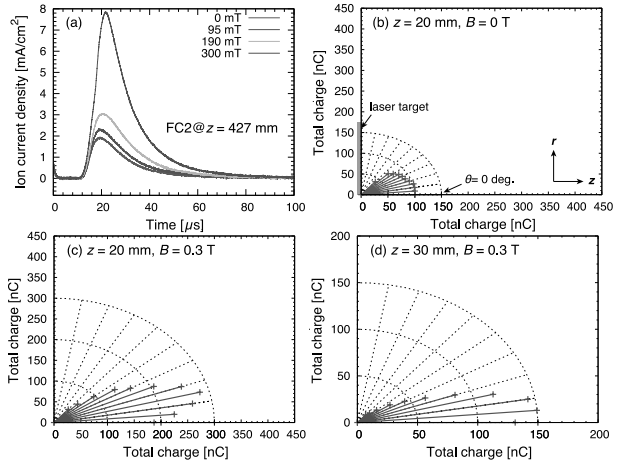

Fig. 3. (a) Typical waveforms of plasma ion flux measured by IC2 with z = 427 mm. The amount of total ion charge detected by IC1 with (b) z = 20 mm, B = 0 T, (c) z = 20 mm, B = 0.3 T, and (d) z = 30 mm, B = 0.3 T.

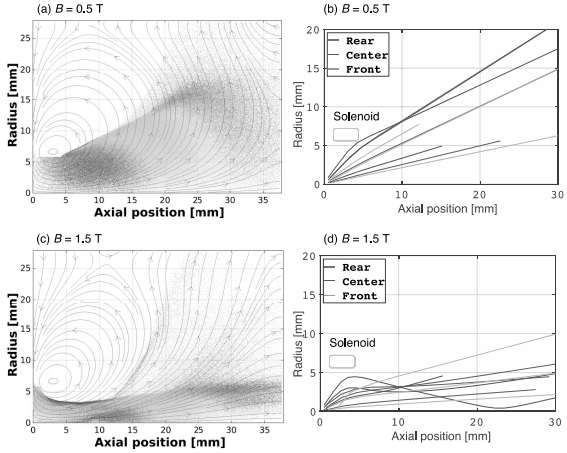

Fig. 4. (a) Ion distribution in the r-z plane with B = 0.5 T. (b) Trajectories of specific ions in the plasma plume. (c) Ion distribution in the r-z plane with B = 1.5 T. (d) Trajectories of specific ions in the plasma plume. Colors in (a) and (c) indicate the initial positions of calculated particles.

directivity of ion flow in the laser-produced plasma in two different ways: 1) magneto-hydrodynamical compression of the core part of the plasma plume caused by magnetic pressure and 2) focusing of ions in the peripheral part of the plasma plume caused by the collective focusing effect. The remarkable enhancement in the plasma ion flux observed downstream far from the target (Fig. 3(a)) is probably due to the collectively focused ions.

Numerical results obtained by the hybrid PIC simulation are shown in Fig. 4. Clearly, the ion directivity is drastically improved by increasing magnetic field from 0.5 T to 1.5 T as shown in Fig. 4(a) and (c). Trajectories of ions having smaller initial velocities (labeled “rear” in Fig. 4(b) and (d)) are bent more strongly than those with larger initial velocities because they spend more time in the strong field region near the solenoid. These results strongly support the mechanisms that we discussed above and qualitatively reproduce the experimental observations. A large difference in the magnetic field strength between the experiment and the simulation is due probably to the underestimation of plasma conductivity in the simulation that determines the strength of the $\boldsymbol{J}\times\boldsymbol{B}$ force acting on the plasma.

4. Conclusion

We proved that the magnetic nozzle can improve the ion directivity of a laser-produced plasma plume and there are probably two mechanisms to enhance the plasma ion flux observed downstream. From the view point of beam extraction, flux enhancement by plasma compression is more preferable because the momentum dispersion in transverse directions becomes minimum in this case. Thus, collective focused ions may be less useful in extracting low emittance ion beams because their transverse momentums are relatively large. By optimizing the strength and distribution of the magnetic field, it may be possible to use a part of focused ions more effectively.

D.5 Numerical Analysis of Particle Dynamics in a Linear Inertial Electrostatic Confinement Fusion Device

Jun HASEGAWA

1. Introduction

In the inertial electrostatic confinement (IEC) fusion device, deuterium ions produced by glow discharge are accelerated toward a high-voltage cathode and electrostatically confined in a negative potential well. The recirculating motion of the deuterium ions is expected to enhance fusion reaction rate between deuterons, thus making the IEC device an attractive candidate for compact neutron generators. Various types of IEC neutron sources have been developed and neutron production rates (NPR) more than 10^8 n/s have been achieved.

On the other hand, the actual behaviors of deuterium particles in the IEC device are very complicated because of huge amount of collisional processes between the particles accompanied by momentum transfer, charge exchange, ionization, dissociation and so on. Particularly, interactions between fast particles (D, D^+, D_2, D_2^+, and D_3^+) and background gas molecules (D_2) determines the velocity distributions of the deuterium particles causing D-D fusion reactions. The cross section of D-D fusion reaction strongly depends on particle velocity in an energy range less than a few hundred keV. Thus, for optimizing the design of the IEC device, it is important to understand correlations between the operational parameters of the IEC device and the velocity distributions of the fast particles that potentially cause fusion reactions.

The purpose of this study is to develop a one-dimensional numerical model including various collisions and reactions between fast ions/atoms and background neutral molecules, and to investigate the dependence of the fusion reaction rate on the discharge parameters. To check the validity of the model, we compare calculated Hα spectra with experimentally observed ones. We evaluate also fusion reaction rates under various discharge conditions.

2. Experimental Setup

Figure 1 shows a cross-sectional view of the linear IEC device developed as a new compact neutron source. The overall structure of the device is axisymmetric. A hollow cathode and two facing anodes made of stainless steel are arranged coaxially on the center axis with gap lengths of 115 mm. The cathode has an inner diameter of 60 mm and a length of 100 mm. The anode consists of coaxially arranged two cylinders having inner diameters of 20 mm and 75 mm. The electrode thickness is 10 mm. The side walls are 8-mm-thick glass tubes having an inner diameter of 134 mm.

Fuel gas is supplied from one end of the device through a solenoid valve (≤10 sccm) and evacuated by a turbo molecular pump from the other end of the device. The pumping speed is limited by a manual valve located before the pump. The gas pressure is maintained to be ~1 Pa by controlling the solenoid valve with a feedback signal from a diaphragm pressure gauge.

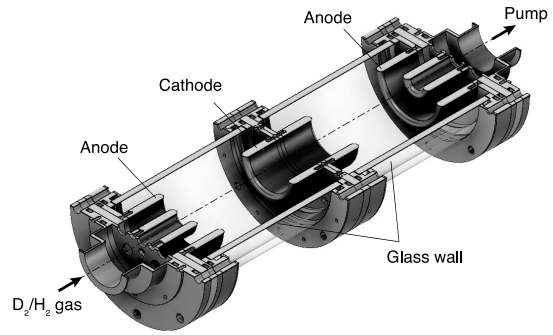

Fig. 1. A cross-sectional view of the linear IEC device.

In the present study, the cathode was negatively biased up to –30 kV by a regulated high-voltage power supply to induce high-voltage glow discharge in hydrogen gas. The power supply was operated in a constant current mode and the discharge voltage was indirectly controlled by changing the hydrogen gas pressure. During operation, a bright plasma column is formed along the center axis of the device.

We performed a spectroscopic measurement of hydrogen Balmer series emission from the discharge plasma using a 50-cm monochromator combined with a high-resolution EMCCD camera. The light emitted from the region inside the hollow cathode was extracted through the anode center hole and focused by a ø30-mm plano-convex lens (f = 300 mm) onto the inlet of an optical fiber connected to the spectrometer. The wavelength resolution of this spectroscopy system is calculated to be ~0.045 nm/px if all aberrations of the optics are ignored.

3. Numerical model

A one-dimensional numerical model based on the Monte Carlo (MC) method was developed to obtain the distribution functions of fast particles $f_i(x, v)$ in the linear IEC device. Here, x and v are, respectively, the position and velocity of hydrogen atoms when they cause Hα emission after charge-exchange reactions with background deuterium/hydrogen molecules. The suffix i denotes the species of parent particles such as H^+, H_2^+, H_3^+, H, and H_2. To calculate the probabilities of various collisional reactions, we used hydrogen cross sections given in the literature. The followings are particularly important because they lead to the Balmer-α emission:

$$H^+ + H_2 \rightarrow H\ (n=3) + \ldots \quad (1)$$

$$H_2^+ + H_2 \rightarrow H\ (n=3) + \ldots \quad (2)$$

$$H_3^+ + H_2 \rightarrow H\ (n=3) + \ldots \quad (3)$$

$$H + H_2 \rightarrow H\ (n=3) + \ldots \quad (4)$$

$H_2 + H_2 \rightarrow H\ (n=3) + ...$ (5)

By reactions (2) and (3), excited hydrogen atoms are produced through the dissociation of fast molecules (H_2 and H_3). Thus, they have a half or a third of the kinetic energy that the parent molecular ions gain in the electrostatic field. Fast neutral atoms (H) and molecules (H_2), which are produced by charge exchange reactions between ions and background molecules, also causes Hα emission through the reactions (4) and (5).

In the case of deuterium gas discharge, the same cross section data was used for deuterium particles having equivalent velocities. In addition, D-D fusion reactions were considered. Since fusion cross sections are much smaller than those for the other atomic processes, they were artificially enhanced ($\times 10^8$) in this model to obtain a sufficient number of fusion reactions within a practical calculation time.

The electrostatic potential calculated in advance by using COMSOL Multiphysics® was imported to the MC code. Because the model treated a weakly ionized plasma, the Debye shielding was ignored. The position and velocity of a particle were advanced by the leap-frog method and recorded in each time step until the particle escapes from the calculation region. By accumulating 10^7 trials and analyzing the particle record, we obtained distribution functions related to specific events such as Hα emission and D-D fusion reaction.

3. Results and Discussion

Figure 2 shows a typical Hα spectrum (solid line) observed with a glow discharge of 30 kV, 10 mA, and 0.57 Pa. In addition to a sharp central peak, broad red- and blue-shifted peaks due to the "beam" components of hydrogen atoms are separately observed on both sides of the central peak. Clearly, these side peaks are composed of Hα emissions originating from different ion species. The highest energy evaluated from the far edge of the side peaks well coincides with the maximum acceleration energy of H^+ ions.

Figure 2 also compares the numerically predicted Hα spectrum (dotted line) with the observed one. Although the relatively high energy parts of the Doppler-shifted components are well reproduced by the MC calculation, there exist large discrepancies between the experiment and

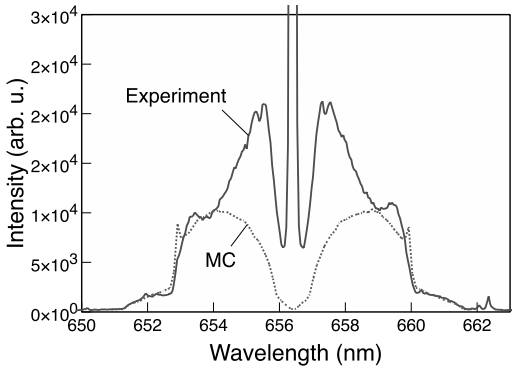

Fig. 2. Comparison between a numerically predicted Hα spectrum and an experimentally obtained one.

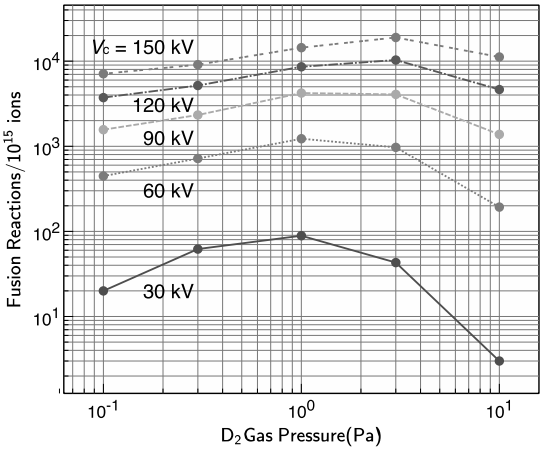

Fig. 3. Dependencies of the number of D-D fusion reactions on discharge voltage and background gas pressure.

the MC calculation. This is probably because the uniform spatial distribution of the initial ions was incorrect. The ion impact ionization (β effect), which is not taken into account in the present MC code, may contribute to the generation of the initial ions much more than expected.

Figure 3 shows the dependencies of the number of fusion reactions on the discharge voltage and the background deuterium gas pressure. One can see that the number of the D-D fusion reactions drastically increases with increasing the discharge voltage. Meanwhile, there is an optimal gas pressure that maximizes the fusion reactions in each discharge condition with fixed cathode voltage. The optimal gas pressure slightly increases from 1 Pa to 3 Pa with increasing discharge voltages from 30 kV to 150 kV, indicating that smaller gap distances are more preferable when we operate the IEC device with higher discharge voltage.

In Fig. 3, the MC calculation predicts that $\sim 4.2\times10^3$ neutrons can be generated by 10^{15} initial ions under a discharge voltage of 90 kV. When the discharge current is 10 mA, we can evaluate the ion production rate to be $0.01\ A/1.6\times10^{-19}\ C \simeq 6.3\times10^{16}\ s^{-1}$. Thus, the NPR in the above discharge condition is estimated to be $4.2\times10^3/10^{15}\times6.3\times10^3 \simeq 2.6\times10^5$ n/s. This is smaller than the NPR obtained in our experiment using the linear IEC device by a factor of about 4. In order to obtain more reliable data, it is necessary to improve the numerical model, but the model is probably useful for examining the scaling rule of NPR.

4. Conclusions

We developed a 1D numerical model based on the MC scheme to predict the spatial and velocity distributions of Hα emitting fast hydrogen atoms generated from various ion species in IEC devices. The model was partly successful in reproducing the experimentally observed Hα emission spectra and neutron production rates. Thus, this numerical approach will be more useful for optimizing the design of IEC devices if its accuracy is more improved.

E. Fundamental Research Division

E.1 Study for nuclear fission and its application

Chikako ISHIZUKA and Satoshi CHIBA

1. Introduction

Nuclear fission has been studied for eighty years since its discovery. However, we still cannot explain the whole property of nuclear fission even of ^{236}U with sufficient predictive power, although empirical models have been applied to practical use. Such practical models may work well in the case of n-induce fission of ^{235}U and ^{239}Pu. On the other hand, in order to develop Accelerator-driven Systems (ADS) and Fast Reactors (FR), and to reduce the TRU wastes, we need high quality data on minor actinides (MA). Experiments to obtain fission data for MA and long-lived fission products (LLFP) have been performed in various facilities. But it is still difficult to cover whole fission data, such as fission fragment mass distributions (FFMDs), thermal energy (total kinetic energy; TKE), prompt and delayed neutrons, and decay heat from the fission products. We are working on the reduction of poisonous nuclear wastes by studying the whole mechanism of nuclear fission process from scission to β-decay, and by developing high-quality nuclear data. In our laboratory, we have also investigated the influence of nuclear data on the decommissioning costs.

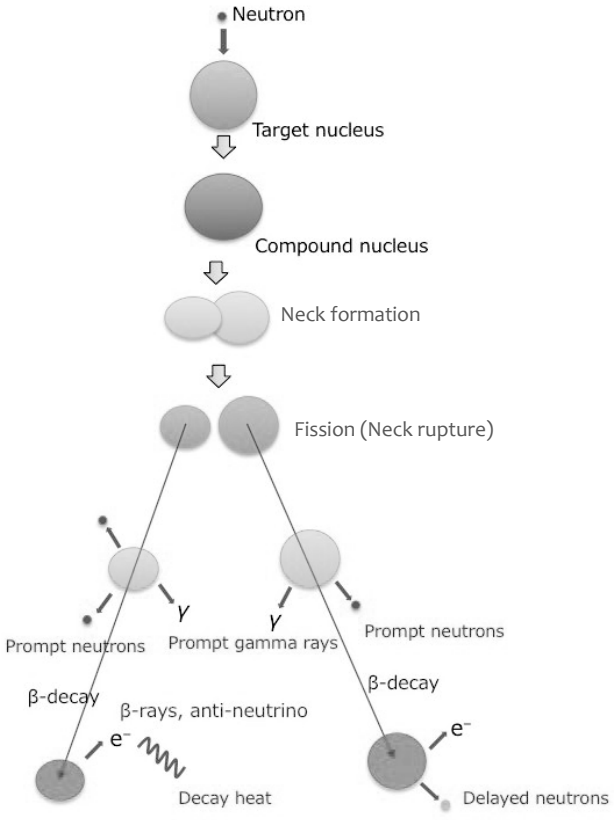

Fig.1 Schematic view of nuclear fission process

2. Fundamental studies for nuclear fission

In our laboratory, we have studied the fundamental mechanism of nuclear fission at low energies using various nuclear-physics theories such as Multidimensional Langevin models, Anti-symmetrized Molecular Dynamics model, and Time-dependent Hartree Fock model. Nuclear fission is the motion of a many-body quantum system. It is still very difficult to describe the whole feature of a nuclear fission process with a single model. Indeed, there is no theoretical model, which can completely simulate the whole process of nuclear fission shown in Fig.1. Therefore, we have adopted different models depending on our purpose.

2.1. Multidimensional Langevin models

Langevin models can reproduce and predict not only the fission product mass yields but also the total kinetic energies of the fission fragments of actinides. In the Lanvin model, a nuclear fission process is regarded as a time-evolution of the nuclear shape of a fissioning nucleus following the equation of motion under the friction force and the random force. Such equation of motion is called the Langevin equation. We have developed the Langevin model by extending degree of freedom to describe a fissioning nuclear shape [1], by improving the potential energy [1], and by [2].

2.2. Anti-symmetrized Molecular Dynamics (AMD) model

The Langevin models cannot directly provide the spins of fission fragments and the division of nuclear excitation energy among fission fragments. Those quantities has been investigated by the Quantum molecular dynamics (QMD). However, a nucleus is a quantum many-body system of fermions such as protons and neutrons. Fermions are anti-symmetric under particle exchange. Therefore we need to extend the QMD to include such anti-symmetrization for more precise description of nuclear fissions, though such extension had not been performed for long time due to the difficulty of the model. Such model with the anti-symmetrization is called the Anti-symmetrized Molecular Dynamics (AMD), which is a very powerful model to describe both nuclear reactions and nuclear structures. We have developed the AMD for the microscopic study of nuclear fission mechanisms and applied it to the ^{236}U fission for the first time.

2.3. Time-dependent Hartree Fock (TDHF) model

In the standard Langevin models, the friction force is provided by the potential derivatives with a macroscopic coefficient evaluated the one-body dissipation model. In order to valid such friction force, we have performed the Time-dependent Hartree Fock (TDHF) calculations. The

TDHF model can derive the friction coefficient considering all nucleon degree of freedom. Then we study the friction coefficient using TDHF to valid the friction strength we have used in the Langevin model.

3. Beta decay of fission products

After prompt neutrons and gammas emitted from the fission fragments, the beta-decays of these nuclei will occur. Neutrinos produced by the beta-decay process play a significant role in the surveillance and in-service inspection in nuclear power plants. In our laboratory, we have studied the anti-neutrino spectrum from aggregate fission products beta-decays based on the gross theory.

4. Evaluation of nuclear data and development of nuclear fission data library for various applications

High precision nuclear data is necessary to economically evaluate the total heat from the fission products and their toxicity. Major nuclear data libraries such as JENDL-4.0 contain ambiguity due to the experimental data and human errors during coding process. In our laboratory, we have investigated the suspicious nuclear data, and have examined its influence on transmutation and decommissioning. For example, we found the possibility of 20% overestimation in the cross section of thermal neutron caption on 102Ru of JENDL-4.0, where Ru-isotopes affect the transmutation efficiency using nuclear reactors. We also evaluated the ambiguity in the fission neutron spectrum in JENDL-4.0, which may influence the activation of reactor structural materials. Nuclear data is the most basic data for nuclear reactors. Therefore we have to pay much attention to its precision, and develop better nuclear data. For this aim, we have studied nuclear fission from the fundamental mechanism.

Acknowledgment

This work was supported by the grant "Research and development of an innovative transmutation system of LLFP by fast reactors" entrusted to the Tokyo Institute of Technology, "Development of prompt-neutron measurement in fission by surrogate reaction method and evaluation of neutron- energy spectra" entrusted to JAEA, and "Concept of a nuclear fuel cycle using an environmental load-reducing light-water reactor" entrusted to Toshiba by the Ministry of Education, Culture, Sports, Science and Technology of Japan (MEXT). The authors also thank the WRHI (World Research Hub Initiative) program of Tokyo Institute of Technology, and IAEA CRP on beta-delayed neutrons (F41030).

Reference

1. Chikako Ishizuka, Mark D. Usang, Fedir A. Ivanyuk, Joachim A. Maruhn, Katsuhisa Nishio, and Satoshi Chiba, Physical Review C 96, 064616 (2017).
2. M. D. Usang, F. A. Ivanyuk, C. Ishizuka, and S. Chiba, Physical Review C 96, 064617 (2017).

E.2 Diagnostics of Microwave Discharge Low-Pressure Argon Plasma by Multi-Optical Emission Line Analysis Based on Collisional-Radiative Model

Hiroshi AKATSUKA, Atsushi NEZU

Conventionally, probe method has been applied to measure electron temperature T_e and density N_e of processing plasma. However, it disturbs the plasma. Therefore, it is required to establish diagnostic method by optical emission spectroscopic (OES) measurement. We proposed the OES diagnostic method for the low-pressure argon plasma. In this work, the applicability for the microwave discharge argon plasma is reported.

The CR model describes excited-state density n_i with the i-th level on the assumption that the essential excitation-kinetic processes are electron collisional excitation/de-excitation and the radiative transition, where the input parameters are T_e, N_e, the ground-state density n_1, the pressure p, the atomic temperature T_a, and so on. Generally, in the rate equations, the relaxation time of n_i is sufficiently longer than that of T_e and N_e. Therefore, we can approximate as $dn_i/dt = 0$ by quasi-steady state approximation. Based on the Ar collisional-radiative (CR) model, the dominant elementary possesses were extracted for the excitation kinetics for several excited states. And, the excitation-kinetic model for the OES diagnostics was established. As a result, the diagnostic model was obtained. In the model, input parameter is 15 optical emission lines (wavelength range: 340.7 – 912.5 nm). Possible measurement range is $1.0 \le T_e$ [eV] ≤ 3.8, and $1.0 \times 10^9 \le N_e$ [cm^{-3}] $\le 5.0 \times 10^{12}$ [1].

For i (Racah symbol) = 24 (6p'), we got Eq. (1) and found that dn_{24}/dt is described with n_i, where i = 8 (4p'[3/2]$_{1,2}$), 19 (5p'), 21 (4d'+6s'), 24 (6p'), 26 (5d'+7s'), 27 (5d+7s), 29 (5f, g), and 30 (7p'). With electron collisional excitation $C_{i,j}$ and de-excitation $F_{i,j}$, atomic collisional excitation $K_{i,j}$ and de-excitation $L_{i,j}$, we have

$$\begin{aligned} dn_{24}/dt \simeq\ & C_{8,24}N_e n_8 + C_{19,24}N_e n_{19} + C_{21,24}N_e n_{21} \\ & -\left(C_{24,26} + C_{24,30} + C_{24,36}\right)N_e n_{24} \\ & +F_{26,24}N_e n_{26} + F_{30,24}N_e n_{30} - F_{24,19}N_e n_{24} \\ & -\left(K_{24,27} + K_{24,29}\right)n_1 n_{24} \\ & +L_{27,24}n_1 n_{27} + L_{29,24}n_1 n_{29} \simeq 0. \end{aligned} \quad (1)$$

In order to evaluate the model, the degree of inflow and outflow population equilibrium for i = 24 was calculated with Eq. (2). We found that N_e is more essential than T_e for the value of f_{ekme}.

$$f_{\mathrm{ekme}}(T_e, N_e) = \frac{POP}{DEP} - 1, \quad (2)$$

where, POP indicates total population inflow to the level and DEP total population outflow from the level [2].

In order to examine the validity of the proposed method, microwave discharge argon plasma was diagnosed with (A) probe measurement: (A-1) under the assumption that the electron density distribution function (EEDF) is Maxwellian, (A-2) together with the measurement of the EEDF by the Druyvesteyn's method, and equivalent T_e measurement; and (B) OES measurement by the present proposed method at points (from the center of the waveguide) = 10, 14, and 18 cm, with the microwave power = 100, 300, and 500 W.

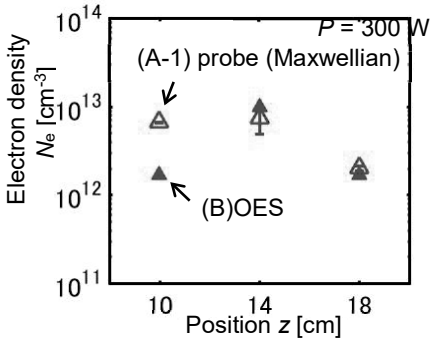

Fig. 1 The position dependence of electron density

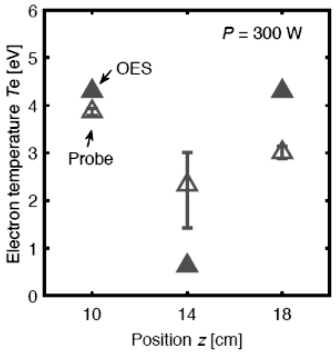

Fig. 2 The position dependence of electron temperature

Concerning N_e diagnosis, the trend of N_e determined with the scheme (B) was in good agreement with the scheme (A-1), which is shown in Fig. 1. Meanwhile, as for T_e diagnosis, it was difficult to evaluate, because the result of the scheme (B) reached the limit value of root-finding range in the numerical procedure, as shown in Fig. 2. However, at least, the result of (A-1) is considered to be reasonable. And by using input with arbitrary shaped EEDF is measured by the OES measurement, and the resultant improvement of the diagnostic result can be expected [3].

Reference

1. Y. Yamashita, H. Akatsuka: 78th Jpn. Soc. Appl. Phys. (JSAP) Autumn Meeting, 2017, September 5 – 8, Fukuoka, Japan, 5a-A413-7 (2017).
2. Y. Yamashita, H. Akatsuka: 39th International Symposium on Dry Process (DPS2017), Nov. 16 – 17, Tokyo, Japan, P-17 (2017).
3. Y. Yamashita, F. Yamazaki, A. Nezu, H. Akatsuka: 65th Jpn. Soc. Appl. Phys. (JSAP) Spring Meeting, 2018, March 17 – 20, Tokyo, Japan, 17p-C204-3 (2018).

E.3 Spectroscopic study on CO b $^3\Sigma^+$ state in microwave discharge CO_2 plasma and the effect of rare-gas admixture

Hiroshi AKATSUKA, Atsushi NEZU

Carbon dioxide plasma is widely applied in practical engineering, for example, decomposition of CO_2 into CO molecule or even synthesis of hydrocarbons for energy storage or for environmental purpose, etc. It should be also remarked that CO molecules are sometimes added even to the semiconductor processing plasmas for the purpose of improvement of selection ratio in the etching process, to which rare gases are also added simultaneously. Therefore, we will investigate spectroscopic characteristics of the third positive system (3PS) of CO molecule in the microwave discharge CO_2 plasma mixed with rare gases for the purpose of experimental understanding of the excitation kinetics of CO b $^3\Sigma^+$ state and its vibrational and rotational temperatures. We will also carry out probe measurement of the CO_2 with rare gas plasmas to understand the electron temperature and density. Based on the dependence of the plasma parameters on the discharge conditions including the rare gas admixture ratio, we would like to discuss the remarkable atomic and molecular processes dominated in the excitation kinetics of CO molecules.

Details of the apparatus were described elsewhere [1]. We applied CO_2 gas with one of rare gases, He, Ar and Kr, to the discharge quartz tube with its i.d. 26 mm. The discharge pressure was set at 1 Torr and the microwave output power was set at 400 – 500 W. In the present study, we determined the vibrational and the rotational temperatures of CO 3PS with the best fitting parameters for the theoretical calculation of the OES spectrum observed experimentally. In the vibrational and rotational fitting, we assumed their distribution function to be Maxwellian. An example of the 3PS spectral fit of CO_2 plasma is shown in Fig. 1.

Figure 2 shows the dependence of the vibrational temperature T_v on the rare gas mixture ratio with a constant total discharge pressure P = 1 Torr and the microwave power 500 W at z = 100 mm. When the rare gas admixture ratio was less than 20%, T_v was to be almost constant, 0.15 – 0.20 eV. Meanwhile, when Kr was added more than 60%, the vibrational temperature of CO b state was found to increase remarkably.

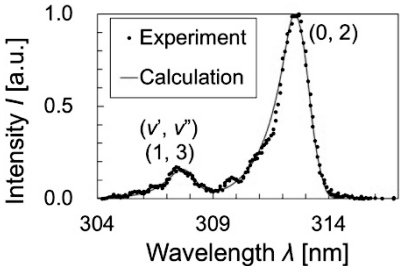

Fig. 1 Theoretical fitting of CO 3PS spectrum for microwave discharge CO_2 plasma without rare gas admixture.

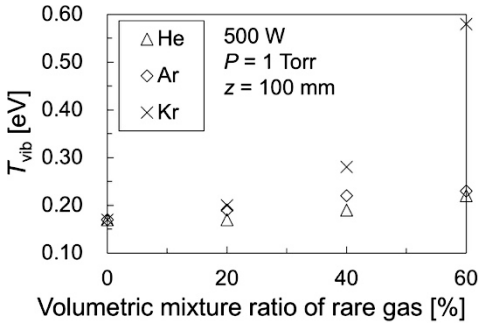

Fig. 2 Dependence of the vibrational temperature T_v on the rare gas mixture ratio. Discharge pressure P = 1 Torr, the microwave power 500 W, at the position z = 100 mm.

Now we consider that this remarkable change of T_v with Kr admixture is attributed to the resonant energy transfer from the Kr metastable level. Figure 3 shows the schematic energy diagram of CO molecule. This figure shows that the metastable state of Kr 5s'[1/2]$_0$ has almost resonant energy level with v = 1 and 2 levels of CO b $^3\Sigma^+$ state. Consequently, the excitation energy of Kr metastable resonantly transfers to these vibrational levels, and it is concluded that the remarkable increase in the vibrational temperature of CO b state was observed [2, 3].

Reference

1. H. Akatsuka, H. Kawano, K. Naoi, H. Matsuura, A. Nezu: Jpn. J. Appl. Phys., Vol.56, No.5, 056102 (2017).
2. Y. Morita, A. Nezu, H. Akatsuka: 10th Asia-Pacific International Symposium on the Basics and Applications of Plasma Technology (APSPT-10), Dec. 15 – 17, Taoyuan, Taiwan, P1-03 (2017).
3. Y. Morita, A. Nezu, H. Akatsuka: 40th International Symposium on Dry Process (DPS2018), Nov. 13 – 15, Nagoya, Japan, P-26 (2018).

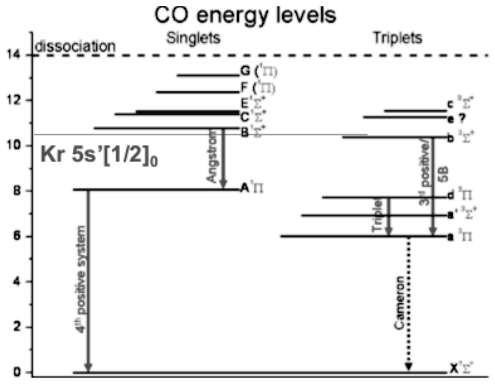

Fig. 3 Schematic energy diagram of CO molecule and Kr metastable.

E.4 Heat Transfer of Submerged Ar Arc Plasma to Water for the Decommissioning of Degraded Nuclear Power Plant

Hiroshi AKATSUKA, Atsushi NEZU

Arc discharge plasma is expected as a basic technology for decommissioning of nuclear reactors, even after severe-accident like Fukushima Daiichi Nuclear Power Plant. Laser technology is considered to be difficult due to color center formation by γ-ray. Hence, arc-cutting technology is one of the promising methods, together with submerged arc discharge plasma. However, the water flow and the heat transfer from the arc plasma to water, submerged structural materials and nuclear fuel debris is not yet understood well. The main objective of the present study is to investigate the water flow characteristics, particularly, to examine the velocity of the bubbles and the heat transfer to the ambient water.

Figure 1 schematically shows the plasma generator and other equipment. Concerning the arc-discharge generator, the anode was made of copper and the cathode of 2%-thoriated tungsten. Further details are given elsewhere [1]. We measured flow velocity distribution in the vicinity of the arc plume ejected into the water. The bubbles formed in the water enable us to trace the water flow by Particle Image Velocimetry (PIV). Figure 2 shows the observed flow velocity, which shows that the flow velocity ranges about 20 – 80 cm/sec, increasing with the increasing arc discharge current, together with the position dependence. Meanwhile, we measured electron temperature T_e and density with spectroscopic measurement of continuum spectrum [2]. Since the argon arc plasma in the present study is generated under atmospheric pressure with large DC current more than 100 A, it is justifiably considered to be in a state of thermodynamic equilibrium. It was found that T_e ranges about 0.6 – 2.2 eV, where it becomes lower as it flows to the downstream direction [2].

We also examined heat flux by measuring the water temperature with thermocouples at various positions in the water. Figure 3 shows the observed heat flux in terms of Nusselt number plotted against the electron temperature. It should be noted that the Nusselt number Nu is defined as

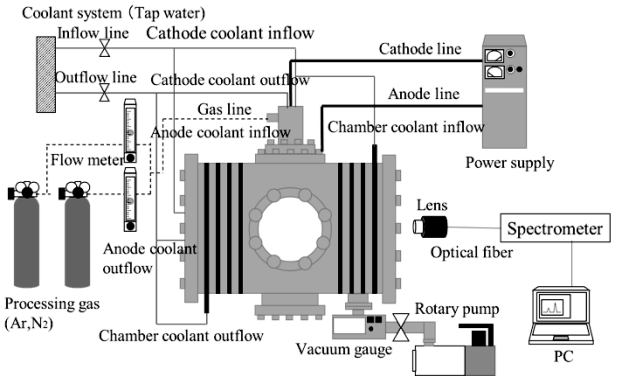

Fig. 1 Experimental set up.

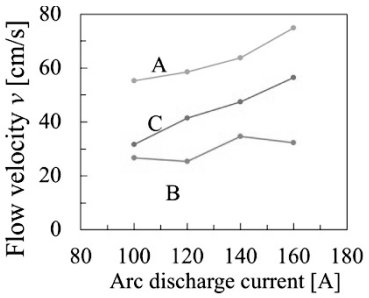

Fig. 2. 3-D Flow velocity measured with PIV method. A, C and C denote the observed position: A - just near the anode nozzle, B - deepest in the bubbles, and C - rising bubbles.

follows:

$$Nu = (h^* C_p D_e)/\lambda_c \,, \qquad (1)$$

where h^* is the heat transfer coefficient for the plasma, C_p is the constant pressure specific heat, D_e is the representative length, taken as plasma column diameter, and λ_c is the thermal conductivity averaged over plasma temperature from the axis to the plasma-wall interface. We found a peak of Nu for $T_e \sim 8000$ K, which can be attributed to the dominant recombination of Ar^+ ion on the interface. It is considered that this temperature range could give us an optimized operation condition in terms of thermal efficiency in the decommission processes of degraded reactors [3].

Reference

1. R. Suzuki, D. Hirotani, Y. Matsuoka, A. Nezu, S. Mori, H. Akatsuka: Plasma Conf. 2017, Nov. 20 – 24, Himeji, Japan, 21P-94 (2017).
2. Y. Matsuoka, D. Hirotani, R. Suzuki, A. Nezu, S. Mori, H. Akatsuka: Joint Tech. Meeting Plasma Sci. and Technol., Pulsed Power Technol. Elec. Discharge, May 15 – 17, Kyoto, Japan, PST-17-024, PPT-17-024, ED-17-024 (2017).
3. J. Kawamura, R. Suzuki, Y. Matsuoka, D. Hirotani, A. Nezu, S. Mori, H. Akatsuka: 10th Asia-Pacific International Symposium on the Basics and Applications of Plasma Technology (APSPT-10), Dec. 15 – 17, Taoyuan, Taiwan, PA04 (2017).

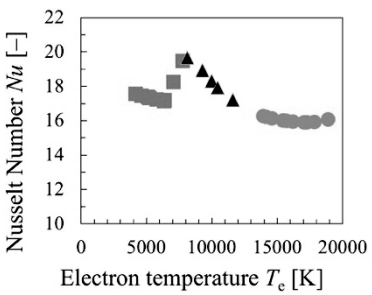

Fig. 3 Nusselt number plotted against the electron temperature on the plasma axis.

II. Co-operative Researches

II. Co-operative Researches

II.1 Co-operative Researches within Tokyo Institute of Technology

(1) Research on Remote Measurement Technology using Robot, Associate Prof. Gen Endo in Department of Mechanical Engineering, Tokyo Institute of Technology
(2) MD simulation study on aqueous electrolyte solutions, J. Habasaki, School of Materials and Chemical Technology
(3) Live imaging system for visualization of DNA damage response in a wide range of eukaryotic organisms based on the life cycle of Ku, Yoichi Tagawa, Hiroshi Iwasaki, Hideo Tsubouchi, Shinji Masuda, Takashi Suzuki, Atsushi Kawakami, Yuya Hattori.
(4) Development of droplet injection ICP-AES/MS for the element analysis in a single cell, Akitoshi Okino.
(5) Possible measurements of nuclear data using laser based neutron sources, Chikako Ishizuka, Satoshi Chiba
(6) Study on prompt-neutron emission mechanism of nuclear fission based on a statistical model, Chikako Ishizuka, Shin Okumura, Satoshi Ciba
(7) Development of quantitative evaluation method for charge polarization using Langevin model, Chikako Ishizuka, Satoshi Chiba
(8) Measurement of Arc Plasmas Generated in Water for the Application to Decommissioning of Fukushima No. 1 Nuclear Power Plant, Graduate Majors Chemical Science and Engineering
(9) Analysis of Nuclear Data important for Non-destructive Assay Technology in the field of nuclear non-proliferation and security, KAKENHI 17K07005

II.2 Co-operative Researches with Outside of Tokyo Institute of Technology

(1) Study on numerical kinetic analysis method by integral kinetic model with delayed neutrons, Hiroki Takezawa, Tokyo City University
(2) High-Temperature Solar Thermal Energy Recovery, Cross-ministerial Strategic Innovation Promotion Program, Cabinet Office, Government of Japan, 2014-2017.
(3) Solid oxide electrolysis cell development for CO_2 reduction, JSPS Grant-in-Aid for Scientific Research (B), 2016-2019.
(4) Carbon Recycling Ironmaking System, Research Committee on Smart Ironmaking System, ISIJ.
(5) Research on accessibility for removal of fuel debris in BWR plant after severe accident, Tohoku University, Japan Atomic Energy Agency.
(6) Research on Thermal-hydrodynamics for Future Light Water Reactor, Energy System and Chemical Technology Development, Prof. Hai Ngoc Duong of Vietnam Academy of Science and Technology.
(7) Research on Two-phase Flow Dynamics for Future Light Water Reactor Development, Director Won-Pil Baek and Manager Chul-Hwa Song of Korea Atomic Energy Research Institute.
(8) Research on Fluid Engineering, Prof. Hideki Kawai of Muroran Institute of Technology.
(9) Research on Multiphase Flow Engineering, Prof. Mituaki Ochi and Assistant Prof. Kenji Kofu of Nihon University.
(10) Research on Treatment, Disposal of Radioactive Waste and Nuclear Safety, Associate Prof. Kazushi Kimoto of Okayama University.
(11) Research on Thermal-hydrodynamics for Future Light Water Reactor, Energy System and Chemical Technology Development, Prof. Horst-Michael Prasser of Swiss Federal Institute of Technology (ETH Zurich).
(12) Property Measurement of High Efficiency Solar Cell, J-Cal Investments, Inc.
(13) Research on Doppler Ultrasonic Flow Rate Measurement Technique, Aichi Tokei Denki Co., Ltd.
(14) Micro/Macro Sclale Evaluation of Buffer Material during Rflooding, Nuclear Safety Research Association (NSRA), Radioactive Waste Disposal Safety Research Center
(15) Research on Nuclear Security for Nuclear Fuel Material Transport Ⅲ, Nulear Fuel Transport Co., Ltd.
(16) Research on Nondestructive Steam Flow Rate Meter, Tokyo Elctric Power Company Holdings, Inc.
(17) Fundamental Research on Application to Actual Power Plant of 3 Dimentional Sensing Technology in Reactor using Pulse Ultrasound, Tokyo Elctric Power Company Holdings, Inc.
(18) Feasibility Study of Mesurement Method for Realtime Visualization and Flow Velocity Measurement of Surrounding Environment, Hitachi-GE Nuclear Energy, Ltd.
(19) Advancement of Doppler Flow Velocity Profile Measurement using Phased Array, Hitachi-GE Nuclear Energy, Ltd.
(20) Research on Development of Flow Rate Measurement Method using Multi Points Simultaneous LDV System, National Institute of Advanced Industrial Science and Technology (AIST) and National Institute of Technology, Toyama College
(21) Advancement Research of Radioactive Substance

Transfer Evaluation Model in Sodium-cooled Fast Reactor, Japan Atomic Energy Agency (JAEA)

(22) Integration of Ultrasonic Measurement System and Robot for Water Leakage Identification and Debris Characteristics Investigation, UK Japan Collaborative Civil Nuclear Research Program, Ministry of Education, Culture, Sports, Science and Technology, Japan (MEXT).

(23) Fabrication of high-purity Pb-Li alloys, National Institutes for Quantum and Radiological Science and Technology, National Institute for Fusion Science, Kyoto University, Tokai University

(24) Development of function sharing interface structure for liquid metal coolant systems, National Institute for Fusion Science, Hirosaki university

(25) Development of liquid Sn divertor for fusion DEMO reactors, National Institute for Fusion Science

(26) Design of Fusion DEMO by Joint Special Design Team, National Institutes for Quantum and Radiological Science and Technology

(27) Study on ion recognition mechanism and separation of f-block element by multidentate *N*,*O*-hybrid donor ligand immobilized gel, Grant-in-Aid for Young Research, Japan Society for the Promotion of Science, 16K18351

(28) Cesium desorption for remediation of Fukushima Radioactive Soils, Grant-in-Aid for JSPS Research Fellow, Japan Society for the Promotion of Science, 17J07598

(29) Study of effective ion recognition and selective separation of f-series elements based on higher oxidation states of Americium, Grant-in-Aid for JSPS Overseas Research Fellowship, Japan Society for the Promotion of Science, 434

(30) Absorption study on specific trivalent lanthanide and valence-different uranium ions by ligand-immobilized soft materials, Masahiko Nakase and Tomoo Yamamura (Inter-University Cooperative Research Program of the Institute for Materials Research, Tohoku University), 17K0086

(31) Synthesis and performance evaluation of titanium acid immobilized zeolite by gel thin-coating method, Hitachi-GE Nuclear Energy Ltd., KY290410.

(32) Study on radioactive Cs removal by subcritical water treatment by utilization of multivalent carboxylic acid, JFE Kankyo Co., KY290028,

(33) Stable solidification of radioactive elements by solid acid dispersed porous glass, Mitsubishi Materials Co., KY290119

(34) Heat calculation of geological repository for high level radioactive waste generated from UO_2 and MOX spent fuels, Radioactive Waste Management Funding and Research Center, JY295037M

(35) Development of cyano-crosslinked coordination polymer material with high sorption ability of platinum group elements for high quality and volume reduction of vitrified glass for high level radioactive wastes, H29 commissioned research from Nagoya University, Japan Science and Technology Agency (JST)

(36) Development of Advanced Micro Analytical System of Radionuclides, Department of Chemical Engineering, University College London UK.

(37) Creation of Photonic Crystal Polymer Device for Metal Ion Sensing, University of South Australia.

(38) Creation of Boron-Incorporating Nanomaterials for Boron Neutron Capture Therapy, International Center for Materials Nanoarchitectonics (WPI-MANA), National Institute for Materials Science (NIMS).

(39) Development of Innovative Analytical System of Radionuclides, Japan Atomic Energy Agency.

(40) Highly Sensitive Detection of Cesium Isotopes, Nuclear Regulation Authority.

(41) Study on Low-Cost Process of SiC/SiC Composites: Japan Aerospace Exploration Agency (JAXA)

(42) Study on Properties of B_4C Neutron-Absorbing Materials for Control Rods: Japan Atomic Energy Agency (JAEA)

(43) Study on Neutron-Irradiation Resistance of Orientation-Controlled Ceramics: National Institute for Materials Science (NIMS)

(44) Sinterability of SiC Ceramics with Al_4SiC_4 Addition and Their Properties: National Institute for Materials Science (NIMS)

(45) Study on the Evaluation of Thermal Shock Fracture Behavior of Ceramics: Tokyo Metropolitan University

(46) Research on Formation and Characterization of Oxide Nanopowder : Vinca Institute, University of Belgrade, Serbia

(47) Development of Porous Ceramics using Natural Minerals for Adsorption and Immobilization of Radioactive Nuclides: Silica Material LLC.

(48) Fundamental Study on Plasma Resistance of Rare-Earth Fluoride Ceramics: Nippon Yttrium Co., Ltd.

(49) Study on Applicability of Alumina-Based Fibers for Ceramics-Based Composites, Denka Co. Ltd., Nitivy Co. Ltd.

(50) Creation of SiC Fiber-Reinforced Composites with Titanium Silicides Matrix, Grant-in Aid for Scientific Research (B), Japan Society for the Promotion of Science

(51) Development of Highly Microstructure-Controlled Ceramic Neutron Absorbers for Improving Safety of Fast Reactors, Innovative Nuclear Research and Development Program, MEXT.

(52) Synthesis and characterization of onion-like carbon with high specific surface area, K. Yamamoto, National Institute of Advanced Industrial Science and Technology (AIST)
(53) Astrobiology Experiments Based on MeV Ion Beams, Division of Materials Science and Chemical Engineering, Faculty of Engineering, Yokohama National University.
(54) Development of a Negative Ion Source for Tandem Accelerators, Atomic Energy Research Laboratory, Tokyo City University.
(55) Selective Irradiation of Cancer Cells by Electrons Emitted from Cancer-Localizing Drugs, Grant-in-Aid for Scientific Research (B), Japan Society for the Promotion of Science.
(56) Development of a Technology to Convert Non-Hazardous Raw Materials into an Anticancer Drug inside a Cancer Cell, Grant-in-Aid for Challenging Exploratory Research, Japan Society for the Promotion of Science.
(57) Biological significance of protein phosphorylating function of DNA-dependent protein kinase in DNA double-strand break repair, Grant-in-Aid for Scientific Research (B) from JSPS.
(58) Structural biology on the effect of hyperthermia on DNA double-strand break recognition protein Ku, Grant-in-Aid for Challenging Research from JSPS.
(59) Unification of effects of radiation and chemical substance and evaluation of personal variance in sensitivity, Research on the Health Effects of Radiation from Ministry of Environment.
(60) Live imaging system for visualization of DNA damage response in a wide range of eukaryotic organisms based on the life cycle of Ku, Integrative Collaboration Research Program of Nuclear Energy from MEXT
(61) Regulation of DNA double-strand break repair through dynamic change in protein secondary structure, Akinari Yokoya (National Institute for Quantum and Radiological Science and Technology).
(62) The control of radiation dependent DNA damage response molecular network, Akihiro Yanagihara, Division of Radiation Biology and Medicine, Department of Medicine, Faculty of Medicine, Tohoku Medical and Pharmaceutical University
(63) Analyze of gene expression alteration after ionizing radiation exposure using chromatin immunoprecipitation sequence method, Hironori Hojo, Center for Disease Biology and Integrative Medicine, The University of Tokyo
(64) Study on Portable Pulsed Neutron Sources, Toshiba Corporation
(65) Development of Highly-Charged Fullerene Ion Source for Induction Synchrotron, KEK
(66) Development of Compact Thermal Neutron Source Using Inertial Electrostatic Confinement, JST
(67) Possible measurements of nuclear data using laser based neutron sources, with Takehito Hayakawa (QST)
(68) Study on prompt-neutron emission mechanism of nuclear fission based on a statistical model, with Toshihiko Kawano (LANL, USA)
(69) Development of quantitative evaluation method for charge polarization using Langevin model, with Katsuhisa Nishio (JAEA)
(70) “Research and development of an innovative transmutation system of LLFP by fast reactors” entrusted to the Tokyo Institute of Technology by the Ministry of Education, Culture, Sports, Science and Technology of Japan (MEXT), with Toshio Wakabayashi (Tohoku Univ.), Yoshiaki Tachi (JAEA), Naoyuki Takaki (Tokyo City Univ.)
(71) "Development of prompt-neutron measurement in fission by surrogate reaction method and evaluation of neutron- energy spectra" entrusted to JAEA by MEXT, with Katsuhisa Nishio (JAEA).
(72) "Concept of a nuclear fuel cycle using an environmental load-reducing light-water reactor" entrusted to Toshiba by MEXT, with Koji Hiraiwa (Toshiba corporation), Takanori Kitada and Satoshi Kitada (Osaka Univ.)
(73) "The study on nuclei and neutron matter using finite-range three-body force" Naoyuki Itagaki (Kyoto Univ.)
(74) Measurement of Vibrational and Rotational Temperature in Spark Discharge Plasma by Optical Emission Spectroscopy, Toyota Central R&D Labs., Inc.
(75) Measurement of Arc Plasmas Generated in Water for the Application to Decommissioning of Fukushima No. 1 Nuclear Power Plant, Kyushu Institute of Technology
(76) Argon Spectral Measurement Using Intensity Ratio Method in Large Helicon Source, Tokyo University of Agriculture and Technology, West Virginia University
(77) Analysis of Instability Phenomenon at Current Interruption in Vacuum Arc Discharge Compared with Silver or Copper Electrode, Miyazaki University, King Mongkut’s University of Technology Thonburi
(78) Assessment of TRU mass balance and nonproliferation by using FAMILY-21 calculation code based on the prediction of nuclear power facility utilization in Japan, Akira Otaki, Japan Atomic Energy Agency.

(79) Quantifying the features of safety and non-proliferation of high temperature gas cooled reactors, Hiroshi Ohashi, Hiroyuki Sato, Japan Atomic Energy Agency.

III. List of Publications

III. List of Publications

Journals

(1) Irwan Liapt Simanullang, Toru Obara: Burnup Performance of a PBR with an Accumulative Fuel Loading Scheme Utilizing Burnable Poison Particles in UO2and ROX Fuels; *Energy Procedia*, Vol. **131**, pp. 61-68 (2017).

(2) Van Khanh Hoang, Toru Obara: Impact of Neutron Spectrum Shift on Breed and Burn Reactor Concept; *Energy Procedia*, Vol. **131**, pp. 33-44 (2017).

(3) Hiroki Osato, Jun Nishiyama, Toru Obara: Study on CANDLE Burning Fast Reactor with Initial Core Using Plutonium from LWR Spent Fuel; *Energy Procedia*, Vol. **131**, pp. 15-20 (2017).

(4) Odmaa Sambuu, Jamyansuren Terbish, Toru Obara, Norov Nanzad, Munkhbat Byambajav: Design parameters in an annular, prismatic HTGR for passive decay heat removal; *Annals of Nuclear Energy*, Vol. **111**, pp. 441-448 (2018).

(5) Delgersaikhan Tuya, Hiroki Takezawa, Toru Obara: Improved approach to multi-region supercritical transient analysis based on the integral kinetic model and Monte Carlo method; *Nuclear Science and Engineering*, Vol. **188**, pp. 33-42 (2017).

(6) Delgersaikhan Tuya, Toru Obara: Supercritical transient analysis in coupled fuel debris systems of symmetric and asymmetric geometry using integral kinetic model; *Annals of Nuclear Energy*, Vol. **109**, pp. 113-119 (2017).

(7) Irwan Liapto Simanullang, Toru Obara: Burnup performance of rock-like oxide (ROX) fuel in small pebble bed reactor with accumulative fuel loading scheme; *Annals of Nuclear Energy*, Vol. **107**, pp. 110-118 (2017)

(8) Julia Abdul Karim, Jun Nishiyama, Toru Obara: Effects of cooling interval time in melt and refining process for CANDLE burning; *Annals of Nuclear Energy*, Vol. **105**, pp.144-149 (2017).

(9) Hiroki Takasu, Shigehiko Funayama, Naoto Uchiyama, Hitoshi Hoshino, Yoshirou Tamura, Yukitaka Kato: "Kinetic analysis of the carbonation of lithium orthosilicate using the shrinking core model"; *J. Ceramics International*, **44** (10), 11835-11839 (2018).

(10) Y. Kato: "Industrial Application of Carbon Recycling Energy System Technology Driven by Nuclear Power"; *Energy Procedia*, **131**, 108–112 (2017).

(11) M. Zamengom, Y. Kato: "Comparison of magnesium hydroxide/expanded Graphite composites for thermal energy storage in cogeneration nuclear power plants"; *Energy Procedia*, 131, 119–126 (2017).

(12) Jun Kariya, Y. Kato: "Development of thermal energy storage material using porous silicon carbide and calcium hydroxide"; *Energy Procedia*, **131**, 395-406 (2017).

(13) M. C. A. Nepomuceno, Y. Kato: "Development of disk-type solid oxide electrolysis cell for CO_2 reduction in an active carbon recycling energy system"; *Energy Procedia*, **131**, 101–107 (2017).

(14) Hiroki Takasu, Yukitaka Kato: "Reactivity enhancement of lithium orthosilicate for thermochemical energy storage material usage"; *Energy Procedia*, **131**, 94-100 (2017).

(15) Emanuela Mastronardo, Lucio Bonaccorsi, Yukitaka Kato, Elpida Piperopoulos, Maurizio Lanza, Candida Milone: "Strategies for the enhancement of heat storage materials performances for $MgO/H_2O/Mg(OH)_2$ thermochemical storage system"; *Applied Therm. Eng.*, **120**, 626-634 (2017).

(16) Hiroki Takasu, Junichi Ryu, Yukitaka Kato: "Application of lithium orthosilicate for high-temperature thermochemical energy storage"; *Applied Energy*, **193**, 74–83 (2017).

(17) Y. Kato, "Principle and Application of Thermochemical Energy Storage"; *Reito* (Refrigeration), **92**, 1077 (2017).

(18) Y. Kato: "Performance Enhancement of Thermochemical Energy Storage Materials by Thermal Conductivity Enhancement"; *Reito* (Refrigeration), **92**, 1075 (2017).

(19) Takehiro Sumita, Kentaro Urata, Yuya Morita, Yoshinao Kobayashi: Dissolution behavior of core structure materials by molten corium in boiling water reactor plants during severe accidents; *Journal of Nuclear Science and Technology*, Vol. **55**, pp. 267-275(2018).

(20) Jiang Liu, Yuya Morita, Kentaro Urata, Takehiro Sumita, Yoshinao Kobayashi: Dissolution behavior of SUS304 stainless steel into Fe-Cr-Ni-BC alloy; *Energy Procedia*, Vol. **131**, pp. 371-378(2017).

(21) Munkhbat Batsaikhan, Ari Hamdani, Hiroshige Kikura: Velocity Measurement on Two-phase Air Bubble Column Flow using Array Ultrasonic Velocity Profiler; International *Journal of Computational Methods and Experimental Measurements*, Vol.6 No. 1, pp.86-97 (2018).

(22) San Shwin, Ari Hamdani, Hideharu Takahashi,

Hiroshige Kikura: Experimental Investigation of Two-Dimensional Velocity on the 90° Double Bend Pipe Flow Using Ultrasound Technique; *World Journal of Mechanics*, Vol. **7**, No. 12, pp.340-359 (2017).

(23) Giedre Zablackaite, Hideo Nagasaka, Hiroshige Kikura:: Microscopic Bubble Behaviour in Suppression Pool During Wetwell Venting; *IOP Conference Series: Materials Science and Engineering*, Vol.**249**, pp.1-8, Paper No.012017 (2017). (Proceedings Journal)

(24) Wongsakorn Wongsaroj, Ari Hamdani, Natee Thong-un, Hideharu Takahashi, Hiroshige Kikura: Ultrasonic Measurement of Velocity Profile on Bubbly Flow Using Fast Fourier Transform (FFT) Technique; *IOP Conference Series: Materials Science and Engineering*, Vol.**249**, pp.1-12, Paper No.012011 (2017). (Proceedings Journal)

(25) Kentaro Kanatani, Takashi Yamamoto, Yutaka Tamaura, Hiroshige Kikura: A model of a solar cavity receiver with coiled tubes; *Solar Energy*, Vol **153**, pp.249-261 (2017).

(26) Munkhbat Batsaikhan, Ari Hamdani, Hiroshige Kikura: Visualisation of air–water bubbly column flow using array Ultrasonic Velocity Profiler; *Theoretical & Applied Mechanics Letters*, Vol.**7**, pp.379-385 (2017).

(27) Keisuke Tsukada, Hiroshige Kikura, Study on Velocity Profile Measurement of saturated Jet Flow by Air-coupled Ultrasound; *Energy Procedia*, Vol **131**, pp.436-443 (2017).

(28) Shun Kimura, Kazumi Kitayama, Kazushi Kimoto, Katsuyuki Kawamura,, Hiroshige Kikura: , Ultrasonic measurement of water content variation in compacted bentonite; *Energy Procedia*, Vol. **131**, pp.428-435 (2017).

(29) Natee Thong-un, Wongsakorn Wongsaroj, Weerachon Treenuson, Jirasak Chanwutitum, Hiroshige Kikura: , Doppler Frequency Estimation using Maximum Likelihood Function for Low Ultrasonic Velocity Profile; *Acoustical Science and Technology*, Vol **38**, No.5, pp. 268-271 (2017).

(30) Masatoshi kondo, Nariaki Okubo, Eriko Irisawa, Atsushi Komatsu, Norito Ishikawa, Teruya Tanaka: Oxidation characteristics of lead-alloy coolants in air ingress accident; *Energy procedia*, Vol. **131**, pp. 386-394, (2017).

(31) Pribadi adhi, Nariaki Okubo, Atushi Komatsu, Masatoshi Kondo, Minoru Takahashi: Electrochemical impedance analysis on solid electrolyte oxygen sensor with gas and liquid reference electrodes for liquid LBE, *Energy Procedia*, Vol. **131**, pp. 420-427, Dec. (2017).

(32) Masatoshi Kondo, Masaomi Ishii, Takayoshi Norimatsu, Takeo Muroga: Experimental study on corrosion and precipitation in non-isothermal Pb-17Li system for development of liquid breeder blanket of fusion reactor; *IOP Conf. Series: Journal of Physics: Conf. Series*, Vol. **877**, (2017).

(33) Teruya Tanaka, Daiji Kato, Takashi Nozawa, Bun Tsuchiya, Masatoshi Kondo, Takeo Muroga. Characterization of functional materials for liquid blanket systems by cathodoluminescence measurement, *Fusion Engineering and Design*, Vol. **125**, pp. 573-576 (2017).

(34) Masatoshi Kondo, Masaomi Ishii, Yoshimitsu Hishinuma, Teruya Tanaka, Takashi Nozawa, Takeo Muroga. Metallurgical study on corrosion of RAFM steel JLF-1 in Pb-Li alloys with various Li concentrations, *Fusion Engineering and Design*, Vol. **125**, pp. 316-325 (2017).

(35) Travis S. Grimes,Colt R. Heathman, Santa Jansone-Popova, Vyacheslav S. Bryantsev, Sriram Goverapet Srinivasan, Masahiko Nakase, Peter R. Zalupski: Thermodynamic, Spectroscopic and Computational Studies of f-Element Complexation by N-hydroxyethyl-diethylenetriamine-N,N',N",N"-tetraacetic Acid; *Inorganic Chemistry*, **Vol.56, No.3**, pp.1722–1733(2017).

(36) Xiangbiao Yin, Lijuan Zhang , Asumi Ochiai, Satoshi Utsunomiya, Hideharu Takahashi, Toshihiko Ohnuki, Kenji Takeshita: Effect of Temperature on K+ and Mg2+ Extracted Desorption of Cs from Vermiculitized Biotite ; *Chemistry Letters*, **Vol.46**, **No.9,** pp.1350-1352(2017).

(37) Xiangbiao Yin, Xinpeng Wang, Hao Wu, Hideharu Takahashi, Yusuke Inaba, Toshihiko Ohnuki, Kenji Takeshita: Effects of NH4+, K+, and Mg2+ and Ca2+ on the Cesium Adsorption/Desorption in Binding Sites of Vermiculitized Biotite ; *Environmental Science & Technology*, **Vol.51**, pp.13886-13894(2017) .

(38) Takashi Onishi, Ken Sekioka, Mitsuo Suto, Kosuke Tanaka, Shinichi Koyama, Yusuke Inaba, Hideharu Takahashi, Miki Harigai, Kenji Takeshita : Adsorption of platinum-group metals and molybdenum onto aluminum ferrocyanide in spent fuel solution; *Energy Procedia*, **Vol.131**, pp.151-156(2017).

(39) Xiaobiao Yin, Nobutake Horiuchi, Satoshi Utsunomiya, Asumi Ochiai, Hideharu Takahashi, Yusuke Inaba, Xinpeng Wang, Toshihiko Ohnuki, Kenji Takeshita: Effective and efficient desorption of Cs from hydrothermal-treated clay minerals for the decontamination of Fukushima radioactive soil; *Chemical Engineering Journal*, **Vol.333**, pp.392-401 (2018).

(40) Masahiko Nakase, Yuto Matsuzawa, Kenji

Takeshita: Modified flow geometry for higher extraction performance with a liquid–liquid centrifugal contactor with Taylor vortices; *Journal of Nuclear Science and Technology*, **Vol.55**, **No.8**, pp.829–837(2018).

(41) Masahiko Nakase, Tohru Kobayashi, Hideaki Shiwaku, Takuya Kawamura, Kenji Takeshita, Tomoo Yamamura, Tsuyoshi Yaita: Extended X-ray absorption fine structure study on gel/liquid extraction of f-block elements; *Nuclear Science and Technology* (accepted)(2018).

(42) Takuya Kawamura, Kenji Takeshita: Extraction and recovery of soft metal ion by porous silica coated by hydrophilic polymer gel with hexavalent nitrogen-donor ligand; *Separation Science and Technology*, **Vol.53**, Issue:9, pp.1319-1326(2018).

(43) Kota Kawai, Hiroshi Sagara, Kenji Takeshita, Masahiro Kawakubo, Hidekazu Asano, Yaohiro Inagaki, Yuichi Niibori, Seichi Sato: High Burn-up Operation and MOX Burning in LWR; Effects of Burn-up and Extended Cooling Period of Spent Fuel on Vitrification and Disposal; *Journal of Nuclear Science and Technology*, **Vol.55**, **No.10**, pp.1130–1140(2018) .

(44) Chunmin Li, Yuezhou Wei, Xinpeng Wang, Xiangbiao Yin: Efficient and rapid adsorption of iodide ion from aqueous solution by porous silica spheres loaded with calcined Mg-Al layered double hydroxide; *Journal of the Taiwan Institute of Chemical Engineers*, **Vol.85**, pp.193-200(2018).

(45) Tatsuya Fukuda, Yoshio Nakano, Kenji Takeshita: Non-isothermal kinetics of the thermal decomposition of gadolinium nitrate; *Journal of Nuclear Science and Technology*, **Vol.55**, Issue10, pp.1193-1197(2018).

(46) Hao Wu, Xiaoxia Zhang, Xiangbiao Yin, Yusuke Inaba, Harigai Miki, Kenji Takeshita: Selective separation of cadmium(II) from zinc(II) by a novel hydrophobic ionic liquid including an N,N,N′,N′-tetrakis(2-methylpyridyl)-1,2-phenylenediamine-4-amido structure: a hard–soft donor combined method; *DaltonTransactions*, **Vol.47**, **No.30**, pp.10063–10070(2018).

(47) Hao Wu , Xiaoxia Zhang , Xiangbiao Yin , Inaba Yusuke, Harigai Miki, Kenji Takeshita: Extraction Behavior of Lanthanides by a Novel Ionic Liquid Including N,N,N′,N′-Tetrakis(2-pyridylmethyl)-1,3-diamino propane-2-amido Structure: A Soft–Hard Donor Combined Strategy; *Chemistry Letters*, 2018, **Vol.47**, **No.6**, pp.732–735(2018).

(48) Haruka Tateno, Ki Chul Park, Takehiko Tsukahara: Direct Extraction of Platinum Group Metals from Nitric Acid Solution Using the Phase Transition of Poly(N-isopropylacrylamide); *Chemistry Letters*, **47**, 318 - 321 (2018).

(49) Ki Chul Park, Haruka Tateno, and Takehiko Tsukahara: Solid phase extraction based on the phase transition of poly(N-isopropylacrylamide): the extraction behaviour of lanthanide(III) ions in highly acidic solutions; *Reaction Chemistry and Engineering*, **3**, 48 - 54 (2018).

(50) Kyojiro Morikawa, Kazuki Matsushita, and Takehiko Tsukahara: Rapid Plasma Etching for Fabrication of Fused Silica Microchannels; *Analytical Sciences*, **33**, 1453 - 1456. (2017).

(51) Yuta Fukatsu, Luc R. Van Loon, Amir Shafizadeh, Daniel Grolimund, Yasuhisa Ikeda, and Takehiko Tsukahara: Effects of Celestite Precipitation in Compacted Illite on the Diffusion of HTO, $^{36}Cl^-$, and $^{22}Na^+$; *Energy Procedia*, **131**, 133 - 139 (2017).

(52) Yuta Fukatsu, Kyojiro Morikawa, Yasuhisa Ikeda, and Takehiko Tsukahara: Temperature and Size Effects on Structural and Dynamical Properties of Water Confined in 1 ~ 10 nm-scale Pores Using Proton NMR Spectroscopy; *Analytical Sciences*, **33**(8), 903 - 909 (2017).

(53) Xiangbiao Yin, Xinpeng Wang, Hao Wu, Toshihiko Ohnuki, Kenji Takeshita, Enhanced desorption of cesium from collapsed interlayer regions invermiculite by hydrothermal treatment with divalent cations, J. Hazardous Materials, 326, (2017) 47-53.

(54) T. Ohnuki, N. Kozai, F. Sakamoto, S. Utsunomiya, K. Kato, Sorption Behavior of Np(V) on Microbe Pure Culture and Consortia, Chem. Lett. 2017, 46, 771. doi.org/10.1246/cl.170068

(55) Genki Furuki, Junpei Imoto, Asumi Ochiai, Shinya Yamasaki, Kenji Nanba, Toshihiko Ohnuki, Bernd Grambow, Rodney C. Ewing, Satoshi Utsunomiya, Caesium-rich micro-particles: A window into the meltdown events at the Fukushima Daiichi Nuclear Power Plant, Scientific reports 7:42731, DOI: 10.1038/srep42731.

(56) Q. Yu, T. Ohnuki, N. Kozai, F. Sakamoto, K. Tanaka, K. Sasaki, Quantitative analysis of radiocesium retention onto birnessite and todorokite, Chemical Geology, 470, 141-151(2017).

(57) 144 Xiangbiao Yin, Lijuan Zhang, Asumi Ochiai, Satoshi Utsunomiya, Hideharu Takahashi, Toshihiko Ohnuki, Kenji Takeshita, Effect of Temperature on K+ and Mg2+ Extracted Desorption of Cs from Vermiculitized Biotite, Chemistry Letter, Vol.46 , No.9, pp. 1350 – 1352(2017).

(58) Yurina Sekine, Ryuhei Motokawa, Naofumi Kozai, Toshihiko Ohnuki, Daiju Matsumura,

Takuya Tsuji, Riku Kawasaki, Kazunari Akiyoshi, Calcium-deficient Hydroxyapatite as a Potential Sorbent for Strontium, Scientific Reports, 7, 2064, DOI:10.1038/s41598-017-02269-z.

(59) Yuriko Nakano , Kenta Ichiyoshi , Keisuke Kawamoto , Ayaka Takeda , Toshihiko Ohnuki , Michael F. Hochella Jr. , Satoshi Utsunomiya, Adsorption of Extracellular Polymeric Substances Derived from S. cerevisiae to Ceria Nanoparticles and the Effects on Their Colloidal Stability, Environments, vol. 4, 48(2017).

(60) Asumi Ochiai , Genki Furuki , Mizuki Suetake , Ryohei Ikehara , Kenji Horie , Mami Takehara , Shinya Yamasaki , Kenji Nanba , Toshihiko Ohnuki , Gareth T. W. Law , Bernd Grambow , Rodney C. Ewing , Satoshi Utsunomiya, Isotopic signature and nano-texture of cesium-rich microparticles: Release of uranium and fission products from the Fukushima Daiichi Nuclear Power Plant, Scientific Reports, Vol. 7, 5409(2017).

(61) Junpei Imoto, Asumi Ochiai, Genki Furuki, Mizuki Suetake, Ryohei Ikehara, Kenji Horie, Mami Takehara, Shinya Yamasaki, Kenji Nanba, Toshihiko Ohnuki, Gareth T. W. Law, Bernd Grambow, Rodney C. Ewing, Satoshi Utsunomiya, Isotopic signature and nano-texture of cesium-rich microparticles: Release of uranium and fission products from the Fukushima Daiichi Nuclear Power Plant, Scientific Reports, 7, 5409, DOI:10.1038/s41598-017-05910-z

(62) Takumi Horiike, Yuma Dotsuta, Yuriko Nakano, Asumi Ochiai, Satoshi Utsunomiya, Toshihiko Ohnuki, and Mitsuo Yamashita, Removal of Soluble Strontium via Incorporation into Biogenic Carbonate Minerals by Halophilic Bacterium Bacillus sp. Strain TK2d in a Highly Saline Solution, Appl. Environ. Microbiol. October 2017; 83:20 11

(63) Shota Masaki, Yuriko Nakano, Kenta Ichiyoshi, Keisuke Kawamoto, Ayaka Takeda, Toshihiko Ohnuki, Michael F. Hochella Jr., Satoshi Utsunomiya, Adsorption of Extracellular Polymeric Substances Derived from *S. cerevisiae* to Ceria Nanoparticles and the Effects on Their Colloidal Stability, Environments, 4, 48, 2017. doi:10.3390/environments4030048.

(64) Tomooki Shiba, Shigetaka Maeda, Hiroshi Sagara, Akihiro Ishimi, Hirofumi Tomikawa: Simple Method to Create Gamma Ray Source Spectrum for Passive Gamma Technique; Energy Procedia, Volume 131, December 2017, Pages 250-257

(65) T. Nagatani, M. Komeda, T. Shiba, M. Maeda, Y. Nauchi, M. Kureta, H. Tomikawa, K. Okumura, H. Sagara, C. Heinberg, K. Hori: Characterization Study of Four Candidate Technologies for Nuclear Material Quantification in Fuel Debris at Fukushima Daiichi Nuclear Power Station; Energy Procedia, Volume 131, December 2017, Pages 258-263.

(66) Masatoshi Kawashima, Hiroshi Sagara: Consideration of Enhanced Safety Based on CMR-concept for Large Fast Reactor; Energy Procedia, Volume 131, December 2017, Pages 230-238.

(67) Rei Kimura, Hiroshi Sagara, Satoshi Chiba: Applicability Study of the Photofission Based Nuclear Material Isotopic Composition Measurement Method on the Thorium Uranium System; Energy Procedia, Volume 131, December 2017, Pages 264-273.

(68) Yoga Peryoga, Hiroshi Sagara and Tomooki Shiba: PHITS Benchmarking for HPGe Detector Efficiency; Energy Procedia, Volume 131, December 2017, Pages 246-249.

(69) H. El-Asaad, H. Sagara, H. Nagai: User Interface of Atmospheric Dispersion Simulation for Nuclear Emergency Countermeasures; Energy Procedia, Volume 131, December 2017, Pages 279-284.

(70) Takeshi Aoki, Hiroshi Sagara and Chi Young Han: Impacts of ^{240}Pu self-shielding effect and uncertainties of $\sigma(n,\gamma)$ at resonance energy on the reactivity controllability in HTGR inert matrix fuel; Progress in Nuclear Science and Technology, Vol. 5, 2017.

(71) Yuhao Jin, Katsumi Yoshida, Zhengcao Li, Tadashi Maruyama, Toyohiko Yano: Precision dilatometer analysis of neutron-irradiated nuclear graphite recovery process up to1673K; *Journal of Nuclear Science and Technology*, Vol. **54,** No**.** 4, pp.424-431 (2017).

(72) Toru Tsunoura, Katsumi Yoshida, Toyohiko Yano, Yukio Kishi: Fabrication, characterization, and fluorine-plasma exposure behavior of dense yttrium oxyfluoride ceramics; *Japanese Journal of Applied Physics*, Vol. **56**, 06HC02 (2017).

(73) Toyohiko Yano, Hiroshi Konishi, Saishun Yamazaki, Mohd Idzat bin Idris, Katsumi Yoshida: Recovery of neutron-irradiation-induced defects of Al_2O_3, Y_2O_3, and yttrium-aluminum

garnet; *Journal of Nuclear Science and Technology*, Vol. **54**, No. 8, pp.891-898 (2017).

(74) Jelena Maletaškić, Nadežda Stanković, Nina Daneu, Biljana Babić, Milovan Stoiljković, Katsumi Yoshida, Branko Matović: Acid leaching of natural chrysotile asbestos to mesoporous silica fibers; *Physics and Chemistry of Minerals*, Vol. **45**, No. 4, pp.343-351 (2017).

(75) Branko Matovic, Jelena Maletaskic, Marija Prekajski Djordjevic, Vesna Maksimovic, Jelena Zagorac, Katsumi Yoshida, Toyohiko Yano: Synthesis and characterization of nanometric gadolinia powders by room temperature solid-state displacement reaction and low temperature calcination; *Journal of the European Ceramic Society*, Vol. **37**, No. 8, pp.2843-2848 (2017).

(76) Jelena Maletaškić, Branko Matović, Nadezda Stanković, Marija Prekajski Djordjević, Jelena Luković, Katsumi Yoshida, Toyohiko Yano: Phase Evolution of Sphene Based Ceramics during Annealing; *Energy Procedia*, Vol. **131**, pp.407-412 (2017).

(77) Mohd Idzat Idris, Saishun Yamazaki, Katsumi Yoshida, Toyohiko Yano: Recovery behavior of SiC_f/SiC composites by post-irradiation annealing up to of 1673 K; *Energy Procedia*, Vol. **131**, pp.413-419 (2017).

(78) Branko Matovic, Marija Prekajski Djordjevic, Jelena Maletaskic, Katsumi Yoshida, Toyohiko Yano: Preparation and properties of hydroxyapatite nano-spheres for immobilization of Sr isotopes; *Energy Procedia*, Vol. **131**, pp.140-145 (2017).

(79) Liang Sun, Yimin Gao, Katsumi Yoshida, Toyohiko Yano, Yefei Li, Yangzhen Liu: Structural, Mechanical, Thermal and Electronic Properties of Novel Ternary Carbide $Al_4Si_2C_5$ under High-Pressure by DFT Calculation; *International Journal of Modern Physics B*, Vol. **31**, No. 3, 1750012 (2017).

~~(80)~~ Liang Sun, Yimin Gao, Katsumi Yoshida, Toyohiko Yano, Wen Wang: Prediction on structural, mechanical and thermal properties of Al_4SiC_4, Al_4C_3 and 4H-SiC under high pressure by first-principles calculation; *Modern Physics Letters B*, Vol. **31**, No. 9, 1750080 (2017).

(81) R. Yamanaka, A.V. Gubarevich, E. Miyazaki, T. Yamaguchi, O. Odawara: Formation of Microparticles from Silicone Contaminants under Simulated Space Environment; *International Journal of Microgravity Science and Application,* Vol.**34**, No.2, p. 340207 (2017).

(82) Y. Hu, H. Fukuda, Y. Oguri: Evaluation of the X-ray Distribution of a Syringe-Needle Type Proton-Induced X-ray Source by Geant4 Simulation; *X-Ray Spectrom.* Vol.**46**, No.5, pp. 356–360 (2017).

(83) Sunatani Y, Kamdar RP, Sharma MK, Matsui T, Sakasai R, Hashimoto M, Ishigaki Y, Matsumoto Y, Iwabuchi K: Caspase-mediated cleavage of X-ray repair cross-complementing group 4 promotes apoptosis by enhancing nuclear translocation of caspase-activated DNase; *Experimental Cell Research*, Vol. **362**, pp. 450-460 (2018).

(84) Someya M, Hasegawa T, Hori M, Matsumoto Y, Nakata K, Masumori N, Sakata K: Local tumor control and DNA-PK activity of peripheral blood lymphocytes in prostate cancer patients receiving radiotherapy; *Journal of Radiation Research*, Vol. **58**, pp. 225-231 (2017).

(85) Hasegawa T, Someya M, Hori M, Matsumoto Y, Nakata K, Nojima M, Kitagawa M, Tsuchiya T, Masumori N, Hasegawa T, Sakata K: Expression of Ku70 predicts results of radiotherapy in prostate cancer; *Strahlentherapie und Onkologie*, Vol. **193**, pp. 29-37 (2017).

(86) Samartha RM, Samartha M, Matsumoto Y: Medicinally important aromatic plants with radioprotective activity; *Future Science OA*, FSO247 (2017).

(87) Mikio Shimada, Hisayo Tsuchiya, Yoshihisa Matsumoto: Effect of different dose rates of ionizing radiation on ciliogenesis in hTERT-RPE1 cells; *Energy Procedia, Elsevier*, Vol. **131C**, pp. 444-447, Dec. 2017.

(88) R. Chiba, Y. Ishikawa, J. Hasegawa, K. Horioka: Time evolution of laser-ablation plumes and induced shock waves in low-pressure gas; *Physics of Plasma*, **24**, 063520 (2017).

(89) Y. Ishikawa, J. Hasegawa, K. Horioka, Y. Iwata: Influence of hydrodynamic behavior of laser ablation plume on cluster formation; *Energy Procedia*, **131**, pp. 319-325 (2017).

(90) S. Kittaka, T. Sodekoda, J. Hasegawa, K. Horioka: Transient Charge Flows Induced by the Evolution of Laser Ablation Plasma; *Plasma and Fusion Res*., **12**, 1201014 (2017).

(91) F.A. Ivanyuk, C. Ishizuka, M.D. Usang, and S. Chiba: *The 4-dimensional Langevin approach to low energy nuclear _ssion*; *EPJ Web of Conferences*, **169**, 00005 (2018).

(92) C. Ishizuka, S. Chiba and N. Carjan: *CHARGE POLARIZATION AND THE ELONGATION OF THE FISSIONING NU-CLEUS AT SCISSION*; *Romanian Reports in Physics*, **70**, 202 (2018).

(93) M. D. Usang, F. A. Ivanyuk, C. Ishizuka, and S. Chiba: *Analysis of the total kinetic energy of _ssion fragments with the Langevin equation*; *Phys. Rev. C*, **96**, 064617-1-13 (2017).

(94) Chikako Ishizuka, Mark D. Usang, Fedir A.

Ivanyuk, Joachim A. Maruhn, Katsuhisa. Nishio, and Satoshi Chiba: *Four-dimensional Langevin approach to low-energy nuclear _ssion of* 236U; *Phys. Rev. C*, **96**, 064616-1-9 (2017).

(95) Chikako Ishizuka, Hiroki Jojima, Mark D. Usang, Satoshi Chiba, and Nicolae Carjan: *The charge polarization and its impact on prompt _ssion neutron multiplicity*; *Energy Procedia*, **131**, 285-291 (2017).

(96) K. Hirose, K. Nishio, S. Tanaka, R. L_eguillon, H. Makii, I. Nishinaka, R. Orlandi, K. Tsukada, J. Smallcombe, M. J. Vermeulen, S. Chiba, Y. Aritomo, T. Ohtsuki, K. Nakano, S. Araki, Y. Watanabe, R. Tatsuzawa, N. Takaki, N. Tamura, S. Goto, I. Tsekhanovich, and A. N. Andreyev: *Role of Multichance Fission in the Description of Fission-Fragment Mass Distributions at High Energies*; Phys. Rev. Lett, **119**, 222501 (2017).

(97) Satoshi Chiba, ToshioWakabayashi, Yoshiaki Tachi, Naoyuki Takaki, Atsunori Terashima, Shin Okumura, Tadashi Yoshida: *Method to Reduce Long-lived Fission Products by Nuclear Transmutations with Fast Spec-trum Reactors*; *Scienti_c Reports*, **7**, Article number: 13961 (2017).

(98) D.S. Martyanov, E.Sh. Soukhovitski~_ , R. Capote, J.M. Quesada, and S. Chiba: *Predicting the optical observables for nucleon scattering on even-even actinides*; *Chinese Physics C*, Vol. **41**, No. 9 094105-1-6 (2017).

(99) Hiroyuki Koura and Satoshi Chiba: *Improvement to the gross theory of* β *decay by inclusion of change in parity*; *Phys. Rev. C*, **95**, 064304-1-6 (2017).

(100) K. Hirose, K. Nishio, H. Makii, I. Nishinaka, S. Ota, T. Nagayama, N. Tamura, S. Goto, A.N. Andreyev, M.J. Vermeulen, S. Gilespie, C. Barton, A. Kimura, H. Harada, S. Meigo, S. Chiba, T. Ohtsuki: Simultaneous measurement of neutron-induced _ssion and capture cross sections for 241Am at neutron energies below _ssion threshold; *Nuclear Instruments and Methods in Physics Research A*, **856**, (2017) 133-138

(101) Tadashi Yoshida, Takahiro Tachibana, and Satoshi Chiba: Analysis of reactor-neutrino spectra fully based on gross theory of beta-decay emphasizing the special role of odd-odd FP nuclide; *EPJ Web of Conferences* **146**, 10003(2017).

(102) Hiroyuki Koura, Tadashi Yoshida, Takahiro Tachibana, and Satoshi Chiba: Improvement of gross theory of beta decay for application to nuclear data; *EPJ Web of Conferences* **146**, 12003(2017).

(103) Yoritaka Iwata : Infinitesimal generators of invertible evolution families ; *Methods Funct, Anal. Topology* **23**, no.1, 26-36 (2017).

(104) Yoritaka Iwata : Alternative infinitesimal generator of invertible evolution families ; *Journal of Applied Mathematics and Physics*, **5**, 822-830 (2017).

(105) J. R. Stone, P. Denielewicz, Y. Iwata: Proton and neutron density distributions at supranoemal density in low- and medium-energy heavy-ion collisions ; *Phys. Rev. C*, **96**, 014612 (2017).

(106) Yoritaka Iwata: Opetator algebra as an application of logarithmic representation of infinitesimal generators ; *J. Phys. Conf. Ser.* ,arXiv :1710. 01858 (accept).

(107) Yoritaka Iwata : Neutrino potential for neutrinoless beta decay ; *Nuclear Physics Review*, vol. **34**, Issue 1, 82-86 (2017).

(108) Yoritaka Iwata:Heavy neutrino potential for neutrinolesss double betadecay ; *Proc.Sci*, arXiv :1710. 07894 (accept).

(109) Hiroshi Akatsuka, Hirokazu Kawano, Koichi Naoi, Haruaki Matsuura, Atsushi Nezu: Experimental Study on Difference in Molecular Rotation Temperatures between Neutral Molecules and Molecular Ions in Nitrogen Plasma and Oxygen Plasma by Optical Emission Spectroscopy measurement; *Japanese Journal of Applied Physics*, Vol. **56**, No. 5, 056102 (2017).

(110) Junya Konno, Atsushi Nezu, Haruaki Matsuura, Hiroshi Akatsuka: Excitation Kinetics of Oxygen $O(^1D)$ State in Low-Pressure Oxygen Plasma and the Effect of Electron Energy Distribution Function; *Journal of Advanced Oxidation Technologies*, Vol. **20**, No. 2, jaots-2017-0002 (2017).

(111) Yurina Honda, Alejandro Álvaro-González, Atsushi Nezu, Hiroshi Akatsuka: Spectroscopic Examination of Fulcher-α Band of Microwave Discharge H_2-D_2 and H_2-He Plasmas; *Energy Procedia*, Vol. **131**, pp.312-318 (2017).

(112) H. Mochizuki, and T. Yano, A passive decay-heat removal system for an ABWR based on air cooling, Nuclear Engineering and Design, 311, (2017), 35-42.

(113) Tadas Kaliatka, Algirdas Kaliatka, Eugenijus Uspuras, M. Vaišnorus, Hiroyasu Mochizuki, W.F.G. van Rooijen, Best estimate approach for the evaluation of critical heat flux phenomenon in the boiling water reactors, Kerntechnik 82, 2, (2017),148-160.

(114) H. Mochizuki, Evaluation of spent fuel pool temperature and water level during SBO, Annals of Nuclear Energy, 109, (2017), 548-556.

(115) H. Mochizuki, Analyses of decay heat removal tests with PRACS and DRACS of a sodium loop using the NETFLOW++ code, Nuclear Engineering and Design, 322, (2017), pp. 345-359.

(116) Keiko Chitose, Hiroyasu Mochizuki, Naoyuki Takaki, Thermal-hydraulic feasibility study of a convex shaped fast reactor core, Energy Procedia, 131 (2017), pp.86-93.

(117) P. S. Uppala, E. Bates, G. Su, I. Di Piazza, H. Mochizuki, H. Ohira, M. Stempniewicz, B. Truong, A. Moisseytsev, L.L. Briggs, T. Sofu, T. Sumner, T. Fei, D. Zhang, D. Sui, W. Hu, L. Maas, B. Vezzoni, M. Marchetti, R. Zanino, D. Caron, W.F. van Rooijen, K. Morita, C. Choi, N. Rtischev, Y. Zhang, K. Mikityuk, etc., Benchmark Analysis of EBR-II Shutdown Heat Removal Tests, PO Box 100, 1400 Vienna, Austria, IAEA, IAEA-TECDOC-1819, ISBN 978-92-0-105517-0 (August, 2017).

International Conference Proceedings

(1) Toru Obara, Delgersaikhan Tuya: Supercritical Kinetic Analysis of Accumulated Fuel Debirs in the Fukushima-Daiichi NPS; *Transactions of the American Nuclear Society*, **117**, 851-852 (2017) Washington, D.C., October 29-November 2, 2017.

(2) Van Khanh Hoang, Jun Nishiyama, Toru Obara: Effect of Compensating for Fuel Losses in Melt and Refining Process for Small CANDLE Reactor; *Transactions of the American Nuclear Society*, **117**, 1487-1488 (2017) Washington, D.C., October 29-November 2, 2017.

(3) Kazuki Kuwagaki, Jun Nishiyama, Toru Obara: Feasibility of Bruning Wave Reactor with Continuous Fuel Movement; *Transactions of the American Nuclear Society*, **117**, 1101-1104 (2017) Washington, D.C., October 29-November 2, 2017.

(4) Hiroki Osato, Jun Nishiyama, Toru Obara: Initial Core Design of CANDLE Bruning Fast Reactor Using Plutonium from LWR Spent Fuel; *Transactions of the American Nuclear Society*, **117**, 1485-1486 (2017) Washington, D.C., October 29-November 2, 2017.

(5) Kazuki Kuwagaki, Jun Nishiyama, Toru Obara; Preliminary Study of Burning Wave Reactor with Continuous Fuel Movement; *Proc. of the Reactor Physics Asia 2017 (RPHA17) Conference*, August 24-25, 2017, Chengdu, China (2017).

(6) Toru Obara, Kazuki Kuwagaki, Jun Nishiyama: Feasibility of Burning Wave Fast Reactor Concept with Rotational Fuel Shuffling; *Proceedings of International Conference of Fast Reactors and Related Fuel Cycles: Next Generation Nculear Systems for Sustainable Development (FR17)*, IAEA-CN245-051, 26-29 June 2017, Yekaterinburg, Russia (2017).

(7) Toru Obara, Van Khanh Hoang, Jun Nishiyama: Concept of small CANDLE reactor with melt and refining process; *Proceedings of 2017 International Congress on Advances in Nuclear Power Plants (ICAPP2017)*, 17739, April 24-28, 2017, Fukui and Kyoto (2017).

(8) Van Khanh Hoang, Jun Nishiyama, Toru Obara: Effect of homogenization of breeding zone in small CANDLE burning reactor with melt and refining process; *Proceedings of 2017 International Congress on Advances in Nuclear Power Plants (ICAPP2017)*, 17696, April 24-28, 2017, Fukui and Kyoto (2017).

(9) S C. Milone, E. Mastronardo, E. Piperopoulos1, Y. Kato, M. Fazio, M. Lanza, S. Galvagno: "Synthetic approaches to efficiency enhancement of heat storage materials"; *European Advanced Energy Materials and Technology Congress*, 25-28 March, 2018, Stockholm.

(10) Y. Kato, H. Nogami: "Development of low carbon emission and material saving ironmaking system, SMART"; *1st International Conference on Energy and Material Efficiency and CO_2 Reduction in the Steel Industry* (EMECR2017), 11-13 October, 2017, Kobe.

(11) H. Takasu, H. Hoshino, Y. Tamura, Y. Kato: "Kinetic analysis of carbonation of lithium orthosilicate for thermochemical energy storage material"; *1st International Conference on Energy and Material Efficiency and CO_2 Reduction in the Steel Industry* (EMECR2017), 11-13 October, 2017, Kobe.

(12) Y. Numata, M. C. A. Nepomuceno, Y. Kato: "Development of Solid Oxide Electrolysis Cells for CO_2 reduction in an Active Carbon Recycling Energy System as applied to iron-making process"; *1st International Conference on Energy and Material Efficiency and CO_2 Reduction in the Steel Industry* (EMECR2017), P-25, 11-13 October, 2017, Kobe.

(13) Yukitaka Kato: [Invited lecture] "High-Temperature Solar Thermal Energy Recovery and Utilization System Development for Energy Carrier Productions"; Plenary: Beyond Power, *SolarPACES2017*, 28 (26-29) September, 2017, Santiago, Chile.

(14) Hiroki Takasu, Hitoshi Hoshino, Yoshiro Tamura, Yukitaka Kato: "Carbonation kinetic study of thermochemical energy storage material of Li_4SiO_4/CO_2"; *International Sorption Heat Pump Conference* (ISHPC2017), 8 (7-10) August, 2017, Tokyo, Japan.
(15) Yukitaka Kato, Massimiliano Zamengo, Keiko Fujioka: "Thermal Conductivity Enhancement Of Thermochemical Energy Storage Material For Performance Improvement"; *International Sorption Heat Pump Conference* (ISHPC2017), 8 (7-10) August, 2017, Tokyo, Japan.
(16) Kentaro Kanatani, Hiroshige Kikura: Condensation Heat Transfer Outside A Veartical Tube With Temperature Variation In The Presence Of Noncondensable Gas; *The 10th International Conference on Boiling and Condensation Heat Transfer (ICBCHT2018)*, March 12-15, 2018, Nagasaki, Japan, pp.1-2, Paper No.A320.
(17) Wongsakorn Wongsaroj, Ari Hamdani, Natee Thong-un, Hideharu Takahashi, Weerachon Treenuson, Hiroshige Kikura: Application of Short Time Fourier Transform in Ultrasonic Velocity Profiler on Bubbly Flow; *The 6th International Electrical Enginnering Congress (iEECON2018)*, March 7-9, 2018, Krabi, Thailand, pp.647-650, Paper No.330.
(18) Jiaju Zhou, Hiroshige Kikura: Masahiro Kawaji, Experimental Investigation of High Viscosity Liquid-liquid Two Phase Diffussion Flow in a Cylindrical Tank for Modeling a Glass Melter; *10th International Symposium on Measurement Techniques for Multiphase Flow (ISMTMF17)*, November 1-4, 2017, Hong Kong SAR, China, pp. 1-8, Paper No.ISMTMF-R001-055.
(19) Tri Vien Tran, Tat Thang Nguyen, Ari Hamdani, Hideharu Takahashi, Hiroshighe Kikura: Measurement of condensation rate and rising velocity of vapor bubbles in subcooled boiling flow using Ultrasonic Velocity Profile method; *10th International Symposium on Measurement Techniques for Multiphase Flow (ISMTMF17)*, December 3-7, 2017, Hong Kong SAR, China, pp. 1-8, Paper No.ISMTMF-R001-057.
(20) Naruki Shoji, Shunsuke Akiguchi, Tomoaki Kyoden, Tsugunobu Andoh, Tadashi Hachiga, Hiroshige Kikura: Real-time Visualization System of Blood Flow Velocity Distribution Using Cross-sectional Multipoint LDV; *The 11th Pacific Symposium on Flow Visualization and Image Processing (PSFVIP-11)*, December 1-3, 2017, Kumamoto, Japan, pp. 1-7, Paper No. PSFVIP11-052.
(21) Masayoshi Kojima, Hiroshige Kikura, Shunsuke Uchida, Hidetoshi Okada: A Safety Analysis Method Based on Harmonization Among Capability Balance; *Comprehensive Capability Value and Risk Priority with Respect to Maintenance Management*, November 13-15, 2017, Yokohama, Japan, Paper No. ASRAM2017-1017.
(22) San Shwin, Ari Hamdani, Hideharu Takahashi, Hiroshige Kikura: VelocityProfile Measurement of Swirling Turbulent Flow Downstream of the Double BendPipe Using Phased Array UVP; *The 12th International Symposium on Advanced Science and Technology in Experimental Mechanics (12th ISEM' 17-Kanazawa)*, November 1-4, 2017, Kanazawa, Japan, pp. 1-6, Paper No.087.
(23) Ari Hamdani, Nobuyoshi Tsuzuki, Gen Endo, Kazushi Kimoto, Hiroshige Kikura: Integration of Ultrasonic Measurement and Robotic System for Measurement in NPP Decommissioning for Fukushima; *2017 ANS Winter Meeting and Nuclear Technology Expo*, October 29 – November 2, 2017, Marriott Wardman Park, Washington DC, United States.
(24) Jevin Tanius Owen, Ari Hamdani, Tomonori Ihara, Hideharu Takahashi, Hiroshige Kikura: Design of New Ultrasonic Transducer with Two Elements for Flow Rate Measurement using Ultrasonic Doppler Method; *ASTECHNOVA 2017 International Energy Conference*, November 1-2, 2017, Yogyakarta, Indonesia.
(25) Shun Kimura, Kazumi Kitayama, Hideharu Takahashi, Katsuyuki Kawamura, Hiroshige Kikura: Longitudinal and Shear wave velocities Measurement in Compacted Bentonite for Water Content; *ASTECHNOVA 2017 International Energy Conference*, November 1-2, 2017, Yogyakarta, Indonesia.
(26) Hiroshige Kikura: Status in Fukushima and Decommissioning Project (Ultrasonic-Robotics Integration for Determination of Leakage from Reactor Vessel and Debris Inspection); *ASTECHNOVA 2017 International Energy Conference*, November 1-2, 2017, Yogyakarta, Indonesia.
(27) Giedre Zablackaite, Hideo Nagasaka, Hiroshige Kikura: Microscopic Bubble Behaviour in Suppression Pool During Wetwell Venting, 14th International Conference on Fluid Control; *Measurements and Visualization (FLUCOME2017)*, October 8-12, 2017, Notre Dame, USA, Paper No.704.
(28) Wongsakorn Wongsaroj, Ari Hamdani, Natee Thong-un, Hideharu Takahashi, Hiroshige Kikura: Ultrasonic Measurement of Velocity Profile on Bubbly Flow Using Fast Fourier Transform (FFT) Technique, *14th International Conference on Fluid Control*; *Measurements and Visualization*

(FLUCOME2017), October 8-12, 2017, Notre Dame, USA, Paper No.551.

(29) Shunsuke Uchida, Hidetoshi Okada, Masanori Naitoh, Masayoshi Kojima, Hiroshige Kikura: Improvement of plant reliability based on fusion of prediction and inspection of wall thinning of piping due to FAC; *5th International Symposium on Materials and Reliability in Nuclear Power Plants & Symposium on Water Chemistry and Corrosion in Nuclear Power plants in Asia-2017 & 3rd Asian Forum on Material Aging Issues in Nuclear System (5th IMRNPP & AWC 2017 & 3rd AF)*, September 26-28, 2017, Shenyang, China, pp.56-67.

(30) Masayoshi Kojima, Hiroshige Kikura, Shunsuke Uchida, Hidetoshi Okada: a New Approach on the Formulation of Maintenance Management Programs with Risk Priority Taken into Account; *5th International Symposium on Materials and Reliability in Nuclear Power Plants & Symposium on Water Chemistry and Corrosion in Nuclear Power plants in Asia-2017 & 3rd Asian Forum on Material Aging Issues in Nuclear System (5th IMRNPP & AWC 2017 & 3rd AF)*, September 26-28, 2017, Shenyang, China, pp.144-155.

(31) Weichen Zhang, Xingguo Wang, Ari Hamdani, Hiroshige Kikura, Junjie Chang, Yasuhiko Ohgiya, Monitoring of Velocity Profile and Wall Thickness in Pipe Flow using Ultrasonic Velocity Profile and Lamb Wave Technique; *5th International Symposium on Materials and Reliability in Nuclear Power Plants & Symposium on Water Chemistry and Corrosion in Nuclear Power plants in Asia-2017 & 3rd Asian Forum on Material Aging Issues in Nuclear System (5th IMRNPP & AWC 2017 & 3rd AF)*, September 26-28, 2017, Shenyang, China, pp.347-360.

(32) Hideharu Takahashi, San Shwin, Ari Hamdani, Tomonori Ihara, Hiroshige Kikura: Development of Phased-array UVP Technique for Turbulent Pipe Flow; *The 28th International Symposium on Transport Phenomena (ISTP-28)*, September 22-24, 2017, Peradeniya, Sri Lanka, pp.1-4, Paper No. ISTP28-53.

(33) Tri Vien Tran, Tat Thang Nguyen, Ari Hamdani, Hideharu Takahashi, Hiroshige Kikura: Measurement of Condensation Rate and Rising Velocity of Vapor Bubbles in Subcooled Flow using Ultrasonic Technique; *The 12th Vietnam conference on Nuclear and Technology (VINANST-12)*, August 2-4, 2017, Nha Trang, Vietnam.

(34) Tat Thang Nguyen, Quang Thai Nguyen, Ngoc Hai Duong, Hiroshige Kikura: CFD Simulations of Natural Cavitating Flow Around High Speed Bodies; *The 2nd Internaional Conference on Advances in Computational Mechanics (ACOME 2017)*, August 2-4, 2017, Phu Quoc Island, Vietnam, pp.141-142.

(35) Tat Thang Nguyen, Quang Thai Nguyen, Ngoc Hai Duong, Hiroshige Kikura: Numerical Experiment of Subcooled Pool Boiling by using CFD Simulation; *The 2nd Internaional Conference on Advances in Computational Mechanics (ACOME 2017)*, August 2-4, 2017, Phu Quoc Island, Vietnam, pp.146-147.

(36) Ryo Nishiwaki, Keisuke Tsukada, Jiaju Zhou, Takuya Kawachi, Hiroshige Kikura: Fundamental Study of Telemetry System with Phased Array Ultrasonic Velocity Profiler Method for Flow Measurement; *25th International Conference on Nuclear Engineering (ICONE25)*, July 2-6, 2017, Shanghai, China, pp.1-5, Paper No. ICONE25-68010.

(37) Munkhbat Batsaikhan, Ari Hamdani, Hiroshige Kikura: Velocity Measurement on Two-phase Air Bubble Column Flow using Array Ultrasonic Velocity Profiler; *9th International Conference on Computational & Experimental Methods in Multiphase & Complex Flow "Multiphase Flow 2017"*, June 20-22, 2017, Tallinn, Estonia, pp.443-453.

(38) Takuya Kawachi, Hiroshige Kikura, Robert Malkin, Bruce W. Drinkwater: Development of Simultaneous Measurement System for Flow Visualization and Surface Reconstruction using Ultrasonic Array Sensors; *9th World Conference on Experimental Heat Transfer, Fluid Mechanics and Thermodynamics (ExHFT-9)*, June 11-15, 2017, Iguazu Falls, Brazil, pp.1-6, Paper No. OC.121.

(39) Munkhbat Batsaikhan, Ari Hamdani, Hiroshige Kikura: Visualisation of Air-water Bubbly Column Flow Using Array Ultrasonic Velocity Profiler; *The 14th Asian Symposium on Visualization (ASV14)*, May 22-26, 2015, Beijing, China, pp.1-11, Paper No. ASV14-MI-03.

(40) Rendy Silva Renata, Kentaro Kanatani, Yutaka Tamaura, Hiroshige Kikura: Numerical Study on Cavity Linear Receiver of the 30kW Cross Linear System Demonstration Plant in India; *International Conference Recent Trends on Energy Storage & Hydrogen Energy*, April 28-29, 2017, Rajiv Gandhi Proudyogiki Vishwavidyalaya, Bhopal, India.

(41) Ryan Naldo Pratama, Kentaro Kanatani, Hiroshige Kikura, Yutaka Tamaura, Investigation of Thermocline on Pilot-scale Rock Bed Thermal Energy Storage System by CFD Simulations; *International Conference Recent Trends on Energy Storage & Hydrogen Energy*, April 28-29, 2017, Rajiv Gandhi Proudyogiki Vishwavidyalaya,

Bhopal, India.
(42) Pribadi Mumpuni Adhi, Masatoshi Kondo, Minoru Takahashi: Study on Performance of Oxygen Sensors with Solid and Liquid Reference Electrodes in Liquid LBE with the Parameters of Oxygen Potential and Temperature, *2017 International Congress on Advances in Nuclear Power Plants*, April 24-28, 2017, Fukui-Kyoto, Japan ICAPP2017-17124.
(43) Masatoshi Kondo, Toru Obara: Plenary presentation, Status of JAPAN LFR activities; *Global Symposium on Lead and Lead Alloy based Nuclear Energy Science and Technology (GLANST 2017)*, September 7-8, 2017 Korea, pp. 39-50.
(44) Masahiko Nakase, Yuto Matsuzawa, Kenji Takeshita: Unique Separation Based on Extraction Kinetics Using a Liquid-liquid Countercurrent Centrifugal Contactor with Taylor Vortices; *International Solvent Extraction Conference 2017 (ISEC2017)*, November 5-9, 2017, Miyazaki, Japan, pp.187-193.
(45) Kazuki Matsushita, Brandt Aileen, Akira Kirishima and Takehiko Tsukahara: *The 21th International Conference on Miniaturized Systems for Chemistry and Life Sciences (MicroTAS 2017)*, October 22-26, 2017, Savannah International Trade & Convention Center, Savannah Georgia, USA.
(46) Kaname Saga, Frederik H. Kriel, Craig Priest and Takehiko Tsukahara: *The 21th International Conference on Miniaturized Systems for Chemistry and Life Sciences (MicroTAS 2017)*, October 22-26, 2017, Savannah International Trade & Convention Center, Savannah Georgia, USA.
(47) Kazuki MATSUSHITA, Takehiko TSUKAHARA: *Global 2017 International Nuclear Fuel Cycle Conference,* September, 25-28, 2017, Grand Walkerhill Seoul, Seoul, South Korea.
(48) Kaname SAGA, Takehiko TSUKAHARA, Ki Chul PARK, Hideyuki SUZUKI, Tetsuro MATSUMURA: *Global 2017 International Nuclear Fuel Cycle Conference,* September, 25-28, 2017, Grand Walkerhill Seoul, Seoul, South Korea.
(49) Takehiko TSUKAHARA, Nutthon YOKACHUKSUSE: *Global 2017 International Nuclear Fuel Cycle Conference,* September, 25-28, 2017, Grand Walkerhill Seoul, Seoul, South Korea.
(50) Min seok Kim, Takehiko TSUKAHARA: *Global 2017 International Nuclear Fuel Cycle Conference,* September, 25-28, 2017, Grand Walkerhill Seoul, Seoul, South Korea.
(51) Haruka TATENO, Takehiko TSUKAHARA: *Actinide 2017,* July 9-14, 2017, Tohoku University, Sendai, Japan.
(52) Masashi Kaneko, Takehiko TSUKAHARA: *Actinide 2017,* July 9-14, 2017, Tohoku University, Sendai, Japan.
(53) T. Takeda, M. Stefanica: Study on Liquid Jet for Neutron Source of BNCT; *19th International Conference on Nuclear Engineering (ICONE20)*, October 24-25, 2012, Paris, France, ICONE20-45600.
(54) H. Sagara, M. Katayama, K. Takao, Y. Naoi, H. Nakamura, C. Y. Han and M. Saito: Academy for Global Nuclear Safety and Security Agent (II) -Nuclear Security Training-; Proc. INMM Annual Mtg. Indian wells, California, 2017.
(55) T. Aoki, H. Sagara, C. Y. Han: Impacts of 240Pu self-shielding effect and uncertainties of σ(n,γ) at resonance energy on the reactivity controllability in HTGR inert matrix fuel; ACTINIDES 2017, Sendai (Japan), July 9-14 (2017).
(56) T.Yoshida: Several learnings from summation calculation of reactor decay heat and antineutrino spectra; *Constants' Meeting on Updation Data Needs for TAGS Measurements*, 19-21 February 2018, IAEA, Vienna, Austria.
(57) Yoritaka Iwata: Spin and isospin response of many-nucleon systems; *EMN Spintronics 2017*, Bangkok, Thailand
(58) Yoritaka Iwata: Cluster structure based on density functional calculations; *WNCP 2017*, Hokkaido University, Japan
(59) Takashi Nishikawa, Yoritaka Iwata, Satoshi Chiba: Study on nuclear friction in terms of time-dependent density functional theory; *Colloque GANIL*, Amboise, France, October 15-20, 2017.
(60) A. Etori, A. Ono, M. Kimura, C. Ishizuka, S. Chiba: Study of fission and nuclear collisions by Antisymmetrized Molecular Dynamics; *Colloque GANIL*, Amboise, France, October 15-20, 2017.
(61) Yoritaka Iwata; Nuclear matter property based on the TDDFT: *NuSYM 2017*, GANIL, Cean, France September 2017.
(62) Yoritaka Iwata; Lie algebra as an application of logarithmic representation of infinitesimal generators; XXV *International conference on Integrable Systems and Quantum symmetries (ISQS25)*, Prague, Czech Republic, June 2017.
(63) Masao Kinoshita, Takayuki Fuyuto, Hiroshi Akatsuka: Measurement of Vibrational and Rotational Temperature in Spark Discharge Plasma by Optical Emission Spectroscopy; *9th International Conference on Modeling and Diagnostics for Advanced Engine Systems (COMODIA 2017)*, July 26 – 28, 2017, Okayama,

Japan, C-307.

(64) Hiroshi Akatsuka, Senna Fukukawa, Atsushi Nezu: The Spectroscopic Characteristics of Nitrogen Molecule Puffed onto Cold Expanding Argon Arc Jet Plasma; *9th International Workshop on Plasma Scientech for All Something (PLASAS-9)*, August 18 – 20, 2017, Kumamoto, Japan, p. 18.

(65) Hiroshi Akatsuka: Diagnostics of N_2-Based Gas Discharge Plasma by Optical Emission Spectroscopy on Atomic and Molecular Processes; *1st Asia-Pacific Conference on Plasma Physics (AAPPS-DPP2017)*, September 18 – 23, 2017, Chengdu, China, Plenary-32.

(66) Yuya Yamashita, Hiroshi Akatsuka: Excitation-Kinetic Model for Argon Processing Plasma Diagnostics by Optical Emission Spectroscopic Measurement Based on Collisional-Radiative Model; *39th International Symposium on Dry Process (DPS2018)*, November 16 – 17, 2017, Tokyo, Japan, pp. 83 - 84.

(67) Yuki Morita, Atsushi Nezu, Hiroshi Akatsuka: Effect of Admixture of Rare Gases on the CO Excited States of Microwave-Excited CO_2 Plasma; *10th Asia-Pacific International Symposium on the Basics and Applications of Plasma Technology (APSPT-10)*, December 15 – 17, 2017, Taoyuan, Taiwan, P1-03.

(68) Jun Kawamura, Ryujiro Suzuki, Yuya Matsuoka, Daisuke Hirotani, Atsushi Nezu, Shinsuke Mori, Hiroshi Akatsuka: Characteristics of Water Flow Induced by the Injection of Arc-Discharge Argon Plasma; *10th Asia-Pacific International Symposium on the Basics and Applications of Plasma Technology (APSPT-10)*, December 15 – 17, 2017, Taoyuan, Taiwan, PA-04.

(69) Koji Kikuchi, Hiroshi Akatsuka: Discussion on Temperatures on the Basis of the Tsallis Entropy Determined by the Excited-State Populations of Hydrogen Atoms in Hydrogen Plasma; *APS March Meeting 2018*, March 5 – 9, 2018, Los Angeles, California, USA, L60.206.

(70) Hiroshi Akatsuka: Some Topics of Low-Temperature Plasma Study as Extensions of Isotope Separation Research; *The 1st Russia-Japan Joint Forum for Education and Research*, March 9, 2018, Tokyo, Japan, Talk-5.

(71) E. Bates, D. Zhang., B. Truong, D. Sui, W. Hu, G. Su, T. Sumner, L. Maas, B. Vezzoni, M. Marchetti, R. Zanino, D. Caron, W.F. Van Rooijen, H. Mochizuki, C. Choi, M. Stempniewicz, N. Rtischev, Y. Zhang, K. Mikityuk, Conclusions of a Benchmark Study on the EBR-II SHRT-45R Experiment, FR17, Yekaterinburg, Russia, 372, (2017), 1-11.

(72) Partha Sarathy U., E. Bates, G. Su, I. Di Piazza, H. Ohira, H. Mochizuki, M. Stempniewicz, B. Truong, A. Moisseytsev and T. Sumner, Thermal Hydraulic Investigation of EBR-II Instrumented Subassemblies during SHRT-17 and SHRT-45R Tests, FR17, Yekaterinburg, Russia, 118, (2017), 1-10.

Oral Presentation in international or domestic conferences

(1) Yukitaka Kato: [Invited Lecture] "Thermochemical energy storage technologies for future low-carbon society"; Research Workshop of Div. of Energy and Resources, Japan Association for Chemical Innovation (JACI), 21 Feb, 2017, Tokyo.

(1) Takeshi Muramoto, Jun Nishiyama, Toru Obara: Criticality safety analysis in falling down of fuel debris in water; *Proc. of 2018 annual meeting of Atomic Energy Society of Japan*, 2F07 (2018).

(2) Kodai Fukuda, Toru Obara, Jun Nishiyama: Radiation Dose by Super Critical Condition of Fuel Debris in Water; *Proc. of 2018 annual meeting of Atomic Energy Society of Japan,* 2F09 (2018).

(3) Kazuki Kuwagaki, Jun Nishiyama, Toru Obara: Possibility of Breed and Burn Reactor with Spiral Fuel Shuffling; *Proc. of 2018 annual meeting of Atomic Energy Society of Japan*, 3F03 (2018).

(4) Delgersaikhan Tuya, Toru Obara: Supercritical transient analysis in hypothetical fuel debris by multi-region based on integral kinetic model; *Proc. of 2017 fall meeting of Atomic Energy Society of Japan*, 2G05 (2017).

(5) Irwan Liapto Simanullang, Toru Obara: Introduction of MOX and Pu-ROX fuels in PBR with accumulative fuel loading scheme; *Proc. of 2017 fall meeting of Atomic Energy Society of Japan*, 3H14 (2017).

(6) Hoang Hai Nguyen, Jun Nishiyama, Toru Obara: Burnup analysis of CANDLE bruning reactor by Monte Carlo based method; *Proc. of 2017 fall meeting of Atomic Energy Society of Japan*, 3H15 (2017).

(7) Jun Nishiyama, Kazuki Kuwagaki, Toru Obara: Feasibility of Breed and Burn reactor with spiral pattern fuel movement; *Proc. of 2017 fall meeting of*

Atomic Energy Society of Japan, 3H17 (2017).
(8) Y. Numata, K. Nakajima, Y. Kato: "SOEC Development for Carbon Dioxide Electrolysis"; *175th Spring Term ISIJ Annual Meeting*, 21 March, 2018, Chiba.
(9) K. Nakaji, K. Nishida, A. Sekimoto, Y. Okano, Y. Kato: "Numerical Analysis of Optimization of Thermochemical Energy Storage System Using EM8"; *20th SCEJ Student Meeting*, 3 March, 2018, Hiroshima.
(10) T. Ohtaki, H. Iguchi, K. Fujioka, Y. Kato: "Reactivity evaluation of thermochemical energy storage materials using calcium chloride / water system in packed bed reactor"; *JSME ICMS 2017 Summer Meeting*, 12 June, 2017, Tokyo.
(11) S. Funayama, Y. Kato: "Evaluation of thermochemical energy storage and output performance of a packed bed of $Ca(OH)_2$ pellets"; *JSME ICMS 2017 Summer Meeting*, 12 June, 2017, Tokyo
(12) H. Takasu, Y. Kato: "Study on high temperature thermochemical energy storage system using lithium orthosilicate"; *Regular Meeting of 54th Committee on ironmaking of JSPS*, Nagoya, 30 June, 2017.
(13) Y. Kato: [Invited Lecture] "Key Points for Social Implementation of Heat Storage Technologies"; *ISISJ Eco-Metallurgy Young Researcher Forum*, 12 July, 2017, Tokyo.
(14) K. Nishida, M. Zamengo, Y. Kato, Y. Okano: "Heat Transfer Phenomena Analysis on MgO/H_2O TcES Packed Bed Reactor"; *SCEJ 49th Autumn Meeting*, 21 September, 2017, Nagoya.
(15) T. Ohtaki, H. Iguchi. K. Fujioka, Y. Kato: "Reactivity evaluation of thermochemical energy storage materials using calcium chloride/water system in packed bed reactor"; *54th Japan Heat Transfer Symposium*, 25 May, 2017, Ohmiya.
(16) K. Nishida, T. Yamamoto, M. Zamengo, Y. Kato, Y. Okano: "Understanding of Heat Transfer in a Packed Bed Reactor Using Thermochemical Heat Storage Material"; *54th Japan Heat Transfer Symposium*, 25 May, 2017, Ohmiya.
(17) Takehiro Sumita, Yoshinao Kobayashi: Investigation on the Dissolution Behavior of Core Structure Materials by Molten Corium in Boiling Water Reactor Plants during Severe Accidents; *The Sixth International Education Forum on Environment and Energy Science*, Canary Islands, Spain, Dec.12th, 2017.
(18) Takehiro Sumita, Yoshinao Kobayashi: Collapse Behavior of Reactor Core Materials in BWR During Severe Accidents; *MIT-Tokyo Tech Workshop on Innovative Nuclear Energy System (MT-INES)*, Cambridge, USA, Oct. 26th, 2017.
(19) Takehiro Sumita, Yoshinao Kobayashi: Investigation on the Fracture Behavior of Core Structure materials by Molten Corium in Boiling Water Reactor Plants during severe accidents; *TITECH-CRIEPI-JAEA Joint Workshop*, Tokyo, JPN, July 4th, 2017.
(20) Takehiro Sumita, Yoshinao Kobayashi: The Fracture Behavior of Solid SS by Molten SS-B4C Eutectic Melt under the Dynamic Condition; *AESJ 2018 Annuak Meeting*, Mar. 26th, 2018.
(21) Takehiro Sumita, Yoshinao Kobayashi: Collapse behavior of stainless steel by molten metallic corium; *Conference for R&D Initiative on Nuclear Decommissioning Technology by the Next Generation (NDEC-3)*, Mar. 19th, 2018.
(22) Takehiro Sumita, Yoshinao Kobayashi, Shigeru Ueda, Toshio Nakagiri: Investigation on the Fracture Behavior of Core Structure Materials by Molten Corium in Boiling Water Reactor Plants during Severe Accidents —Fracture Mode of Stainless Steel by molten Fe-Cr-Ni-B-C—; *AESJ 2017 Fall Meeting*, Sep. 13th, 2017.
(23) Hiroshige Kikura, Hideharu Takahashi, Ari Hamdani, Yutaka Tamaura,"Revitalizics" and Fundamental Study of Cross Linear Concentration System in Tokyo Tech; *International Round Table Conference on CSV and PV for Cost Effective Solar Power*, March 28, 2018, Bhopal, India.
(24) Hideharu Takahashi, Hiroshige Kikura, Ari Hamdani, Yutaka Tamura, Fundamental Study on Heat Storage System using Pebble; *International Round Table Conference on CSV and PV for Cost Effective Solar Power*, March 28, 2018, Bhopal, India.
(25) Kenta Matsumasa, Naruki Shoji, Takuya Kawachi, Hideharu Takahashi, Hiroshige Kikura: A Fundamental Study on Underwater Shape Mapping Using Ultrasound; *The 57th Student Research Workshop of the Japan Society of Mechanical Engineers Kanto Branch*, March 16, 2018, Tokyo, Japan, Paper No. 711. in Japanese.
(26) Atsushi Ito, Hiroshige Kikura, Hideharu Takahashi, Fundamental study of air-coupled ultrasound locationing system for robot transport; *The 11th Student Research Workshop of the Atomic Energy Society of Japan Kanto-Koetsu Branch*, March 1, 2018, Tokyo, Japan, A04. in Japanese.
(27) Kanichi Oyama, Tetsu Kikuhara, Hideharu Takahashi, Makoto Hirose, Hiroshi Sagara, Hiroshige Kikura: Study on Analytical Safety Assessment on Sabotage Against Spent Nuclear Fuel Transportation using High Energy Density Devices; *The 11th Student Research Workshop of the Atomic Energy Society of Japan Kanto-Koetsu Branch*, March 1, 2018, Tokyo, Japan, A09. in

Japanese.
(28) Giedre Zablackaite, Hideharu Takahashi, Hideo Nagasaka, Hiroshige Kikura: Microscopic Bubble Behaviour in Suppression Pool during Wetwell Venting; *The 11th Student Research Workshop of the Atomic Energy Society of Japan Kanto-Koetsu Branch*, March 1, 2018, Tokyo, Japan, B23.
(29) Hiroshige Kikura, Rob Malkin: Study of an ultrasonic measurement system and its robotic deployment into vessels for the combined assessment of debris condition and water leakage; *2018 Annual Meeting of Atomic Energy Society of Japan*, March 26-28, 2018, Osaka, Japan, 1O_PL01. in Japanese.
(30) Hironobu Kiuchi, Shun Kimura, Hideharu Takahashi, Hiroshige Kikura, Daisuke Sasa, Shuichi Omori: Fundamental study on the three-dimensional object shape imaging method using air-coupled ultrasonic sensing; *2018 Annual Meeting of Atomic Energy Society of Japan*, March 26-28, 2018, Osaka, Japan, 1A04. in Japanese.
(31) Shun Kimura, Kazumi Kitayama, Kazushi Kimoto, Hideharu Takahashi, Katsuyuki Kawamura, Hiroshige Kikura: A study on ultrasonic measurement for water distribution investigation in compacted bentonite; *2018 Annual Meeting of Atomic Energy Society of Japan*, March 26-28, 2018, Osaka, Japan, 2L08. in Japanese.
(32) Masayoshi Kojima, Hiroshige Kikura, Hideharu Takahashi, Shunsuke Uchida, Hidetoshi Okada: Risk Based Strategies for Inspection and Maintenance of Nuclear Power Plants 6. Maintenance Management Based on Reliability Evaluation Method Combining PFM and FMEA; *2018 Annual Meeting of Atomic Energy Society of Japan*, March 26-28, 2018, Osaka, Japan, 3K10. in Japanese.
(33) Hidetoshi Okada, Shunsuke Uchida, Masanori Naitoh, Yasuhiro Chimi, Shigeki Kasahara, Satoshi Hanawa, Masayoshi Kojima, Hideharu Takahashi, Hiroshige Kikura: Risk Based Strategies for Inspection and Maintenance of Nuclear Power Plants 7. Improvement of Plant Reliability Based on Fusion of Prediction and Inspection on IGSCC; *2018 Annual Meeting of Atomic Energy Society of Japan*, March 26-28, 2018, Osaka, Japan, 3K11. in Japanese.
(34) Shun Kimura, Kazumi Kitayama, Kazushi Kimoto, Katsuyuki Kawamura, Hiroshige kikura: A Study of the Effect of a Degree of Saturation on Elastic Properties in Unsaturated Compacted Bentonite by Ultrasonic Velocities Measurement; *The Sixth International Education Forum on Environment and Energy Science*, December 15-19, 2017, Tenerife, Spain, Paper No.D131.
(35) Kanichi Oyama, Hideharu Takahashi, Makoto Hirose, Hiroshige Kikura: nclusive Study on Damage Calculation for Sabotage of Spent Nuclear Fuel Package; *38th Annual Meeting of the Institute of Nuclear Materials Management Japan Chapter*, November 21-22, 2017, Tokyo, Japan, P3808. in Japanese.
(36) Tatsuya Fuji, Koki Aotsuka, Yoshihiko Oishi, Hideki Kawai, Hideki Murakawa, Hiroshige Kikura: Effect of low frequency broadband component generated nearby fixed wall in Taylor-Couette flow with small aspect ratio; *Muroran Visualization Symposium 2017*, November 3-4, 2017, Muroran, Japan, OS4-2, pp.1-4. in Japanese.
(37) Yutaro Kato, Yoshihiko Oishi, Hideki Kawai, Hiroshige Kikura: Ultrasound Measurement of Isolated Mixed Region in Taylor-Couette Flow with different size particles; *Muroran Visualization Symposium 2017*, November 3-4, 2017, Muroran, Japan, OS4-3, pp.1-4. in Japanese.
(38) Takuya Kawachi, Ryo Nishiwaki, Shun Kimura, Hideharu Takahashi, Hiroshige Kikura: Development of Echo-PIV using Aperture Synthesis Method; *Muroran Visualization Symposium 2017*, November 3-4, 2017, Muroran, Japan, OS4-5, pp.1-4. in Japanese.
(39) Hiroshige Kikura: MIT-TIT Workshop, October 27, 2017, USA.
(40) Shun Kimura, Hironobu Kiuchi, Takuya Kawachi, Hiroshige Kikura, Daisuke Sasa, Shuichi Omori: Fundamental study on three dimensional shape measurement by air-coupled ultrasonic aperture synthesis; *The 16th Young Researcher Research Workshop of the Atomic Energy Society of Japan Kanto-Koetsu Branch*, October 19, 2017, Tokyo, Japan. .in Japanese.
(41) Kentaro Kanatani, Takashi Yamamoto, Yutaka Tamaura, Hiroshige Kikura: A model of a solar cavity receiver with coiled tubes, *Mechanical Engineering Congress, 2017 Japan*, September, 2017, Saitama, Japan, J0540103. in Japanese.
(42) Shun Kimura, Kazumi Kitayama, Hideharu Takahashi, Kazushi Kimoto, Katsuyuki Kawamura, Hiroshige Kikura: Fundamental Study on Measurement of Water Content and Elastic Property of Compacted Bentonite Buffer Material using Ultrasound Speed; *61th Annual Meeting of The Clay Science Society of Japan*, September 25-27, 2017, Toyama, Japan, A14. in Japanese.
(43) Toshiya Kono, Kazushi Kimoto, Hiroshige Kikura: Development of an immersion ultrasonic imaging method for the shape reconstruction of nuclear fuel debris; *2017 Fall Meeting of Atomic Energy Society of Japan*, September 13-15, 2017, Hokkaido, Japan, 2D20. in Japanese.

(44) Shun Kimura, Kazumi Kitayama, Hideharu Takahashi, Kazushi Kimoto, Katsuyuki Kawamura, Hiroshige Kikura: A Study on Evaluation of Elastic Properties in Unsaturated Compacted Bentonite by Ultrasonic Measurement; *2017 Fall Meeting of Atomic Energy Society of Japan*, September 13-15, 2017, Hokkaido, Japan, 2H21. in Japanese.

(45) Ryo Nishiwaki, Shun Kimura, Hideharu Takahashi, Gen Endo, Hiroshige Kikura: Fundamental study of ultrasonic velocity profiler method for flow measurement and robot; *2017 Fall Meeting of Atomic Energy Society of Japan*, September 13-15, 2017, Hokkaido, Japan, 1P12. in Japanese.

(46) Masayoshi Kojima, Hiroshige Kikura, Shunsuke Uchida, Hidetoshi Okada: Risk Based Strategies for Inspection and Maintenance of Nuclear Power Plants 3. Maintenance management based on reliability evaluation in consideration of responding capability against failure modes; *2017 Fall Meeting of Atomic Energy Society of Japan*, September 13-15, 2017, Hokkaido, Japan, 3F01. in Japanese.

(47) Hidetoshi Okada, Shunsuke Uchida, Masanori Naitoh, Masayoshi Kojima, Hiroshige Kikura: Risk Based Strategies for Inspection and Maintenance of Nuclear Power Plants 4. An Example for Risk Based Inspection for the Events Originating FAC Related Causes; *2017 Fall Meeting of Atomic Energy Society of Japan*, September 13-15, 2017, Hokkaido, Japan, 3F02. in Japanese.

(48) Shunsuke Uchida, Hidetoshi Okada, Masanori Naitoh, Satoshi Hanawa, Masayoshi Kojima, Hiroshige Kikura: Risk Based Strategies for Inspection and Maintenance of Nuclear Power Plants 5. An Example for Risk Based Inspection for the Events Originating IGSCC Related Causes; *2017 Fall Meeting of Atomic Energy Society of Japan*, September 13-15, 2017, Hokkaido, Japan, 3F03. in Japanese.

(49) Jiaju Zhou, Hiroshige Kikura, Masahiro Kawaji, Experimental Investigation of Liquid-liquid Two Phase Diffusion Flow in a Cylindrical Tank for Vitrification of High Level Liquid Wastes; *17th International Topical Meeting on Nuclear Reactor Thermal Hydraulics (NURETH17)*, September 3-8, 2017, Xian China, pp.1-12, Paper No. 20841.

(50) Antonin Povolny, Hiroshige Kikura, Marco Pellegrini, Masanori Naitoh, Improving Accuracy of CFD Modelling for Direct Contact Condensation in a Suppression Pool; *17th International Topical Meeting on Nuclear Reactor Thermal Hydraulics (NURETH17)*, September 3-8, 2017, Xian China, pp.1-14, Paper No.20656.

(51) Shun Kimura, Hironobu Kiuchi, Hiroshige Kikura, Daisuke Sasa, Shuichi Omori: Fundamental study on reconstructed image of three dimensional shape by air-coupled ultrasound; *2017 JSEM Annual Conference on Experimental Mechanics*, August 28-30, 2017, Okayama, Japan, B103. in Japanese.

(52) Naruki Shoji, Tomoaki Kyoden, Shunsuke Akiguchi, Tadashi Hachiga, Hiroshige Kikura: Application to flow rate measurement in circular pipe using multi-point LDV; *2017 JSEM Annual Conference on Experimental Mechanics*, August 28-30, 2017, Okayama, Japan, C116. in Japanese.

(53) Kentaro Kanatani, Hiroshige Kikura: Condensation heat transfer outside a vertical tube with temperature variation in the presence of noncondensable gas; *The 64th National Congress of Theoretical and Applied Mechanics*, August 22-24, 2017, Tokyo, Japan, Paper No.OS2-02-01. in Japanese.

(54) San Shwin, Ari Hamdani, Hideharu Takahashi, Hiroshige Kikura: Effect of Swirling Inlet at Downstream of the Double Bent Pipe Using Phased Array UVP; *45th Symposium on Visualization*, July 18-19, 2017, Tokyo, Japan, A103, pp.1-4.

(55) Tri Vien Tran, Tat Thang Nguyen, Ari Hamdani, Keisuke Tsukada: Hideharu Takahashi, Hiroshige Kikura: Measurement of condensation rate and rising velocity of vapor bubbles in subcooled boiling flow using ultrasonic technique; *45th Symposium on Visualization*, July 18-19, 2017, Tokyo, Japan, A104, pp.1-4.

(56) Yutaro Kato, Yoshihiko Oishi, Hideki Kawai, Hiroshige Kikura: Ultrasound measurement of Isolated Mixed Region in Taylor-Couette flow with small aspect ratio; *45th Symposium on Visualization*, July 18-19, 2017, Tokyo, Japan, A105, pp.1-4. in Japanese.

(57) Hiroshige Kikura: Nuclear Human Resource Development in Tokyo Institute of Technology; *25th International Conference on Nuclear Engineering (ICONE25)*, July 2-6, 2017, London, England. (Panelist)

(58) Marco Pellegrini, Antonio Buccio, Shunsuke Uchida, Masanori Naitoh, Daisuke Yamauchi, Shinya Mizokami, Antonin Povolny, Hiroshige Kikura, L. Araneo, F. Cozzi, M. Ricotti, H. Ninokata; Contribution to Ipresca from the Institute of Applied Energy, *IPRESCA Kick-off meeting & International Workshop on Pool Scrubbing*, June 21-22, 2017, Frankfurt, Germany.

(59) Hiroshige Kikura: Integration of Ultrasonic Measurement and Robotic System for Measurement in Nuclear Power Plant Decommission; *2017 China-Japan NDT*

Symposium, May 18-19, 2017, Suzhou, China.
(60) Zhang Weichen, Wang Xingguo, Yasuhiko Ougiya, Hiroshige Kikura: A Study of the Effect of Pipe Damage on the Flow Measurement Using Ultrasonic Velocity Profiler; *2017 China-Japan NDT Symposium*, May 18-19, 2017, Suzhou, China.
(61) Hiroshige Kikura, Hideharu Takahashi: Progress of Fluid Measurement by Ultrasound Doppler (Application to Ultrasonic Velocity Profiler Method (UVP) and Phased Array Measurement); *4th JSME RC270 Sectional Meeting*, April 7, 2017, Tokyo, Japan. in Japanese.
(62) Pribadi Mumpuni Adhi, Masatoshi Kondo, Minoru Takahashi: Study on Performance of Oxygen Sensors with Solid and Liquid Reference Electrodes in Liquid LBE with the Parameters of Oxygen Potential and Temperature, *2017 International Congress on Advances in Nuclear Power Plants*, April 24-28, 2017, Fukui-Kyoto, Japan ICAPP2017-17124.
(63) Masatoshi Kondo, Toru Obara: Status of JAPAN LFR activities; *Global Symposium on Lead and Lead Alloy based Nuclear Energy Science and Technology (GLANST 2017)*, September 7-8, 2017 Korea, pp. 39-50, Plenary presentation.
(64) Masatoshi Kondo, Yoshimitsu Hishinuma, Takayoshi Norimatsu, Takeo Muroga: Dynamic behaviors of corrosion-erosion and mass transfer in non-isothermal Pb-17Li system; *13th International Symposium on Fusion Nuclear Technology*, Kyoto, Japan, September 25-29, 2017, OA4-2. 3.
(65) Masatoshi Kondo, Yuu Nakajima, Teruya Tanaka, Takayoshi Norimatsu: Study on neutron transport and material activation for development of inertial fusion reactor; *International conference on computation in science and engineering (ICCSE 2017)*, Bandung, Indonesia, July 10-12, 2017, Keynote speech: Key 06.
(66) Takeo Muroga, Masatoshi Kondo. Material issues for liquid metal coolant nuclear systems, First IAEA workshop on challenges for coolants in fast spectrum system: chemistry and materials, Vienna, Austria, Jul. 5-7, 2017.
(67) Masatoshi Kondo: DEVELOPMENT OF SOLID ELECTROLYTE CERAMIC SENSORS FOR OXYGEN AND HYDROGEN MONITORING IN FAST REACTORS AND FUSION REACTORS; *4th Conference of the Serbian Society for Ceramic Materials*, The book of abstracts, June 14-16, 2017, Invited lecture: I-18.
(68) Kenji Takeshita: Recovery of Radioactive Cecium from Clay Minerals in Soil Contaminated by Fukushima Daiichi NPP Accident; *15th Japan-Korea International Symposium on Resource Recycling and Material Science*, Osaka, Japan, April 18, 2017.
(69) Kota Kawai, Hiroshi Sagara, Kenji Takeshita, Masahiro Kawakubo, Hidekazu Asano, Yaohiro Inagaki, Yuichi Niibori, Seichi Sato: Effects of High Burn-Up Operation of LWR and Extended Cooling Period of Spent Fuel on High-Level Waste Properties for Vitrification and Storage; *2017 International Congress on Advances in Nuclear Power Plants (ICAPP '17)* , Fukui and Kyoto, Japan, April 24-28, 2017.
(70) Travis S. Grimes, Masahiko Nakase, Nicholas C. Schmitt, Bruce J. Mincher: Further Studies on the Behavior of Higher Valence Americium in Acidic Solution; *40th Annual Actinide Separations Conference*, San Diego, USA, May 24-26, 2017.
(71) Ryuji Sannomiya*, Xiangbiao Yin, Kenji Takeshita: Recovery of Cesium from Contaminated Soil by Hydrothermal Treatment with Metal Ions; *RCWM2017 (Research Conference on Cementitious Composites in Decommissioning and Waste Management)*, Fukushima, Japan, June 20, 2017.
(72) Lijuan Zhang*, Kenji Takeshita, Hideharu Takahashi: Removal of Cs from Clay Minerals by Hydrothermal Treatment Using Organic Acids; *RCWM2017 (Research Conference on Cementitious Composites in Decommissioning and Waste Management)* , Fukushima, Japan, June 20, 2017.
(73) T. S. Grimes, C. Heathman, S. Jansone-Popova, V. S. Bryantsev, S. Goverapet Srinivasan, *M. Nakase*, P. R. Zalupski: Modified aqueous holdback reagents for improved actinide/lanthanide separations; *72nd Annual Northwest Regional Meeting of the American Chemical Society (NORM2017)*, Corvallis, USA, June 25-28, 2017.
(74) Kenji Takeshita: Extraction Chromatographic Separation of Am(III) and Eu(III) by Porous Silica coating TPPEN-NIPA Gel; *Actinide2017*, Sendai, Japan, July 9-14, 2017, ThB-5.
(75) M. Cibula, Y. Inaba, K. Takeshita, H. Narita: Separation of platinum group metals in HNO3 using thiodiglycolamide and amide-containing tertiary amine extractants; *Actinide2017* , Sendai, Japan, July 9-14, 2017, ThB-5.
(76) *M.Nakase*, T.Kobayashi, H.Shiwaku, T.Kawamura, K.Takeshita, T.Yamamura, T.Yaita : Extended X-ray absorption fine structure study on gel/liquid extraction of f-block elements ; *Actinide2017* , Sendai, Japan, July 9-14, 2017, ThB-5
(77) Kenji Takeshita, Yusuke Inaba, Hideharu Takahashi, Jun Onoe, Hirokazu Narita : Effect of Introduction of Simultaneous Adsorption

System of PGMs and Mo from HLLW on Vitrification Process; *The 4th Japan-China Academic Symposium on Nuclear Fuel Cycle (ASNFC 2017)*, Lanzhou, China, July 17-21, 2017.

(78) Xiaobiao Yin, Hideharu Takahashi, Yusuke Inaba, Kenji Takeshita: Effective and Efficient Removal of Cs from Clay Minerals for Volume Reduction of Radioactive Soli in Fukushima; *The 4th Japan-China Academic Symposium on Nuclear Fuel Cycle (ASNFC 2017)*, Lanzhou, China, July 17-21, 2017.

(79) Kenji Takeshita, Yin Xiangbiao, Hideharu Takahashi, Yusuke Inaba, Kazuo Utsumi, Nobutake Horiuchi, Takahiro Chikazawa, Junichi Munazawa: Rapid ion exchange of Cs from classified solid by metal ion containg subcritical water and volume reduction of vitrified glasses (1) oveall research plan and overview; *6th Annual Conference on Environmental Radiation Decontamination*, Fukushima, Japan, July 19-20, 2017, S8-1.

(80) Kenji Takeshita, Yin Xiangbiao, Hideharu Takahashi, Yusuke Inaba, Kazuo Utsumi, Nobutake Horiuchi, Takahiro Chikazawa: Rapid ion exchange of Cs from classified solid by metal ion containg subcritical water and volume reduction of vitrified glasses (2)Cs removal experiments by metal containing subcritical water; *6th Annual Conference on Environmental Radiation Decontamination*, Fukushima, Japan, July 19-20, 2017, S8-2.

(81) Yusuke Inaba, Miki Harigai, Hideharu Takahashi, Kazuo Utsumi, Kenji Takeshita, Nobutake Horiuchi, Takahiro Chikazawa, Junichi Munazawa: Rapid ion exchange of Cs from classified solid by metal ion containg subcritical water and volume reduction of vitrified glasses (3) Cs vitrification into glass by from subctirical water; *6th Annual Conference on Environmental Radiation Decontamination*, Fukushima, Japan, July 19-20, 2017, S8-3.

(82) Hideharu Takahashi, Yusuke Inaba, Kazuo Utsumi, Kenji Takeshita, Nobutake Horiuchi, Takahiro Chikazawa: Rapid ion exchange of Cs from classified solid by metal ion containg subcritical water and volume reduction of vitrified glasses (4) Cs vitrification into borosillicate glass containing solid acid ; *6th Annual Conference on Environmental Radiation Decontamination*, Fukushima Japan, July 19-20, 2017, S8-4.

(83) Nobutake Horiuchi, Takahiro Chikazawa, Hideharu Takahashi, Yusuke Inaba, Yin Xiangbiao, Kazuo Utsumi, Kenji Takeshita: Rapid ion exchange of Cs from classified solid by metal ion containg subcritical water and volume reduction of vitrified glasses (5) system assessment and future perspective; *6th Annual Conference on Environmental Radiation Decontamination*, Fukushima, Japan, July 19-20, 2017, S8-5.

(84) Kenji Takeshita, Xiangbiao Yin, Hideharu Takahashi, Yusuke Inaba, Kazuo Utsumi, Nobutake Horiuchi, Takahiro Chikazawa: Recovery of Cs from Contaminated Soil by Subcritical Water Containing Metal Ions and Its Solidification using Inorganic Materials for Volume Reductionn(1) oveall research plan and overview; *The Japan Atomic Energy Society Fall 2017*, SapporoJapan, September 13-15, 2017 , 3I01.

(85) Nobutake Horiuchi, Takahiro Chikazawa, Xiangbiao Yin, Hideharu Takahashi, Yusuke Inaba, Kazuo Utsumi, Kenji Takeshita: Recovery of Cs from Contaminated Soil by Subcritical Water Containing Metal Ions and Its Solidification using Inorganic Materials for Volume Reduction(2) Cs removal from contaminated soil by rapid ion exchange in subcritical water condition; *The Japan Atomic Energy Society Fall 2017*, Sapporo, Japan, September 13-15, 2017, 3I02.

(86) Xiangbiao Yin, Nobutake Horiuchi, Takahiro Chikazawa, Asumi Ochiai, Satoshi Utsunomiya, Hideharu Takahashi, Yusuke Inaba, Toshihiko Ohnuki, Kenji Takeshita: Recovery of Cs from Contaminated Soil by Subcritical Water Containing Metal Ions and Its Solidification using Inorganic Materials for Volume Reduction (3)Mechanism of Enhanced Cs Desorption from Clay Minerals under Hydrothermal Condition; *The Japan Atomic Energy Society Fall 2017*, Sapporo, Japan, September 13-15, 2017, 3I03.

(87) Hideharu Takahashi, Yusuke Inaba, Miki Harigai, Kazuo Utsumi, Kenji Takeshita, Nobutake Horiuchi, Takahiro Chikazawa, Junichi Munazawa: Recovery of Cs from Contaminated Soil by Subcritical Water Containing Metal Ions and Its Solidification using Inorganic Materials for Volume Reduction (4) Cs selective recovery by subcritical water and Cs vitrification into glass; *The Japan Atomic Energy Society Fall 2017*, Sapporo, Japan, September 13-15, 2017, 3I04.

(88) Kouta Kawai, Kenji Takeshita: Effects of heat generation from highly vitrificated glass on environment of near field in disposal site; *The Japan Atomic Energy Society Fall 2017*, Sapporo, Japan, September 13-15, 2017, 1H13.

(89) Ippei Amamoto, Hidekazu Kobayashi, Yasuo Shobu, Takashi Ohnishi, Akiko Koshizaka, Yoshio Hasegawa, Yusuke Inaba, Kazuo Utsumi, Kenji Takeshita, Jun Onoe: Development of Recovery Process of Platinum-group Metals from HLLW for

Stable Production and Volume Reduction of Homogeneous Vitrified Object(24)Comprehensive evaluation of adsorbent for PGM separation; *The Japan Atomic Energy Society Fall 2017*, Sapporo, Japan, September 13-15, 2017, 2A21.

(90) Kota Kawai, Kenji Takeshita, Eef Weet Jens, Alexey Stankovskiy, Edouard Mbala Malambu, Gert Van Den Eynde: Thermal analysis in the near-field of a geological repository taking into account generated heat distribution by gamma rays ; *International Nuclear Fuel Cycle Conference (GLOBAL2017)*, Seoul, Korea, September 24-29, 2017.

(91) Kota Kawai, Kenji Takeshita: Effects of extended cooling period of spent fuel from LWR and nuclides separation on vitrification and disposal; *MIT-Tokyo Tech Workshop on Innovative Nuclear Energy System (MT-INES)*, Cambridge, USA, October 26-28, 2017.

(92) Masahiko Nakase, Kenji Takeshita: Development of compact, rapid and highly efficient separation process based on a liquid-liquid countercurrent centrifugal contactor with Taylor vortices; EU-Japan Symposium on Back-End Systems for Reduction of Radiotoxicity and Final Waste Volume, Tokyo, Japan, November 1-2, 2017.

(93) Hidekazu Asano, Masahiro Kawakubo, Kazuhiro Tsubono: Integration of backend process for HLW geological disposal in consideration of nuclides partitioning and advanced vitrification technique; *EU-Japan Symposium on Back-End Systems for Reduction of Radiotoxicity and Final Waste Volume*, Tokyo, Japan, November 2, 2017.

(94) Kenji Takeshita, Yusuke Inaba, Hideharu Takahashi, Jun Onoe, Hirokazu Narita: Development of Simultaneous Adsorption System of PGMs and Mo from High-level Liquid Waste; *the 21st International solvent extraction conference (ISEC2017)*, Miyazaki, Japan, November 5-9, 2017, OD10.

(95) Michal Cibula, Yusuke Inaba, Kenji Takeshita, Hirokazu Narita: Mutual Separation of Platinum Group Metals in HNO3 Using Amide-Type Extractants; *the 21st International solvent extraction conference (ISEC2017)* , Miyazaki, Japan, November 5-9, 2017, OD09.

(96) Masahiko NAKASE, Yuto MATSUZAWA, Kenji TAKESHITA: Unique Separation Based on Extraction Kinetics Using a Liquid-liquid Countercurrent Centrifugal Contactor with Taylor Vortices; *the 21st International solvent extraction conference (ISEC2017)*, Miyazaki, Japan, November 5-9, 2017, OD23.

(97) Hidekazu Asano: Radionuclide migration and safety assessment of geological disposal program forhigh-level radioactive waste; *The 16th Isonomic Science Research Association,* Tokyo, Japan, March 16, 2018.

(98) M. Sato, Y. Niibori, Y. Inagaki, G. Chiba, K. Takeshita, M. Kawakubo, K. Tsubonou, H. Asano: Technical options of radioactive waste management for the second half of the 21st Century, in consideration of Pu utilization and less environmentally impacted geological disposal(1) background, viewpoints and research plan; *The Japan Atomic Energy Society Annual Meeting in the Spring of 2018*, Osaka, Japan , March 26-28, 2018.

(99) H. Asano, M. Kawakubo, K. Tsubonou, M. Sato: Technical options of radioactive waste management for the second half of the 21st Century, in consideration of Pu utilization and lessenvironmentally impacted geological disposal, (2)A case study on CEA's report; *The Japan Atomic Energy Society Annual Meeting in the Spring of 2018* , Osaka, Japan, March 26-28 , 2018.

(100) Kouta Kawai, Tomohiro Okamura, Eriko Minari, Masahiro Kawakubo, Hidekazu Asano, Kenji Takeshita: Technical options of radioactive waste management for the second half of the 21st Century, in consideration of Pu utilization and less environmentally impacted geological disposal (3) Effects of various nuclear fuel cycle scenarios on property of spent fuel and waste glass; *The Japan Atomic Energy Society Annual Meeting in the Spring of 2018*, Osaka, Japan, March 26-28, 2018.

(101) Tomohiro Okamura, Kouta Kawai, Eriko Minari, Hidekazu Asano, Kenji Takeshita: Technical options of radioactive waste management for the second half of the 21st Century, in consideration of Pu utilization and lessenvironmentally impacted geological disposal, (2)A case study on CEA's report; *The Japan Atomic Energy Society Annual Meeting in the Spring of 2018*, Osaka, Japan, March 26-28, 2018.

(102) Eriko Minari, Kouta Kawai, Tomohiro Okamura, Masahiro Kawakubo, Hidekazu Asano, Kenji Takeshita: Technical options of radioactive waste management for the second half of the 21st Century, in consideration of Pu utilization and less environmentally impacted geological disposal (5) Effects of MA separation on occupied area per waste package in the case of extended cooling period of UO2 spent fuel; *The Japan Atomic Energy Society Annual Meeting in the Spring of 2018*, Osaka, Japan, March 26-28, 2018.

(103) Kenji Takeshita, Kouta Kawai, Tomohiro Okamura, Eriko Minari, Masahiro Kawakubo, Kazuhiro Tsubonou, Hidekazu Asano, Go Chiba, Yaohiro Inagaki, Yuichi Niibori, Masatomo Sato: Technical options of radioactive waste

management for the second half of the 21st Century, in consideration of Pu utilization and less environmentally impacted geological disposal (6) Suggestion for back-end system research and development of load reduction of geological repository; *The Japan Atomic Energy Society Annual Meeting in the Spring of 2018*, Osaka, Japan, March 26-28, 2018.

(104) Kazuki MATSUSHITA, Takehiko TSUKAHARA: Creation of New Analysis System Using Self-assembled Monolayers on Glass Substrate; *Global 2017 International Nuclear Fuel Cycle Conference,* September, 25-28, 2017.

(105) Kaname SAGA, Takehiko TSUKAHARA, Ki Chul PARK, Hideyuki SUZUKI, Tetsuro MATSUMURA: Phase Transition-based Solvent Extraction Using Thermoresponsive Polymer and Alkyl Diamide Amine; *Global 2017 International Nuclear Fuel Cycle Conference,* September, 25-28, 2017.

(106) Takehiko TSUKAHARA, Nutthon YOKACHUKSUSE: Synthesis of Novel Diaza-Crown Ether Extractant and Its Application to Supercritical Carbon Dioxide Extraction of Strontium Ions; *Global 2017 International Nuclear Fuel Cycle Conference,* September, 25-28, 2017.

(107) Takehiko Tsukahara: Advanced microchip-based separation analysis system of radionucleides; *2018 Annual Meeting of Atomic Energy Society of Japan*, Osaka, March 26-28, 2018.

(108) Shen Chen, Kaname Saga, and Takehiko Tsukahara: Development of novel analytical device of radionuclides using photonic crystal polymer (1) Creation of Core/Shell photonic crystal for lanthanide sensing; *2018 Annual Meeting of Atomic Energy Society of Japan*, Osaka, March 26-28, 2018.

(109) Kaname Saga, Frederik H. Kriel, Craig Priest, and Takehiko Tsukahara: Development of novel analytical device of radionuclides using photonic crystal polymer (2) Feasibility study for realizing on-chip anion analysis; *2018 Annual Meeting of Atomic Energy Society of Japan*, Osaka, March 26-28, 2018.

(110) Shuichiro Yoneoka, Yasuhiro Nakagawa, Mitsuhiro Ebara, and Takehiko Tsukahara; Synthesis and Performances Evaluation of Boron Containing Thermoresponsive Polymer Nanomicelle; *2018 Annual Meeting of Atomic Energy Society of Japan*, Osaka, March 26-28, 2018.

(111) Kaname Saga, Frederik H. Kriel, Craig Priest, and Takehiko Tsukahara: Development of photonic crystal polymer-based analytical system of radionuclides; *NDEC-3 (The Third Conference for R&D Initiative on Nuclear Decommissioning Technology by the Next Generation)*, October 2, 2018.

(112) Ochiai A, Imoto J, Furuki G, Ikehara R, Suetake M, Yamasaki S, Nanba K, Ohnuki T, Grambow B, Ewing R & Utsunomiya S, Nuclear Fuel Fragments Released from the Fukushima Daiichi Nuclear Power Plant, *Goldschmidt Conference 2017*, Paris, France, Aug. 13-18, 2017.

(113) Imoto J, Ochiai A, Furuki G, Ikehara R, Suetake M, Horie K, Takehara M, Yamasaki S, Nanba K, Ohnuki T, Law G, Grambow B, Ewing R & Utsunomiya S, Isotopic Signature and Nano-Scale Texture of Cesium-Rich Micro-Particles: Release of Uranium and Fission Products from the Fukushima Daiichi Nuclear Power Plant, *Goldschmidt Conference 2017*, Paris, France, Aug. 13-18, 2017.

(114) Jiang M, Ohnuki T & Utsunomiya S, Comparison of Biomineralization Process of Middle REE (Sm) by Different Microorganisms: Yeast and Bacteria, *Goldschmidt Conference 2017*, Paris, France, Aug. 13-18, 2017.

(115) Furuki G, Ikehara R, Suetake M, Ochiai A, Imoto J, Yamasaki S, Nanba K, Ohnuki T & Utsunomiya S., Migration of Cs-Rich Microparticles Released from the FDNPP in the Surface Environments, *Goldschmidt Conference 2017*, Paris, France, Aug. 13-18, 2017.

(116) Horiike T, Dotsuta Y, Nakano Y, Utsunomiya S, Kozai N, Ohnuki T, Hriljac J & Yamashita M, Bioremediation of Radioactive Strontium Contaminated Sea Water by Biogenic Ca-Carbonate *Goldschmidt Conference 2017*, Paris, France, Aug. 13-18, 2017.

(117) Nakano Y, Ohnuki T & Utsunomiya S, Effects of Extracellular Polymeric Substances on the Aggregation of CeO2 Nanoparticles, *Goldschmidt Conference 2017*, Paris, France, Aug. 13-18, 2017.

(118) S. Yamasaki, N. Kozai, K. Tanaka, T. Ohnuki, KINETIC STUDY ON URANIUM(VI) REDUCTION BY FLAVINS AND ANTHRAQUINONES- ELECTROCEHMICAL APPROACH FOR UNDERSTANDING THE EXTRACELLER REDUCTIONt, Migratioon 2017, Barcelona, Spain, Sept. 10-15, 2017.

(119) Toshihiko Ohnuki, Naofumi Kozai, Kazuya Tanaka, Takumi Horiike, Mitsuo Yamashita,Yuma Dotsuda, Yuriko Nakano, Satoshi Utsunomiya, J. A. Hriljac, T.-Y. Chen, M. Karmaoui, S. Savva, A. Mayora, Japan UK collaboration on developing novel restoration materials for clean-up of radionuclides in the environment, AESJ 2018 Spring meeting, Osaka, Japan, March. 26-28,

2018

(120) Tomoaki Kato, Toshihiko Ohnuki, Qianqian Yu: Removal of Sr using the mix solution of MnO_4^- and biomass, AESJ 2018 Spring meeting, Osaka, Japan, March. 26-28, 2018.

(121) Taro Kanbe, Kenta Nakagawa: Development of Liquid Target for Neutron Capture Therapy Using Accelerator, (1) An outline of the target for NCT; *2012 Annual Meeting of Atomic Energy Society of Japan*, Fukui, March 30-35, 2012, K46.

(122) Hiroshi Sagara, Tatsuya Katabuchi: Nuclear data and its preparedness for developing non-destructive assay technique for non-proliferation and nuclear security -overview -; AESJ 2018 Annual Meeting, Osaka Univ., (2018).

(123) NUR HUSNA MD HANIPAH, Hiroshi Sagara, Yoga Peryoga, Chi Young Han: Applicability of LaBr3 (Ce) Detector for 154Eu Quantification in Molten Fuel Material and Waste Categorization by Using Passive Gamma; AESJ 2018 Annual Meeting, Osaka Univ., (2018).

(124) Chikara Fujinawa, Hiroshi Sagara, Chi Young Han: Performance evaluation of light water reactor fuel in inherent safety and non-proliferation features —U3Si2 fuel—; AESJ 2018 Annual Meeting, Osaka Univ., (2018).

(125) Takeshi Aoki, Hiroshi Sagara, Sunil S. Chirayath: Feasibility study of TRISO fuel for efficient Pu incineration and 3S feature enhancement (3) Required measurement accuracy for the Pu verification technique); Proc. 38th INMMJ Annual Mtg., Tokyo, Nov. 21－22 (2017).

(126) Hamza El-Asaad, Haruyasu Nagai, Hiroshi Sagara, Chi Young Han: User Interface Development of Atmospheric Dispersion Simulations for Nuclear Emergency Countermeasures (II). Evaluation of Interface Application for Fukushima Daiichi Disaster Case Scenario; Proc. 38th INMMJ Annual Mtg., Tokyo, Nov. 21－22 (2017).

(127) Tetsu Kikuhara, Sunil Sunny Chirayath, Masahide Katayama, Hiroshi Sagara: Damaging mechanism of structural materials by hypervelocity projectile impact - Robustness of reinforced concrete and estimation of delay time-; Proc. 38th INMMJ Annual Mtg., Tokyo, Nov. 21－22 (2017).

(128) Chikara Fujinawa, Hiroshi Sagara, Chi Young Han: Feasibility study on Accident Tolerant Fuel for light water reactors with intensive safety and proliferation resistance (3) Burnup performance of U3Si2 fuel); Proc. 38th INMMJ Annual Mtg., Tokyo, Nov. 21－22 (2017).

(129) Rei Kimura, Hiroshi Sagara, Satoshi Chiba, Effect of photon absorption adjusting on nuclear fuel material isotopic composition measurement based on the photofission reaction; Proc. 38th INMMJ Annual Mtg., Tokyo, Nov. 21－22 (2017).

(130) Nur Husna Md Hanipah, Yoga Peryoga , Hiroshi Sagara, Tomooki Shiba,and Chi Young Han, "Evaluation of the minimum detectable activity of 154Eu in fuel debris by using LaBr3 (Ce) detector; Proc. 38th INMMJ Annual Mtg., Tokyo, Nov. 21－22 (2017).

(131) Yoga Peryogaa, Hiroshi Sagaraa, Tomooki Shiba: Modified infinite thickness method for uranium enrichment measurement; Proc. 38th INMMJ Annual Mtg., Tokyo, Nov. 21－22 (2017).

(132) Masahide Katayama, Ryo Matsuzawa and Hiroshi Sagara: Numerical analysis methods and their case studies on the severe accidents in LWRs; Proc. 38th INMMJ Annual Mtg., Tokyo, Nov. 21－22 (2017).

(133) Hiroshi Sagara: Activity report of Special Committee for Nuclear Data in the period of 2015 and 2016, Nuclear Security-(3) Data needs from the field of nuclear security -; AESJ Fall Mtg., 2017.

(134) Katsumi Yoshida, Muhammad Fajar, Toyohiko Yano, Tetsuo Uchikoshi, Tohru S. Suzuki: Fabrication of Textured B_4C Ceramics by Slip Casting in a Strong Magnetic Field and Their Mechanical and Thermal Properties; *12th Pacific Rim Conference on Ceramic and Glass Technology (PacRim12)*, Hawaii, USA, May 23, 2017, PACRIM-S11-018-2017.

(135) Katsumi Yoshida, Ryo Shirata, Takashi Ajito, Toyohiko Yano, Masaki Kotani, Takuya Aoki, Toshio Ogasawara: Mechanical Properties of SiC_f/SiC Composites with Carbon and Boron Nitride Interfacial Coatings Formed by Electrophoretic Deposition Method; *12th Pacific Rim Conference on Ceramic and Glass Technology (PacRim12)*, Hawaii, USA, May 24, 2017, PACRIM-S12-014-2017.

(136) Katsumi Yoshida, Makoto Takahashi, Toyohiko Yano: Effects of Boron and Aluminum Additives on Microstructure of Porous SiC Ceramics with In-Situ Grain Growth; *4th Conference of The Serbian Society for Ceramic Materials*, Belgrade, Serbia, June 15, 2017, I-6.

(137) Jelena Maletaskic, Branko Matovic, Vesna Maksimovic, Marija Prekasjki-Djordjevic, Katsumi Yoshida, Toyohiko Yano: Sintering behavior and mechanical properties of sintered $CaTiSiO_5$ (sphene); *4th Conference of The Serbian Society for Ceramic Materials*, Belgrade, Serbia, June 15, 2017, P-36.

(138) Thanataon Pornphatdetaudom, Toyohiko Yano, Katsumi Yoshida: Macroscopic Length Recovery of Neutron-Irradiated Aluminum Nitride at a Fluence up to 4.4 x 10^{23} n/m^2 at 573 K; *The 10th International Conference on the Science and Technology for Advanced Ceramics(STAC-10)*, Yokohama, August 2, 2017, 2pP025.

(139) Toru Tsunoura, Katsumi Yoshida, Toyohiko Yano, Takuya Aoki, Toshio Ogasawara: Wet Oxidation Behavior of Titanium Aluminum Carbide; *The 10th International Conference on the Science and Technology for Advanced Ceramics (STAC-10)*, Yokohama, August 2, 2017, 2pP026.

(140) Katsumi Yoshida, Muhammad Fajar, Toyohiko Yano, Tohru S. Suzuki, Tetsuo Uchikoshi: Mechanical and Thermal Properties of Texture-Controlled B_4C Ceramics with Al_2O_3 Additives by Strong Magnetic Field; *The 10th International Conference on the Science and Technology for Advanced Ceramics (STAC-10)*, Yokohama, August 3, 2017, 3aCh004.

(141) Yan You, Masamitsu Imai, Katsumi Yoshida, Toyohiko Yano: Study of helium bubbles in fast neutron irradiated B_4C; *The 10th International Conference on the Science and Technology for Advanced Ceramics (STAC-10)*, Yokohama, August 3, 2017, 3aCh008.

(142) Katsumi Yoshida, Toyohiko Yano, Masaki Kotani, Takuya Aoki, Toshio Ogasawara: Formation of Carbon Interphase on Polycrystalline and Amorphous SiC Fibers in SiC/SiC Composites by Electrophoretic Deposition; *6th International Conference on Electrophoretic Deposition: Fundamentals and Applications*, Gyeongju, Korea, October 3, 2017.

(143) Thanataon Pornphatdetaudom, Toyohiko Yano, Katsumi Yoshida: Microstructure and Physical Property Changes of Neutron Irradiated Aluminum Nitride and Those Recovery Behavior by Annealing; *18th International Conference on Fusion Reactor Materials (ICFRM-18)*, Aomori, November 8, 2017, 8PT-108.

(144) Alexander James Leide, Richard I Todd, Steve G Roberts, Katsumi Yoshida, Mike Gorley, David E J Armstrong: Reaction-Bonded Silicon Carbide for Fusion Applications; *18th International Conference on Fusion Reactor Materials (ICFRM-18)*, Aomori, November 8, 2017, 8PT-16.

(145) Toru Tsunoura, Riku Akatsu, Katsumi Yoshida, Toyohiko Yano: Sintering behavior of yttrium oxyfluoride ($Y_5O_4F_7$) ceramics; *The 39th International Symposium on Dry Process (DPS2017)*, Tokyo, November 17, 2017, P-11.

(146) Ryuki Tahara, Toru Tsunoura, Katsumi Yoshida, Toyohiko Yano: Fabrication of dense yttrium oxyfluoride ceramics by hot-pressing and their electrical properties; *The 39th International Symposium on Dry Process (DPS2017)*, Tokyo, November 17, 2017, P-10.

(147) Daisuke Endo, Katsumi Yoshida, Junichi Tatami, Eiji Takahashi, Yoshihisa Yamaoka: Photoacoustic imaging to evaluate internal defects in ceramics; *37th Annual Meeting of the Laser Society of Japan*, Tokushima, January 7, 2017, 07pI4.

(148) Katsumi Yoshida: Neutron Irradiation Damage of SiC-Based Ceramics; *3rd PD-SiC's Workshop 2018*, Tokyo, January 19, 2017.

(149) Muhammad Fajar, Tohru S. Suzuki, Katsumi Yoshida, Toyohiko Yano: Fabrication of Textured Boron Carbide Ceramics with Alumina Addition using Slip Casting by Strong Magnetic Field for Neutron Absorber of Fast Breeder Reactor; *10th Student Meeting of the Kanto-Koetsu Division of the Atomic Energy Society of Japan*, Tokyo, March 10, 2017, A07.

(150) Thanataon Pornphatdetaudom, Toyohiko Yano, Katsumi Yoshida: Transition on Macroscopic Length, Lattice Parameter, Microstructure of Aluminum Nitride after Iradiation and its Recovery Behavior; *10th Student Meeting of the Kanto-Koetsu Division of the Atomic Energy Society of Japan*, Tokyo, March 10, 2017, B06.

(151) Takashi Ajito, Katsumi Yoshida, Toyohiko Yano: Fabrication of Amorphous SiC Fiber-Reinforced SiC Matrix Composites with Carbon Interphase Formed by Electrophoretic Deposition Method and Their Mechanical Properties; *Annual Meeting of The Ceramic Society of Japan, 2017,* Tokyo, March 17, 2017, 1H18.

(152) Ryo Shirata, Katsumi Yoshida, Toyohiko Yano: BN Coating on SiC Fibers by Electrophoretic Deposition Method using BN Suspension with Different Dispersants; *Annual*

Meeting of The Ceramic Society of Japan, 2017, Tokyo, March 17, 2017, 1H19.

(153) Ryuki Tahara, Katsumi Yoshida, Toyohiko Yano: Fabrication of Dense Yttrium Oxyfluoride Ceramics by Hot-Pressing and Their Properties; *Annual Meeting of The Ceramic Society of Japan, 2017*, Tokyo, March 19, 2017, 3H06.

(154) Toru Tsunoura, Katsumi Yoshida, Toyohiko Yano, Takuya Aoki, Toshio Ogasawara: High Temperature Bending Behavior of SiC Particle-Reinforced Si Composites; *Annual Meeting of The Ceramic Society of Japan, 2017*, Tokyo, March 19, 2017, 3H10.

(155) Shuhei Toike, Katsumi Yoshida, Toyohiko Yano, Tadahiko Takada: Fabrication of Porous Ceramics using Natural Minerals for Radioactive Contaminated Water Purification; *The 2nd International Forum on the Decommissioning of the Fukushima Daiichi Nuclear Power Station*, Fukushima, July 3, 2017.

(156) Toru Tsunoura, Katsumi Yoshida, Toyohiko Yano, Takuya Aoki, Toshio Ogasawara: High temperature bending behavior of SiC fiber-reinforced Si composites; *The Japan Society of Mechanical Engineers Annual Meeting 2017*, Saitama, September 4, 2017, S0420103.

(157) Daiki Chiba, Syuichi Wakayama, Takahiro Matsueda, Katsumi Yoshida: The development of the thermal shock test for ceramics under various thermal stress; *The Japan Society of Mechanical Engineers Annual Meeting 2017*, Saitama, September 4, 2017, S0420202.

(158) Toru Tsunoura, Katsumi Yoshida, Toyohiko Yano, Takuya Aoki, Toshio Ogasawara: High temperature bending behavior of SiC fiber-reinforced Si-$TiSi_2$ eutectic alloy matrix composites; *The 30th Fall Meeting of The Ceramic Society of Japan*, Kobe, September 20, 2017, 2L04.

(159) Ryo Shirata, Katsumi Yoshida, Toyohiko Yano: Effect of particle size in BN interphase layers formed by electrophoretic deposition method on mechnical properties of SiC_f/SiC composites; *The 30th Fall Meeting of The Ceramic Society of Japan*, Kobe, September 20, 2017, 2L06.

(160) Takuya Aoki, Toru Tsunoura, Katsumi Yoshida, Toyohiko Yano, Toshio Ogasawara: Processing and characterization of SiC-fiber-reinforced composites by melt-infiltration method; *The 30th Fall Meeting of The Ceramic Society of Japan*, Kobe, September 20, 2017, 2L08.

(161) Ryosuke S.S. Maki, Katsumi Yoshida, Toyohiko Yano: Evaluation of Thermal Shock Resistance of B_4C-Based Ceramics with High Frequency Induction Heating Furnace; *The 30th Fall Meeting of The Ceramic Society of Japan*, Kobe, September 20, 2017, 2L19.

(162) Thanataon Pornphatdetaudom, Toyohiko Yano, Katsumi Yoshida: Major Effects of Neutron Irradiation on AlN Macroscopic Properties Changes and Recovery Behavior under Isochronal Annealing; *The 30th Fall Meeting of The Ceramic Society of Japan*, Kobe, September 21, 2017, 3L17.

(163) Muhammad Fajar, Katsumi Yoshida, Toyohiko Yano, Tohru S. Suzuki, Tetsuo Uchikoshi: Densification of textured B_4C ceramic with Al_2O_3 additive fabricated by slip casting in high magnetic field; *The 30th Fall Meeting of The Ceramic Society of Japan*, Kobe, September 21, 2017, 3L20.

(164) Shota Azuma, Tetsuo Uchikoshi, Katsumi Yoshida, Tohru S. Suzuki: Fabrication of Dense-Packing/Porous Multi-Layered Microstructure by Electrophoretic deposition; *The 30th Fall Meeting of The Ceramic Society of Japan*, Kobe, September 20, 2017, 2PL08.

(165) Shota Azuma, Tetsuo Uchikoshi, Katsumi Yoshida, Tohru S. Suzuki: Development of Highly Microstructure-Controlled B_4C Neutron Absorbers for Fast Reactors; *IMR, Tohoku University Oarai Workshop 2017*, Sendai, October 4, 2017.

(166) Anna Gubarevich , Katsumi Yoshida, Toyohiko Yano: Neutron-Irradiation Effects of Silicon Carbide Related Ceramics; *IMR, Tohoku University Oarai Workshop 2017*, Sendai, October 4, 2017.

(167) Katsumi Yoshida: Effects of Aluminum and Boron Additives on Microstructure and Properties of Silicon Carbide Ceramics; *AIMS SiC Fiber Advancement Project Workshop*, Tokyo, December 25, 2017.

(168) A. Gubarevich, J. Habasaki: Long-range charge order and electrostatic screening in ionic liquids and concentrated electrolyte solutions; *8th International Discussion Meeting on Relaxations in Complex Systems*, Wisla, Poland, July 23-28, 2017.

(169) A. Gubarevich, K. Yoshida, T. Yano: Control of secondary phases formation in combustion synthesis of nanolaminated ternary carbides; *6th International Symposium on Advanced Ceramics (ISAC-6)*, Sendai, Japan, March 12-14, 2017.

(170) A. Gubarevich, J. Habasaki: Structure and charge correlations in the water-in-salt solutions studied by molecular dynamics simulation; *The 98th Annual Meeting of Chemical Society of Japan*, Funabashi, Japan, March 21-23, 2017.

(171) K. Kobayashi , R. Aoki, H. Abe, Y.

Kebukawa, H. Shibata, S. Yoshida, H. Fukuda, K. Kondo, Y. Oguri, V.S. Airapetian: Formation of Amino Acid Precursors in Primitive Planetary Atmosphere by Galactic and Solar/Stellar Cosmic Rays; *Astrobiology Science Conference 2017 (AbSciCon 2017)*, Mesa Convention Center and the Phoenix Marriott Mesa, Mesa, Arizona, USA, April 24-28, 2017, #3259.

(172) T. Sato, S. Enomoto, Y. Kebukawa, S. Yoshida, I. Yoda, H. Fukuda, Y. Oguri, K. Kobayashi: Stability of Amino Acid Precursors in Various Space Environments; *Japan Geoscience Union Meeting 2017*, Makuhari Messe, Chiba, Japan, May 20-24, 2017, BAO01-P02.

(173) K. Naito, S. Enomoto, Y. Kebukawa, H. Fukuda, Y. Oguri, K. Kobayashi: Stability of Amino Acid Precursors in Simulated Submarine Hydrothermal Vent Environments; *Japan Geoscience Union Meeting 2017*, Makuhari Messe, Chiba, Japan, May 20-24, 2017, BAO01-P03.

(174) K. Kobayashi, R. Aoki, Y. Kebukawa, H. Shibata, H. Fukuda, K. Kondo, Y. Oguri, V.S. Airapetian: Prebiotic Formation of Amino Acid Precursors in Primitive Earth Atmosphere by Cosmic Rays and Solar Energetic Particles; *Japan Geoscience Union Meeting 2017*, Makuhari Messe, Chiba, Japan, May 20-24, 2017, BAO01-P04.

(175) K. Kobayashi, R. Aoki, Y. Kebukawa, H. Shibata, H. Fukuda, Y. Oguri, V.S. Airapetian: Roles of Solar Energetic Particles in Production of Bioorganic Compounds in Primitive Earth Atmosphere; *18th International Conference on Origin of life (ISSOL 2017)*, San Diego, CA, USA, July 16-21, 2017.

(176) K. Kobayashi, T. Ito, S. Enomoto, Y. Kebukawa, H. Mita, Y. Muramatsu, T. Ouchi, S. Hamanaka, H. Fukuda, Y. Oguri: Is the Strecker Synthesis a Major Formation Pathway of Amino Acids in Space?"; *European Astrobiology Network Association* (*EANA) 2017*, Aarhus, Denmark, August 12-16, 2017.

(177) K. Kondo, K. Kawauchi, H. Kurita, T. Takahashi, Y. Oguri: Role of Insulator Sleeves in the Electro-Magnetic Shock Tube to Produce Well-Defined Dissociated-Hydrogen Targets for Beam Interaction Experiment; *10th International Conference on Inertial Fusion Sciences and Applications (IFSA2017)*, Palais du Grand Large, Saint Malo, France, September 11-15, 2017.

(178) W. Teng, Y. Oguri, S. Kaseda, H. Fukuda: Homogenization of PIXE Targets Prepared by Drop-and-Dry Method Using Non-Ionic Surfactant; *33rd PIXE Symposium in Japan*, Uji Campus, Kyoto University, Kyoto, Japan, October 19-21, 2017, #3-1.

(179) Yoshihisa Matsumoto: Implication of DNA double-strand break repair in cancer, aging and development; *The 12th International conference & 5th Asian Congress on Environmental Mutagens*, Songdo Convensia (Incheon, Korea), 12-16 November 2017, SY1-4.

(180) Mukesh Kumar Sharma, Ali Reza Amiri Moghani, Mikoto Fukuchi, Shoji Imamichi, Anie Day Asa De Castro, Rujira Wanotayan, Mikio Shimada, Yoshihisa Matsumoto: XRCC4 phosphorylation as an in situ indicator for DNA-PK activity; *The 12th International conference & 5th Asian Congress on Environmental Mutagens*, Songdo Convensia (Incheon, Korea), 12-16 November 2017, OS02-8.

(181) Akitoshi Okino, Satoshi Kohno, Mari Aida, Tomoko Miyake, Takahiro Iwai, Hidekazu Miyahara, Mikio Shimada, Yoshihisa Matsumoto, Takashi Aoi, Koichi Chiba: Development of Droplet Injection ICP-AES/MS and Elemental Analysis of Single Human Cancer/Osteosarcoma Cell; *7th Asia-Pacific Winter Conference on Plasma Spectrochemistry*, 12-17 November 2017, Kunibiki Messe (Matsue), Keynote Lecture.

(182) Kaima TSUKADA, Mikio Shimada, Yoshihisa Matsumoto: Development of p53-based DNA Damage Response Visualization System; *The 6th International Education Forum on Environment and Energy Science*, Dec. 2017.

(183) Anie Day ASA, Rujira WANOTAYAN, Mikio Shimada, Yoshihisa Matsumoto: DNA double strand break repair and V(D)J recombination function of XRCC4 mutants associated with microcephaly and growth defect; *2017 Radiation Research Society annual meeting*, Oct. 2017.

(184) Tomoko Miyake, Hiroaki Kawano, Jumpei Hosoda, Mikio Shimada, Hidekadzu Miyahara, Koichiro Takao, Yoshihisa Matsumoto, Akitoshi Okino: Analysis of components in CO2 plasma bubbled-up water; *23rd International Conference on Plasma Chemistry*, ISPC23 Proceedings, p. 712, Aug. 2017.

(185) Jumpei Hosoda, Tomoko Miyake, Hiroaki Kawano, MIkio Shimada, Yuriko Matsumura, hidekadzu miyahara, Atsuo Iwasawa, Yoshihisa Matsumoto, Akitoshi Okino: Measurement of reactive species in Plasma Babbled-up Water affecting human cultured cells; *The International Conference on Phenomena in Ionized Gases (ICPIG) 2017*, Proceedings of the XXXIII International Conference on Phenomena in Ionized Gases 2017, p246, Jul. 2017.

(186) Kaima Tsukada, Mikio Shimada, Yoshihisa Matsumoto: In situ visualization system for DNA damage response in human cells based on p53

regulation mechanism; *Kyoto University, Radiation Biology Center International Symposium*, Dec. 2017.

(187) Akane Yamasaki, Mikio Shimada, Yoshihisa Matsumoto: Function of histone chaperone Anti-silencing function 1 (Asf1) in DNA damage response of human cells; K*yoto University, Radiation Biology Center International Symposium*, Dec. 2017.

(188) Naoya Kase, Mikio Shimada, Hirofumi Nakano, Hiroyuki Nakamura, Yoshihisa Matsumoto: The functional analysis of DNA repair factor PNKP and susceptibility to synthetic lethality of BRCA1/2 mutation; *Kyoto university, Radiation Biology Center International Symposium*, Dec. 2017.

(189) Jumpei Hosoda, Hiroaki Kawano, Tomoko Miyake, Mikio Shimada, Yuriko Matsumura, Shuichi Miyahara, Yoshihisa Matsumoto, Atsuo Iwasawa, Akitoshi Okino: Measurement of reactive species in Plasma Babbled-up Water affecting human cultured cells; *Plasma Conference 2017 (PLASMA2017)*, Plasma Conference 2017 Conference & Exhibition Program, p. 20, Nov. 2017.

(190) Akitoshi Okino, Satoshi Kohno, Mari Aida, Tomoko Miyake, Takahiro Iwai, Hidekazu Miyahara, Mikio Shimada, Yoshihisa Matsumoto, Takashi Aoi, Koichi Chiba: Development of Droplet Injection ICP-AES/MS and Elemental Analysis of Single Human Cancer/Osteosarcoma Cell; *7th Asia-Pacific Winter Conference on Plasma Spectrochemistry*, p. 30, Nov. 2017.

(191) Satoshi Kohno, Mari Aida, Tomoko Miyake, Takahiro Iwai, Hidekazu Miyahara, Mikio Shimada, Yoshihisa Matsumoto, Takashi Aoi, Koichi Chiba, AKITOSHI OKINO: Intracellular calcium analysis of single human cell using droplet injection ICP-OES/MS; *7th Asia-Pacific Winter Conference on Plasma Spectrochemistry*, p. 121, Nov. 2017.

(192) Satoshi Kohno, Mari Aida, Tomoko Miyake, Takahiro Iwai, Wataru Inami, Yoshimasa Kawata, Hidekazu Miyahara, Mikio Shimada, Yoshihisa Matsumoto, Koichi Chiba, AKITOSHI OKINO: Development of Droplet Injection ICP-AES/MS and Elemental Analysis of Single Human Cell; *The 2nd International Symposium on Biomedical Engineering*, p. 216-217, Nov. 2017.

(193) Naoya Kase, Mikio Shimada, Hirofumi Nakano, Hiroyuki Nakamura, Yoshihisa Matsumoto: The functional analysis of DNA repair factor PNKP and susceptibility to synthetic lethality of BRCA1/2 mutation; *ConBio 2017*, Dec. 2017.

(194) Akane Yamasaki, Mikio Shimada, Yoshihisa Matsumoto: Function of histone chaperone Anti-silencing function 1 (Asf1) in DNA damage response of human cells; *ConBio2017*, Dec. 2017.

(195) Mikio Shimada, Naoya Kase, Kaima Tsukada, Yoshihisa Matsumoto: DNA damage response and cell cycle checkpoint in iPSCs; *60th annual meeting of Japanese radiation research society*, Oct. 2017.

(196) Mikio Shimada: Analysis of mechanism of genome stability by DNA repair factors after ionizing radiation exposure; *60th annual meeting of Japanese radiation research society*, Award lecture, Oct. 2017.

(197) Kaima Tsukada, Mikio Shimada, Yoshihisa Matsumoto: In situ visualization system for DNA damage response in human cells based on p53 regulation mechanism; *60th annual meeting of Japanese radiation research society*, Oct. 2017.

(198) Hisayo Tsuchiya, Mikio Shimada, Junya Kobayashi, Yoshihisa Matsumoto: Effect of low dose rate irradiation in DNA double strand breaks repair defect cells; *60th annual meeting of Japanese radiation research society*, Oct. 2017.

(199) Anie Day ASA, Rujira WANOTAYAN, Mikio Shimada, Yoshihisa Matsumoto: DNA double-strand break repair and V(D)J recombination function of XRCC4 mutants associated with microcephaly and growth defect; *60th annual meeting of Japanese radiation research society*, Oct. 2017.

(200) Naoya Kase, Mikio Shimada, Hirofumi Nakano, Hiroyuki Nakamura, Yoshihisa Matsumoto: The functional analysis of DNA repair factor PNKP and susceptibility to synthetic lethality of BRCA1/2 mutation; *60th annual meeting of Japanese radiation research society*, Oct. 2017.

(201) Akane Yamasaki, Mikio Shimada, Yoshihisa Matsumoto: Function of histone chaperone Anti-silencing function 1 (Asf1) in DNA damage response of human cells; *60th annual meeting of Japanese radiation research society*, Oct. 2017.

(202) Satoshi Kohno, Mari Aida, Tomoko Miyake, Takahiro Iwai, Wataru Inami, Yoshimasa Kawata, Hidekazu Miyahara, Mikio Shimada, Yoshihisa Matsumoto, Koichi Chiba, AKITOSHI OKINO: Development of Droplet Injection ICP-AES/MS and Elemental Analysis of Single Human Cell; 2017 Research Center for Biomedical Engineering, p. 74, Mar. 2018.

(203) Mikio Shimada: Ionizing radiation dependent centrosome amplification; *Ibaraki University Department of Science Symposium, 11th Quantum Medicine meeting*, Jan. 2018.

(204) Kaima TSUKADA, Mikio Shimada, Yoshihisa Matsumoto: Development of

p53-based DNA Damage Response Visualization System; *ConBio017*, Dec. 2017.

(205) Kaima TSUKADA, Mikio Shimada, Yoshihisa Matsumoto: Development of p53-based DNA Damage Response Visualization System; 2*017 Annual meeting of Young Radiation Biologists' Association of Japan*, Sep. 2017.

(206) Satoshi Kohno, Mari Aida, Tomoko Miyake, Takahiro Iwai, Wataru Inami, Yoshimasa Kawata, Hidekazu Miyahara, Mikio Shimada, Yoshihisa Matsumoto, Koichi Chiba, AKITOSHI OKINO: Development of Droplet Injection ICP-AES/MS and Elemental Analysis of Single Human Cell; *66th Annual meeting of the Japan Society for Analysis Chemistry*, p. 29, Sep. 2017.

(207) Akane Yamasaki, Mikio Shimada, Yoshihisa Matsumoto: Function of histone chaperone Anti-silencing function 1 (Asf1) in DNA damage response of human cells; *017 Annual meeting of Young Radiation Biologists' Association of Japan*, Sep. 2017.

(208) Naoya Kase, Mikio Shimada, Hirofumi Nakano, Hiroyuki Nakamura, Yoshihisa Matsumoto: The functional analysis of DNA repair factor PNKP and susceptibility to synthetic lethality of BRCA1/2 mutation; *017 Annual meeting of Young Radiation Biologists' Association of Japan*, Sep. 2017.

(209) Yoshihisa Matsumoto, Hisayo Tsuchiya, Mikio Shimada, Junya Kobayashi: Effect of low dose rate irradiation in DNA double strand breaks repair defect cells; *The 78th Annual meeting of the Japanese Cancer Association*, Sep. 2017.

(210) Satoshi Kohno, Mari Aida, Tomoko Miyake, Takahiro Iwai, Wataru Inami, Yoshimasa Kawata, Hidekazu Miyahara, Mikio Shimada, Yoshihisa Matsumoto, Koichi Chiba, AKITOSHI OKINO: Development of Droplet Injection ICP-AES/MS and Elemental Analysis of Single Human Cell; *2017 Tsukuba Seminar*, Jul. 2017.

(211) Kaima TSUKADA, Mikio Shimada, Yoshihisa Matsumoto: Development of p53-based DNA Damage Response Visualization System; *2017 The regular meeting of the Japanese Biochemical Society Kanto Branch,* Jun. 2017.

(212) Kaima TSUKADA, Mikio Shimada, Yoshihisa Matsumoto: Development of p53-based DNA Damage Response Visualization System; *56th Annual meeting of Japanese Society for Medical and Biological Engineering*, May. 2017.

(213) Satoshi Kohno, Mari Aida, Tomoko Miyake, Takahiro Iwai, Wataru Inami, Yoshimasa Kawata, Hidekazu Miyahara, Mikio Shimada, Yoshihisa Matsumoto, Koichi Chiba, AKITOSHI OKINO: Development of Droplet Injection ICP-AES/MS and Elemental Analysis of Single Human Cell; *77th Annual meeting of The Japan Society for Analytical Chemistry*, p. 21, May. 2017.

(214) Satoshi Kohno, Mari Aida, Tomoko Miyake, Takahiro Iwai, Wataru Inami, Yoshimasa Kawata, Hidekazu Miyahara, Mikio Shimada, Yoshihisa Matsumoto, Koichi Chiba, AKITOSHI OKINO: Development of Droplet Injection ICP-AES/MS and Elemental Analysis of Single Human Cell; *2017 Annual meeting of the Spectroscopical Society of Japan*, p. 4, May. 2017.

(215) Kohei Okutomo, Eiki Hotta, Kei Takakura, Jun Hasegawa, Toshiyuki Kohno: Study on Emission Spectra of Hydrogen Discharge Plasma in Inertial Electrostatic Confinement Device; *IEEJ Joint Technical Meeting on Plasma, Pulsed Power, and Discharge,* Kyoto, July 13-15, 2017, PPT-17-009.

(216) Itagaki Tomonobu, Kohei Okutomo, Eiki Hotta, Jun Hasegawa, Kei Takakura, Toshiyuki Kohno: Energy Distribution of Particles in Linear Inertial Electrostatic Confinement Fusion Neutron Source; 2017 *Annual Meeting of Atomic Energy Society of Japan*, Sapporo, September 13-15, 2017, 1N03.

(217) R. Chiba, P. S. Szabo, H. Biber, B. M. Berger, R. Stadlmayr, J. Hasegawa, F. Aumayr: Potential Sputtering of Planet Surface by Highly Charged Ions in Solar Wind; *2017 Autumn Meeting of Physical Society of Japan*, Morioka, September 21-24, 2017, 22pA18-8.

(218) Kohei Okutomo, Itagaki Tomonobu, Jun Hasegawa, Kei Takakura, Eiki Hotta, Toshiyuki Kohno: Investigation of Particle Velocity Distributions in an Inertial Electrostatic Confinement Fusion Device by Optical Emission Spectroscopy; *Plasma 2017*, Himeji, November 20-24, 2017, 21P-93.

(219) Yuta Ishikawa, Jun Hasegawa, Yasushi Iwata, Kazuhiko Horioka: Size Measurement Of Silicon Clusters Generated By Laser Ablation In Rarefied Helium; *Plasma 2017*, Himeji, November 20-24, 2017, 21P-109.

(220) Jun Hasegawa, Tomonobu Itagaki, Kohei Okutomo, Kei Takakura, Eiki Hotta, Toshiyuki Kohno: Inverse Analysis of Particle Velocity Distributions in a Linear-type Inertial Confinement Fusion Device; *Plasma 2017*, Himeji, November 20-24, 2017, 21P-84.

(221) Jun Hasegawa, Kohei Okutomo, Tomonobu Itagaki, Eiki Hota, Kei Takakura, Toshiyuki Kohno: Numerical Analysis of Particle Dynamics in a Linear-type Inertial Electrostatic Confinement Fusion Device; NIFS

(222) Makoto Tsukamoto, Hiroki Fujii, Jun Hasegawa, Kazuhiko Horioka: Control of Laser

Produced Plasma Flow by Magnetic Nozzle; NIFS

(223) Tomonobu Itagaki, Kohei Okutomo, Jun Hasegawa, Eiki Hotta, Kei Takakura, Toshiyuki Kohno: Spectroscopic analysis of Linear shaped Inertial Electrostatic Confinement Fusion (IECF) device; NIFS

(224) Kazuya Hashimoto, Jun Hasegawa, Kazuhiko Horioka: Development of Highly Charged Fullerene Ion Source for Induction Synchrotron; NIFS

(225) Eiki Hotta, Kohei Okutomo, Tomonobu Itagaki, Kei Takakura, Jun Hasegawa: Characteristics of a Linear Inertial Electrostatic Confinement Fusion Neutron Source; *2018 Annual Meeting of IEEJ*, Fukuoka, March 14-16, 2018, 1-152.

(226) Jun Hasegawa, Kohei Okutomo, Tomonobu Itagaki, Kei Takakura, Eiki Hotta: Analysis of a Linear Inertial Electrostatic Confinement Fusion Neutron Source; *2018 Annual Meeting of IEEJ*, Fukuoka, March 14-16, 2018, 1-153.

(227) Kei Takakura, Kohei Okutomo, Tomonobu Itagaki, Jun Hasegawa, Toshiyuki Kohno, Eiki Hotta, Mitsuhiro Maida, Haruo Miyadera, Kenichi Yoshioka, Koichi Nitto: Characteristics of an Imaging Plate Scanner for Neutron Radiography; *2018 Annual Meeting of Atomic Energy Society of Japan*, Osaka, March 26-28, 2018, 1H19.

(228) C. Ishizuka, S. Chiba, K. Tsubakihara and N. Carjan: Evaluation of charge polarization of the fissioning nucleus based on our 4D-Langevin model; *2018 Annual Meeting of Atomic Energy Society of Japan*, Tokyo University of Science, March 22-25, 2018, 22pK305-13.

(229) K. Tsubakihara, C. Ishizuka, S. Okumura, T. Yoshida, S. Chiba: Independent Yields Derived from Nuclear Shell Correction and Boltzmann Weight and Their Validation; *2018 Annual Meeting of Atomic Energy Society of Japan*, Tokyo University of Science, March 22-25, 2018, 22pK305-14.

(230) Y. Ishii, A. Etori, A. Ono, S. Chiba: Study of multi-nucleon transfer reactions on heavy elements; *2018 Annual Meeting of Atomic Energy Society of Japan*, Tokyo University of Science, March 22-25, 2018, 23pK302-12.

(231) A. Etori, A. Ono, M. Kimura, C. Ishizuka, S. Chiba: Study on Nuclear Fission by Antisymmetrized Molecular Dynamics; *2018 Annual Meeting of Atomic Energy Society of Japan*, Tokyo University of Science, March 22-25, 2018, 23pK302-13.

(232) A. Etori, A. Ono, M. Kimura, C. Ishizuka, S. Chiba: Study of fission by Antisymmetrized Molecular Dynamics; *2017 Symposium on nuclear data*, Ibaraki Japan, November 16-17, 2017.

(233) Shin Okumura, Mark Dennis Usang, Toshihiko Kawano, Satoshi Chiba; Calculation s of prompt neutron multiplicities and isomer production ratios by the statistical model; *2017 Symposium on nuclear data*, Ibaraki Japan, November 16-17, 2017, B9.

(234) T. Nishikawa, Y. Iwata, S. Chiba: Microscopic Friction Coefficient and potential for fission Analysis; *2017 Symposium on nuclear data*, Ibaraki Japan, November 16-17, 2017.

(235) K. Kean, Y. Iwata, et al: Microscopic Friction Coefficient and potential for fission Analysis; *2017 Symposium on nuclear data*, Ibaraki Japan, November 16-17, 2017.

(236) Yoritaka Iwata, Yasuhiro Takei: High precision calculation of heavy-ion collisions based on the spectral method; *2017 Fall Meeting of the Atomic Energy Society of Japan*, Hokkaido, September 13-15, 20171G21.

(237) Riku Nakamura, Kenichi Tanaka, Satoshi Chiba: Study on concrete permeation calculation for decommissioning (2) Calculation of composition sensitivity coefficient; *2017 Fall Meeting of the Atomic Energy Society of Japan*, Hokkaido, September 13-15, 20172D03.

(238) Kosuke Tsubakihara, Chikako Ishizuka, Tadashi Yoshida, Satoshi Chiba: Evaluation of independent fission yields including the shell correction effects; *2017 Fall Meeting of the Atomic Energy Society of Japan*, Hokkaido, September 13-15, 20172M01.

(239) Kun Ratha Kean, Satoshi Chiba, Katsuhisa Nishio, Kentaro Hirose, Mark Vermeulen, Hiroyuki Makii, Riccardo Orlandi, Kazuaki Tsukada: Fission Probability of Actinide Nuclei Obtained Using 18O-induced Multi-Nucleon Transfer Channels; *2017 Fall Meeting of the Atomic Energy Society of Japan*, Hokkaido, September 13-15, 20172M02.

(240) Mark Dennis Usang, Fedir A. Ivanyuk, Chikako Ishizuka, Satoshi Chiba: Pairing effects on _ssion observables with 3D-Langevin calculation using microscopic transport coefficients; *2017 Fall Meeting of the Atomic Energy Society of Japan*, Hokkaido, September 13-15, 20172M03.

(241) Chikako Ishizuka, Mark Dennis Usang, Satoshi Chiba: The charge polarization of ^{236}U fission fragments with the shape-4D Langevin model; *2017 Fall Meeting of the Atomic Energy Society of Japan*, Hokkaido, September 13-15, 20172M04.

(242) Takashi Nishikawa, Yoritaka Iwata, Shatoshi Chiba: The nuclear friction coefficient derived from Time-Dependent Density Functional Theory; *2017 Fall Meeting of the Atomic Energy Society of*

Japan, Hokkaido, September 13-15, 20172M05.

(243) Atsuhiko Etori, Akira Ono, Chikako Ishizuka, Satoshi Chiba: Study of fission and nuclear collisions by Antisymmetrized molecular dynamics(2); *2017 Fall Meeting of the Atomic Energy Society of Japan*, Hokkaido, September 13-15, 20172M06.

(244) Tadashi Yoshida, Takahiro Tatibana, Shin Okumura, Satoshi Chiba: Investigation of Reactor-Neutrino Spectral Anomaly based on Gross Theory of Beta-Decay; *2017 Fall Meeting of the Atomic Energy Society of Japan*, Hokkaido, September 13-15, 20172M07.

(245) Shin Okumura, Mark Dennis Usang, Toshihiko Kawano, Satoshi Chiba: Calculations of prompt neutron multiplicities and isomer production ratios by the statistical model; *2017 Fall Meeting of the Atomic Energy Society of Japan*, Hokkaido, September 13-15, 20172M08.

(246) Satoshi Chiba: Activities of Special Committee for Nuclear Data in the period of FY 2015 and 2016; *2017 Fall Meeting of the Atomic Energy Society of Japan*, Hokkaido, September 13-15, 20172MPL01.

(247) Koji Hiraiwa, Kennichi Yoshioka, Shungo Sakurai, Rei Kimura, Satoshi Wada, Tsukasa Sugita, Haruka Kajiwara, Takanori Kitada, Satoshi Takeda, Shatoshi Chiba: Concept of a nuclear fuel cycle using an environmental load-reducing light-water reactor (1)Outline of the Studies and the Results; *2017 Fall Meeting of the Atomic Energy Society of Japan*, Hokkaido, September 13-15, 20172M16.

(248) Takanori Kitada, Satoshi Takeda, Koji Hiraiwa, Satoshi Chiba: Concept of a nuclear fuel cycle using an environmental load-reducing light-water reactor (3) Toxicity reduction by adding poison (1); *2017 Fall Meeting of the Atomic Energy Society of Japan*, Hokkaido, September 13-15, 20172M17.

(249) Satoshi Chiba, Makoto Takahashi, Toshio Wakabayashi, Naoyuki Takaki, Yoshihiro Tachi, Atsunori Terashima, Shin Okumura, Tadashi Yoshida: R&D of Transmutation System of LLFP by using Fast Reactors (1) Outline of the Project; *2017 Fall Meeting of the Atomic Energy Society of Japan*, Hokkaido, September 13-15, 20173H03.

(250) Toshio Wakabayashi, Makoto Takahashi, Satoshi Chiba, Naoyuki Takaki, Yoshihiro Tachi,: R&D of Transmutation System of LLFP by using Fast Reactors (2) Characteristics of Transmutation; *2017 Fall Meeting of the Atomic Energy Society of Japan*, Hokkaido, September 13-15, 20173H04.

(251) Atsunori Terashima, Shin Okumura, Satoshi Chiba: R&D of Transmutation System of LLFP by using Fast Reactors (3) Evaluation of Nuclides Produced by Transmutation of LLFP; *2017 Fall Meeting of the Atomic Energy Society of Japan*, Hokkaido, September 13-15, 20173H05.

(252) Yoritaka Iwata: TDHF approach to nuclear fission; *Mini workshop on Nuclear Fission in Tokyo and Tokai 2017*, Tokyo Institute of Technology, Tokyo, April 2017.

(253) Yuya Matsuoka, Daisuke Hirotani, Ryujiro Suzuki, Atsushi Nezu, Shinsuke Mori, Hiroshi Akatsuka: Characteristic of Argon Plasma Arc Immersed into Water; *Joint Technical Meeting on Plasma Science and Technology, Pulsed Power Technology and Electrical Discharge, IEE Japan*, Kyoto, May 13 – 15, 2017, PST-17-024, PPT-17-024, ED-17-044.

(254) Senna Fukukawa, Atsushi Nezu, Hiroshi Akatsuka: Vibrational and Rotational Temperatures of N_2 B and C States Puffed onto Argon Arc Jet Plume; *Technical Meeting on Plasma Science and Technology, IEE Japan*, Nagoya, pp. 9-14, August 11 – 12, 2017, PST-17-061.

(255) Senna Fukukawa, Atsushi Nezu, Hiroshi Akatsuka: Spectroscopic Study on N_2 Molecule Puffed onto Expanding Argon Arc-Jet Plume; *78th Japan Society of Applied Physics (JSAP) Autumn Meeting*, Fukuoka, September 5 – 8, 2017, 5a-A413-2.

(256) Yuya Yamashita, Hiroshi Akatsuka: Excitation Kinetic Model for Argon Process Plasma Diagnostics by Spectroscopic Measurement Based on Collisional-Radiative Model; *78th Japan Society of Applied Physics (JSAP) Autumn Meeting*, Fukuoka, September 5 – 8, 2017, 5a-A413-7.

(257) Hirotaka Horita, Hiroshi Akatsuka, Amy M. Keesee, Daisuke Kuwahara, Shunjiro Shinohara: Argon Spectral Measurement Using Intensity Ratio Method in Large Helicon Source; *Plasma Conference 2017*, Himeji, November 20 – 24, 2017, 21P-72.

(258) Ryujirou Suzuki, Daisuke Hirotani, Yuya Matsuoka, Atsushi Nezu, Shinsuke Mori, Hiroshi Akatsuka: Measurement of Arc Plasmas Generated in Water for the Application to Decommissioning of Fukushima No. 1 Nuclear Power Plant; *Plasma Conference 2017*, Himeji, November 20 – 24, 2017, 21P-94.

(259) Senna Fukukawa, Atsushi Nezu, Hiroshi Akatsuka: Non-equilibrium Characteristics of N_2 B and C States Puffed onto Argon Arc-Jet Plume; *Plasma Conference 2017*, Himeji, November 20 – 24, 2017, 23P-88.

(260) Yurina Honda, Yasuka Onishi, Alejandro Álvaro-González, Atsushi Nezu, Hiroshi

Akatsuka: Optical Emission Spectroscopic Characteristics of Fulcher Band of Microwave Discharge $H_2 \cdot D_2$ Mixed Plasma; *2017 Joint Meeting of "Development of Plasma Science with Synergistic Effect of Atomic/Molecular process Research and of Passive/Active Spectroscopic Observation" and "Seminar of Atomic and Molecular Data Application Forum"*, Toki, December 20 – 22, 2017, http://www.am-data-forum.com/seminar29/abstract_Akatsuka.pdf.

(261) Hirotaka Horita, Daisuke Kuwahara, Hiroshi Akatsuka, Shunjiro Shinohara: Spectroscopic Measurement of Argon Plasma for High-Density Helicon Plasma Source with Collisional Radiative Model; *2017 Joint Meeting of "Development of Plasma Science with Synergistic Effect of Atomic/Molecular process Research and of Passive/Active Spectroscopic Observation" and "Seminar of Atomic and Molecular Data Application Forum"*, Toki, December 20 – 22, 2017, http://www.am-data-forum.com/seminar29/abstract_Horita.pdf.

(262) Yuya Matsuoka, Hiroshi Akatsuka: Measurement of Excitation Temperature and Electron Density of Submerged Arc Discharge Plasma; *2017 Joint Meeting of "Development of Plasma Science with Synergistic Effect of Atomic/Molecular process Research and of Passive/Active Spectroscopic Observation" and "Seminar of Atomic and Molecular Data Application Forum"*, Toki, December 20 – 22, 2017, http://www.am-data-forum.com/seminar29/abstract_Matsuoka_Y.pdf.

(263) Hiroshi Akatsuka: Up to Now and Tomorrow of Optical Emission Spectroscopy Measurement of Plasmas; *2018 Annual Meeting of the Institute of Electrical Engineers of Japan*, Fukuoka, March 14 – 16, 2018, S2-2.

(264) Noritsugu Kamata, Narong Mungkung, Pakpoom Chansri, Toshifumi Yuji, Hiroyuki Kinoshita, Hiroshi Akatsuka: Analysis of Instability Phenomenon at Current Interruption in Vacuum Arc Discharge Compared with Silver or Copper Electrode; *2018 Annual Meeting of the Institute of Electrical Engineers of Japan*, Fukuoka, March 14 – 16, 2018, 1-158.

(265) Yuya Yamashita, Fuminori Yamazaki, Atsushi Nezu, Hiroshi Akatsuka: Diagnostics of Microwave Discharge Low-Pressure Argon Plasma by Multi-Optical Emission Line Analysis Based on Collisional- Radiative Model; *65h JSAP Spring Meeting,* Tokyo, March 17 – 20, 2018, 17p-C204-3.

(266) Yoshiro Hakozaki, Hiroshi Onishi, Atsushi Nezu, Hiroshi Akatsuka: OES Measurement of Electron Temperature of Non-equilibrium Atmospheric-Pressure Ar Plasma; *65h JSAP Spring Meeting,* Tokyo, March 17 – 20, 2018, 17p-C204-5.

(267) Koji Kikuchi, Hiroshi Akatsuka: Discussion on the Excitation Temperature of Non - Equilibrium Plasma Using Tsallis Entropy; *2018 Annual (73rd) Meeting of the Physical Society of Japan*, Noda, March 22 – 25, 2018, 23pK601-5.

BULLETIN OF THE
LABORATORY FOR ADVANCED NUCLEAR ENERGY

Vol.3 2018

2019年2月　印刷

編集兼
発行者　東京工業大学科学技術創成
研究院先導原子力研究所
責任者　竹　下　健　二
〒152-8550 東京都目黒区大岡山2丁目12-1
電話　03－5734－3052
FAX　03－5734－2959

印刷所　昭和情報プロセス㈱
東京都港区三田5－14－9

Printed by
SHOWA JOHO PROCESS
Minato-ku, Tokyo, Japan